

# DOCTORAL PROGRAMME

---

## INFORMATION MANAGEMENT

Specialization in Geographical Information Systems

### A REMOTE SENSING APPROACH TO THE QUANTIFICATION OF LOCAL TO GLOBAL SCALE SOCIAL-ECOLOGICAL IMPACTS OF ANTHROPOGENIC LANDSCAPE CHANGES

**Rajchandar Padmanaban**

*A thesis submitted in partial fulfillment of the requirements for the  
of Doctor in Information Management*

**February, 2019**

**NOVA Information Management School**  
**Instituto Superior de Estatística e Gestão de Informação**  
Universidade Nova de Lisboa



UNIVERSIDADE  
**NOVA**  
DE LISBOA

# **A Remote Sensing Approach to the Quantification of Local to Global Scale Social-Ecological Impacts of Anthropogenic Landscape Changes**

This thesis is approved by:

**Professor Dr. Pedro Cabral, Supervisor**

*NOVA Information Management School (NOVA IMS), Universidade Nova de,  
Lisboa, Campus de Campolide, 1070-312 Lisboa, Portugal.*

**Dr. Avit K. Bhowmik, Co-Supervisor**

*Assistant Professor, Department of Risk and Environmental Studies,  
Karlstad University,  
Universitetsgatan 2, 651 88 Karlstad, Sweden.*



# A REMOTE SENSING APPROACH TO THE QUANTIFICATION OF LOCAL TO GLOBAL SCALE SOCIAL-ECOLOGICAL IMPACTS OF ANTHROPOGENIC LANDSCAPE CHANGES

## DISSERTATION

to attain

the degree of doctor at the *Universidade Nova de Lisboa (NOVAIMS)*, Portugal,

on the authority of the Dean, **Prof. Dr. Pedro Saraiva** and the Coordinator of

the Ph.D. in Information Management, **Prof. Dr. Tiago Oliveira**

on account of the assessment of the graduation committee, to be submitted

on 20<sup>th</sup>, February 2019

by

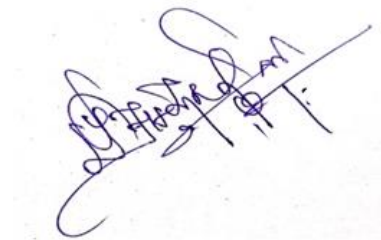
**RAJCHANDAR PADMANABAN**

from

Suchindrum, Kanyakumari District, Tamilnadu

## Declaration

I herewith declare that I have independently drawn up my Ph.D. dissertation entitled **“A remote sensing approach to the quantification of local to global scale social-ecological impacts of anthropogenic landscape changes”**. All aids and sources have been clearly specified, and the contribution of other scientists or authors have been clearly documented. I further certify that proper citations to the previously reported work have been given and no data has been quoted verbatim from other publications without giving due acknowledgement and without the permission of the author(s). I have never received any paid assistance by any sort of Ph.D. service agencies. The dissertation has neither identically nor in a similar form been submitted for any scientific examination in Portugal, Europe or in another country. Moreover, the dissertation has neither earlier nor simultaneously been submitted at any other university or faculty. I am fully aware that the Ph.D. title can be revoked as a result of failure to regard any of the aforementioned points and legal consequences are also possible.



**RAJCHANDAR PADMANABAN**

*NOVA Information Management School (NOVA IMS), Universidade Nova de Lisboa,  
Campus de Campolide, 1070-312 Lisboa, Portugal.*

Copyright © by

**RAJCHANDAR PADMANABAN**

All rights reserved

## Abstract

Landuse and Landcover (LULC) is the common aspect that influences several ecological issues, environmental degradations, changes in Land Surface Temperature (LST), hydrological changes and ecosystem function at regional to global level. Research on the drivers and progressions of LULC change has been key to developing models that can project and predict future LULC extent, level and patterns under different assumptions of socioeconomic, ecological and environmental situations. Rapid and extensive urbanization and Urban Sprawl (US), propelled by rapid population growth leads to the shrinkage of productive agricultural lands, boosting mining, decrease in surface permeability and the emergence of Urban Heat Islands (UHI), and in turn, adversely affects the provision of ecosystem services. Mining for resources extraction may lead to geological and associated environmental changes due to ground movements, collision with mining cavities, and deformation of aquifers. Geological changes may continue in a reclaimed mine area, and the deformed aquifers may entail a breakdown of substrates and an increase in ground water tables, which may cause surface area inundation. Consequently, a reclaimed mine area may experience surface area collapse, i.e., subsidence, and degradation of vegetation productivity.

The greater changes in LULC, US, LST and vegetation dynamics due to increasing human population not only affects inland forest and wetland, it also directly influences coastal forest lands such as mangroves, peat swamps and riparian forest and threats to ecosystem services. Mangroves provide valuable provisioning (e.g. aquaculture, fisheries, fuel, medicine, textiles), regulation (e.g. shoreline protection, erosion control, climate regulation), supporting (nutrient cycling, nursery habitat), and cultural (recreation and tourism) ecosystem services with an important impact on human well-being. However, the mangrove forest is highly threatened due to climate changes, and human activities which ignore the ecological and economic value of these habitats, contributing to its degradation. There is an increasing number of studies about mangrove distribution, changes and re-establishment activities, denoting a growing attentiveness on the value of these coastal wetland ecosystems. Most of these studies address mangrove degradation drivers at regional or local levels.

However, there has not been yet enough assessment on the drivers of mangrove degradation at global level. Thus, complexity of inland and coastal landscape degradation should be addressed using multidisciplinary methodology and conditions. Therefore, this dissertation aimed to assess the impact of LULC associated with vegetation, temperature and wetland changes. To understand the relation among three different types of landscape changes associated with anthropogenic activities: Urbanization, Geological changes and Forest degradation at local to global level, we have selected thirty-three global regions.

In chapter 2, We employed the Random Forest (RF) classification on Landsat imageries from 1991, 2003, and 2016, and computed six landscape metrics to delineate the extent of urban areas within a 10km suburban buffer of Chennai city, Tamilnadu, India. The level of US was then quantified using Renyi's entropy. A land change model was subsequently used to project land cover for 2027. A 70.35% expansion in urban areas was observed mainly towards the suburban periphery of Chennai between 1991 and 2016. The Renyi's entropy value for year 2016 was 0.9, exhibiting a two-fold level of US when compared to 1991. The spatial metrics values indicate that the existing urban areas became denser and the suburban agricultural, forests and particularly barren lands were transformed into fragmented urban settlements. The forecasted land cover for 2027 indicates a conversion of 13,670.33 ha (16.57% of the total landscape) of existing forests and agricultural lands into urban areas with an associated increase in the entropy value to 1.7, indicating a tremendous level of US. Our study provides useful metrics for urban planning authorities to address the social-ecological consequences of US and to protect ecosystem services.

In chapter 3, We studied landscape dynamics in Kirchheller Heide, Germany, which experienced extensive soil movement due to longwall mining without stowing, using Landsat imageries between 2013 and 2016. A Random Forest image classification technique was applied to analyse landuse and landcover dynamics, and the growth of wetland areas was assessed using a Spectral Mixture Analysis (SMA). We also analyzed the changes in vegetation productivity using a Normalized Difference Vegetation Index (NDVI). We observed a 19.9% growth of wetland area within four years, with 87.2% growth in the coverage of two major waterbodies in the reclaimed mine area. NDVI values indicate that the productivity of 66.5% of vegetation of the Kirchheller Heide was degraded due to



changes in ground water tables and surface flooding. Our results inform environmental management and mining reclamation authorities about the subsidence spots and priority mitigation areas from land surface and vegetation degradation in Kirchheller Heide.

In chapter 4, We demonstrated the advantage of fusing imageries from multiple sensors for LULC change assessments as well as for assessing surface permeability and temperature and UHI emergence in a fast-growing city, i.e. Tirunelveli, Tamilnadu, India. IRS-LISSIII and Landsat-7 ETM+ imageries were fused for 2007 and 2017, and classified using a Rotation Forest (RF) algorithm. Surface permeability and temperature were then quantified using Soil-Adjusted Vegetation Index (SAVI) and Land Surface Temperature (LST) index, respectively. Finally, we assessed the relationship between SAVI and LST for entire Tirunelveli as well as for each LULC zone, and also detected UHI emergence hot spots using a SAVI-LST combined metric. Our fused images exhibited higher classification accuracies, i.e. overall kappa coefficient values, than non-fused images. We observed an overall increase in the coverage of urban (dry, real estate plots and built-up) areas, while a decrease for vegetated (cropland and forest) areas in Tirunelveli between 2007 and 2017. The SAVI values indicated an extensive decrease in surface permeability for Tirunelveli overall and also for almost all LULC zones. The LST values showed an overall increase of surface temperature in Tirunelveli with the highest increase for urban built-up areas between 2007 and 2017. LST also exhibited a strong negative association with SAVI. South-eastern built-up areas in Tirunelveli were depicted as a potential UHI hotspot, with a caution for the Western riparian zone for UHI emergence in 2017. Our results provide important metrics for surface permeability, temperature and UHI monitoring, and inform urban and zonal planning authorities about the advantages of satellite image fusion.

In chapter 5, We identified mangrove degradation drivers at regional and global levels resulted from decades of research data (from 1981 to present) of climate variations (sea-level rising, storms, precipitation, extremely high water events and temperature), and human activities (pollution, wood extraction, aquaculture, agriculture and urban expansion). This information can be useful for future research on mangroves, and to help delineating global planning strategies which consider the correct ecological and economic value of mangroves protecting them from further loss.

## Resumo (Abstract in Portuguese)

O uso e a cobertura da Terra (UCT) são o aspeto comum que influencia várias questões ecológicas, degradações ambientais, mudanças na temperatura da superfície terrestre, mudanças hidrológicas, e de funções dos ecossistemas a nível regional e global. A investigação sobre os determinantes e progressão da mudança de UCT tem sido fundamental para o desenvolvimento de modelos que podem projetar e prever a extensão, o nível e os padrões futuros de UCT sob diferentes hipóteses de situações socioeconómicas, ecológicas e ambientais. A rápida e extensa urbanização e expansão urbana impulsionada pelo rápido crescimento populacional, levou ao encolhimento de terras agrícolas produtivas, impulsionando a mineração, a diminuição da permeabilidade da superfície e o surgimento de ilhas urbanas. Por outro lado, tem afetado negativamente a produção de serviços de ecossistemas. A mineração para extração de recursos pode levar a mudanças geológicas e ambientais devido a movimentos do solo, colisão com cavidades de mineração e deformação de aquíferos. As mudanças geológicas podem continuar numa área de mina recuperada, e os aquíferos deformados podem acarretar uma quebra de substratos e um aumento nos lençóis freáticos, causando a inundação na superfície. Consequentemente, uma área de mina recuperada pode sofrer um colapso à superfície, provocando o afundamento e a degradação da produtividade da vegetação.

As mudanças na UCT, no crescimento urbano rápido, na temperatura da superfície terrestre e na dinâmica da vegetação devido ao aumento da população humana não afetam apenas a floresta interior e as zonas húmidas. Estas também influenciam diretamente as terras florestais costeiras, tais como mangais, pântanos e florestas ribeirinhas, ameaçando os serviços de ecossistemas. Os mangais proporcionam um aprovisionamento valioso (por exemplo, aquacultura, pesca, combustível, medicamentos, têxteis), a regulação (por exemplo, proteção da linha de costa, controlo da erosão, regulação do clima), os serviços de ecossistema de apoio (ciclo de nutrientes, habitats) e culturais (recreação e turismo) com um impacto importante no bem-estar humano. No entanto, a floresta de mangal é altamente ameaçada devido às mudanças climáticas e às atividades humanas que ignoram o valor ecológico e económico desses habitats, contribuindo para a sua degradação. Há um número

crescente de estudos sobre distribuição, mudança e atividades de restabelecimento de mangais, denotando uma crescente atenção sobre o valor desses ecossistemas costeiros de zonas húmidas. A maioria desses estudos aborda os fatores de degradação dos mangais a nível regional ou local. No entanto, ainda não há avaliação suficiente sobre os determinantes da degradação dos mangais a nível global. Assim, a complexidade da degradação da paisagem interior e costeira deve ser abordada usando uma metodologia multidisciplinar. Portanto, esta dissertação teve, também, como objetivo avaliar o impacto do UCT associado à vegetação, temperatura e mudanças de zonas húmidas. Para compreender a relação entre a dinâmica da paisagem associada às atividades antrópicas a nível local e global, selecionámos quatro áreas de estudo, duas da Ásia, uma da Europa e outro estudo a nível global.

No capítulo 2, empregamos a classificação *Random Forest* (RF) nas imagens Landsat de 1991, 2003 e 2016, e computamos seis métricas de paisagem para delinear a extensão das áreas urbanas numa área de influência suburbana de 10 km da cidade de Chennai, Tamil Nadu, Índia. O nível de crescimento urbano rápido foi quantificado usando a entropia de Renyi. Um modelo de UCT foi posteriormente usado para projetar a cobertura de terra para 2027. Uma expansão de 70,35% nas áreas urbanas foi observada principalmente para a periferia suburbana de Chennai entre 1991 e 2016. O valor de entropia do Renyi para 2016 foi de 0,9, exibindo uma duplicação do nível de crescimento urbano rápido quando comparado com 1991. Os valores das métricas espaciais indicam que as áreas urbanas existentes se tornaram mais densas e as terras agrícolas, florestas e terras particularmente áridas foram transformadas em assentamentos urbanos fragmentados. A previsão de cobertura da Terra para 2027 indica uma conversão de 13.670,33 ha (16,57% da paisagem total) de florestas e terras agrícolas existentes em áreas urbanas, com um aumento associado no valor de entropia para 1,7, indicando um tremendo nível de crescimento urbano rápido. O nosso estudo fornece métricas úteis para as autoridades de planeamento urbano para lidarem com as consequências socio-ecológicas do crescimento urbano rápido e para proteger os serviços de ecossistemas.

No capítulo 3, estudamos a dinâmica da paisagem em Kirchheller Heide, Alemanha, que experimentou um movimento extensivo do solo devido à mineração, usando imagens Landsat entre 2013 e 2016. Uma técnica de classificação de imagem *Random Forest* foi aplicada para analisar dinâmicas de UCT e o crescimento das áreas de zonas húmidas foi avaliado usando uma Análise de Mistura Espectral. Também analisámos as mudanças na produtividade da vegetação usando um Índice de Vegetação por Diferença Normalizada (NDVI). Observámos um crescimento de 19,9% da área húmida em quatro anos, com um crescimento de 87,2% de dois principais corpos de água na área de mina recuperada. Valores de NDVI indicam que a produtividade de 66,5% da vegetação de Kirchheller Heide foi degradada devido a mudanças nos lençóis freáticos e inundações superficiais. Os resultados informam as autoridades de gestão ambiental e recuperação de mineração sobre os pontos de subsidência e áreas de mitigação prioritárias da degradação da superfície e da vegetação da terra em Kirchheller Heide.

No capítulo 4, demonstramos a vantagem de fusionar imagens de múltiplos sensores para avaliações de mudanças de UCT, bem como para avaliar a permeabilidade, temperatura da superfície e a emergência do ilhas de calor numa cidade em rápido crescimento, Tirunelveli, Tamilnadu, Índia. As imagens IRS-LISSIII e Landsat-7 ETM + foram fusionadas para 2007 e 2017, e classificadas usando um algoritmo de *Random Forest* (RF). A permeabilidade de superfície e a temperatura foram então quantificadas usando-se o Índice de Vegetação Ajustada pelo Solo (SAVI) e o Índice de Temperatura da Superfície Terrestre (LST), respectivamente. Finalmente, avaliamos a relação entre SAVI e LST para Tirunelveli, bem como para cada zona de UCT, e também detetamos a emergência de pontos quentes de emergência usando uma métrica combinada de SAVI-LST. As nossas imagens fusionadas exibiram precisões de classificação mais altas, ou seja, valores globais do coeficiente *kappa*, do que as imagens não fusionadas. Observámos um aumento geral na cobertura de áreas urbanas (áreas de terrenos secos e construídas), e uma diminuição de áreas com vegetação (plantações e florestas) em Tirunelveli entre 2007 e 2017. Os valores de SAVI indicaram uma extensa diminuição na superfície de permeabilidade para Tirunelveli e também para quase todas as classes de UCT. Os valores de LST mostraram um aumento global da temperatura da superfície em Tirunelveli, sendo o maior aumento para as áreas urbanas entre 2007 e 2017.

O LST também apresentou uma forte associação negativa com o SAVI. As áreas urbanas do Sudeste de Tirunelveli foram representadas como um potencial ponto quente, com uma chamada de atenção para a zona ribeirinha ocidental onde foi verificada a emergência de uma ilha de calor em 2017. Os nossos resultados fornecem métricas importantes sobre a permeabilidade da superfície, temperatura e monitoramento de ilhas de calor e informam as autoridades de planeamento sobre as vantagens da fusão de imagens de satélite.

No capítulo 5, identificamos os fatores de degradação dos mangais a nível regional e global resultantes de décadas de dados de investigação (de 1981 até o presente) de variações climáticas (aumento do nível das águas do mar, tempestades, precipitação, eventos extremos de água e temperatura) e atividades humanas (poluição, extração de madeira, aquacultura, agricultura e expansão urbana). Estas informações podem ser úteis para investigações futuras sobre mangais e para ajudar a delinear estratégias de planeamento global que considerem o valor ecológico e económico dos mangais, protegendo-os de novas perdas.

## Original Contributions

### List of Publications:

- (1) Padmanaban, Rajchandar, Avit K. Bhowmik, Pedro Cabral, Alexander Zamyatin, Oraib Almegdadi, and Shuangao Wang. "Modelling urban sprawl using remotely sensed data: A case study of Chennai city, Tamilnadu." *Entropy* 19, no. 4 (2017): 163. Source: <https://www.mdpi.com/1099-4300/19/4/163/htm>
- (2) Padmanaban, Rajchandar, Avit K. Bhowmik, and Pedro Cabral. "A remote sensing approach to subsidence and vegetation degradation in a reclaimed mine area." *ISPRS Int.J. Geo-Inf* 6, no. 6 (2017): 401. Source: <https://www.mdpi.com/2220-9964/6/12/401>
- (3) Padmanaban, Rajchandar, Avit K. Bhowmik, and Pedro Cabral. "Satellite image fusion to detect changing surface permeability and emerging urban heat islands in a fast-growing city." *PloS one* 14.1 (2019): e0208949.  
Source: <https://journals.plos.org/plosone/article?id=10.1371/journal.pone.0208949>
- (4) Padmanaban, Rajchandar, Avit K. Bhowmik, and Pedro Cabral. "What drives global mangrove degradation? (In preparation)"

### Conferences:

- (1) Padmanaban, Rajchandar, "Mangrove degradation", National conference on Recent Innovations in Engineering, Science and Management (RJEM) 2018 sponsored by Indian Space Research Organization and organized by Department of Civil Engineering, Dr. N.G.P Institute of Technology, Coimbatore on September 28, 2018.

## Newsletter and Newspaper proceedings:

(1) Padmanaban, Rajchandar and Avit K. Bhowmik, "Swallowing valuable land - Rapid urban expansion leaves India mega city Chennai without essential ecosystem services",

Stockholm Resilience Centre Newsletter (2017), Source:

<https://www.stockholmresilience.org/research/research-news/2017-05-10-swallowing-valuable-land.html>.

(2) Padmanaban, Rajchandar and Avit K. Bhowmik, "Urbanization of Tirunelveli city might warm it up" The Hindu Newspaper (2019), Source:

<https://www.thehindu.com/sci-tech/science/urbanisation-of-tirunelveli-city-might-warm-it-up/article26037548.ece>.

(3) Padmanaban, Rajchandar and Avit K. Bhowmik, "Hot in the city", Stockholm Resilience Centre Newsletter (2019), Source:

<https://www.stockholmresilience.org/research/research-news/2019-02-01-hot-in-the-city.html>

## Papers related to the thesis (Not included in the dissertation):

(1) Fakhruddin, Bapon, Rubini Mahalingam, and Rajchandar Padmanaban. "Sustainable development goals for reducing the impact of sea level rise on mangrove forests." *Indian Journal of Geo-Marine Sciences* 47, no. 10 (2018): 1947-1958.

Source: <https://run.unl.pt/handle/10362/50862>.

(2) Padmanaban, Rajchandar, S. Karuppasamy, and Rubini Narayanan. "Assessment of pollutant level and forecasting water pollution of Chennai Coastal, Tamilnadu using R." *Indian Journal of Geo-Marine Sciences* 47, no. 7 (2018): 1420-1429.

Source: <https://run.unl.pt/handle/10362/41873>.

(3) Padmanaban, Rajchandar and Marco Painho. "Urban Agent Based Model of Urban Slum Dharavi, Mumbai, India." *Journal of Earth Sciences and Engineering* 2 (2016): 1110. Source: <http://cafetinnova.org/innova/archiveList/IJEE/2017/06/10.21276ijee.2017.10.0601.pdf>.





## Dedication

*To my Mother, Muthulakshmi Padmanabhan*

*To my Father, Padmanabhan Durai Raj*

- Thank you being my inspiration

## Acknowledgments

**“காலத்தி னாற்செய்த நன்றி சிறிதெனினும்  
ஞாலத்தின் மாணப் பெரிது” - திருக்குறள்**

*“Although an action of help done timely, might be little in nature, it is truly larger than the world itself”- Thiruvalluvar (A Tamil Poet), Kural (Couplet).*

First and Foremost, I am very grateful to my mother, my father, my mother tongue “Tamil” and the almighty nature for the blessings to complete this project. My heartfelt gratitude goes to NOVAIMS Dean, **Prof. Dr. Pedro Saraiva** and the Coordinator of the PhD in Information Management, **Prof. Dr. Tiago Oliveira** for the acceptance of my PhD dissertation. I wish my special thanks to the former PhD Coordinator **Dr. Fernando Bacao** for the kind support from the beginning of my PhD application at NOVAIMS.

I wish to express my honest appreciation and thanks to my promoter and supervisor **Prof. Dr. Pedro Cabral**, NOVA Information Management School (NOVA IMS), Universidade Nova de Lisboa, Campus de Campolide, 1070-312 Lisboa, Portugal, for esteemed daily supervision, assistance, and encouragement. I am thankful that you provided me the opportunity to work on this research project. You believed in me from the beginning and lend your hand when I faced difficulties in research. Your direction, advice, coordination, support, technical guidance, and openness for innovative ideas has moulded this dissertation with science contribution in the field of Geographic Information System and Remote Sensing. I wish to describe my full-hearted thankfulness to **Dr. Avit.K. Bhowmik**, Assistant Professor, Department of Risk and Environmental Studies, Karlstad university, Universitetsgatan 2, 651 88 Karlstad, Sweden, my co-supervisor. Your energetic discussion and critical commenting on research work have helped me to be proficient to emphasise my research finding and succeeded the publication resulting from this dissertation to the top journals. You and Dr. Pedro Cabral have sharpened my technical, writing and reasoning skills and helped me to reach that far in my research. Once again thank you for your excellent supervision.

I am so grateful to all associates of the NOVAIMS. Principally, I would like to heartfelt acknowledge and thank **Dr. Fernando Bacao, Dr. Marco Painho and Dr. Cristina Marreiros** from NOVAIMS for their valuable support and direction to complete all the credit courses. I am also thankful to all members and colleagues of the NOVA Information Management School. **Mr. Yuri Vidal Santiago de Mendonça** (Brazil) thanks a lot for helping me with learning a little bit Portuguese and it was great to share the same office and home with you. **Mr. Dahmane Sheikh** (Belgium), **Mr. Sohaib Zafar Ansari** (Portugal) and **Mr. Ziad El Abbass** (Morocco), I am grateful and happy that you guys spent lot of time with me in Lisbon when I was stressed and lonely. All my friends and PhD colleagues in NOVAIMS, **Meer Qaisar Javed, Luis Jose Pinto da Fonseca, Iolanda Marcia de Almeida Fernandes Castro Barbeitos, Andre Ferraz Saraiva, Ricardo Galante Coimbra, and Frank Bivar Franque**, thank you guys for the great time and lively discussions during course hours and free time. My special thanks to my well-wisher and my master program Assistant Professor **Dr. Karuppasamy Sudalaimuthu**, SRM University Chennai for great support and advice during the past eight years.

My grateful thanks to my colleagues in University V.O.C. College of Engineering, Anna university, Tuticorin, **Dr. Jeyanthi** (Dean), **Dr. Aadish Kumar** (Head of the Department, Civil Engineering), **Dr. Collins Johnny, Dr. Mathumathi, Mr. S.Muthupackiaraj, Mrs. A.L. Swarna, Mr. Ashok Subramanian, Mrs. Snowfy Nivetha, Mrs. Mariammal, Mrs. Nisha Gunasekaran, Ms. Revathy, Mr. Siva Mahendra Krishnan, Mr. M. Albert Pradeep, Ms. M. Uma and Ms. Gayathri Devi** for your great support and pleasant working stay during my Tamilnadu visit. My hearty cheers and thanks to my students in 2<sup>nd</sup>, 3<sup>rd</sup> and 4<sup>th</sup> year, Bachelor of Engineering, Geoinformatics from University V.O.C. College of Engineering, Anna University, Thoothukudi, Tamilnadu.

I am grateful to my elder brother **Raj Sundar Padmanaban** for great support and advice. I am heartily thankful to my sister **Praveena Pramananthan**, you helped me in lots of situations especially when I was down with sickness and when I faced financial crisis during my stay in Germany, yes your part of money also included in my thesis work. Thank you very much my dear sister. **Karthikesan Pramananthan**, you lend me a hand in many circumstances when I encountered financial crisis, you helped me to find a part time job, yes that earning aided me

to pay a part of my tuition fees. **Mr. Matthias Hinz** (Germany), **Ms. Oraib Almegdadi** (Jordan), **Ms. Stephanie Walter** (Germany), **Mr. Shuangao Wang** (China), **Ms. Deeba Lakshmi** (Tamilnadu), **Mr. Essaki Raja** (Tamilnadu), **Mr. Mijail Naranjo** (Ecuador) **Mrs. Rubini Narayanan** (United Kingdom) and **Mrs. Yoga** (Germany), you guys helped me in many ways even I am not in Germany, you guys have taken very good care on my career. Your advice, financial aid and help are more precious and timely accountable.

My special great hearty cheers and thanks to my dearest brother **Mohammed Shamsudeen**, the days with you are unforgettable, even though you are younger than me you gave me comfort and happiness when I felt sad and faced many problems during PhD thesis. And your small surprises and tons of cares could never be replaced. My heartily thanks to my cousin **Dharani** and sister **Barathi @ Kamatchi** in Tamilnadu. You both have always been there via Facebook, WhatsApp and Instagram making me feel at home. Both your love and care are priceless.

I wish to extend my genuine thanks and gratefulness to all my friends and relatives for their valuable support, care, and love. Without their support, knowledge and encouragement, this effort would never have been accomplished.



# Index

Declaration	v
Abstract	vii
Resumo (Abstract in Portuguese)	x
Original Contribution	xiv
Dedication	xvii
Acknowledgments	xviii
List of Tables	xxvii
List of Figures	xxx
Acronyms	xxxiv
<b>1 Introduction</b>	<b>39</b>
1.1 Global Anthropogenic Landscape Changes.....	39
1.2 Landscape Change and the Urbanization Process.....	40
1.3 Geological Changes Induced by Mining.....	44
1.4 Forest Landscape Degradation.....	47
1.5 Motivation.....	49
1.6 Research Hypotheses.....	55
1.7 Research Objectives.....	56
1.8 Outline of the Dissertation.....	58
1.9 Research Methodology.....	60
1.10 Path of Research.....	62
<b>2 Modelling Urban Sprawl using Remotely Sensed Data</b>	<b>67</b>
2.1 Introduction.....	67
2.2 Study Area.....	68
2.3 Materials and Methods.....	70
2.3.1 Data and Pre-Processing.....	70
2.3.2 Landuse and Landcover (LULC) Mapping, and Accuracy Assessment.....	70
2.3.3 Quantification of Extent and Level of Urban Sprawl (US).....	73
2.3.3.1 Extent of US.....	73
2.3.3.2 Level of US.....	75

2.3.4 Prediction of Urban Extent for 2027.....	75
2.4 Results and Discussion.....	78
2.4.1 The Extent and Patterns of US between 1991 and 2016.....	78
2.4.2 Change in US Level.....	81
2.4.3 US Extent and Level Prediction for 2027.....	82
2.5 Concluding Remarks.....	84
<b>3 A Remote Sensing Approach to Environmental Monitoring in a Reclaimed Mine Area</b>	<b>88</b>
3.1 Introduction.....	88
3.2 Study Area.....	90
3.3 Materials and Methods.....	92
3.3.1 Satellite Data.....	92
3.3.2 Image Processing.....	93
3.3.3 Land-Use and Landcover Classification and Accuracy Assessment.....	93
3.3.4 Wetland Coverage and Surface Flooding.....	95
3.3.5 Vegetation Productivity and Coverage.....	96
3.4. Results and Discussion.....	97
3.4.1 Landscape Dynamics During 2013–2016.....	97
3.4.2 Emergence and Growth of Waterbodies.....	99
3.4.3 Vegetation Productivity.....	100
3.5 Outlook.....	103
<b>4 Satellite Image Fusion to Detect Changing Surface Permeability and Emerging Urban Heat Islands in a Fast-growing City</b>	<b>107</b>
4.1 Introduction.....	107
4.2 Study area.....	110
4.3 Materials and Methods.....	112
4.3.1 Data.....	112
4.3.2 Image Pre-processing.....	112
4.3.3 Image Fusion.....	113
4.3.4 Image Classification.....	115
4.3.5 Accuracy Assessment.....	117

4.3.6 Surface Permeability Assessment.....	117
4.3.7 Land Surface Temperature Measurement.....	118
4.3.8 Emergence Potential for Urban Heat Islands.....	119
4.4 Results and Discussion.....	120
4.4.1 Landuse and Landcover Changes.....	120
4.4.2 Changes in Soil Permeability and Surface Temperature.....	124
4.4.3 Urban Heat Islands Emergence.....	132
4.5 Concluding Remarks.....	135
<b>5 What Drives Mangrove Degradation?</b>	<b>138</b>
5.1 Introduction.....	138
5.2 Methods.....	140
5.2.1 Document search and Categorization.....	140
5.2.2 Data Interpretation and Analysis.....	142
5.3 Results.....	142
5.3.1 Global Distribution of Mangrove Forest.....	142
5.3.2 Drivers in Mangrove Forest Degradation.....	147
5.3.2.1 Environmental Drivers on Mangrove degradation and Impacts.....	150
5.3.2.1.1 Global Sea Level Rise and Extreme High Water Occurrences..	150
5.3.2.1.2 Extreme Events in a Warming Environment.....	151
5.3.2.1.3 Changes in Temperature and Precipitation Patterns.....	153
5.3.2.2 Anthropogenic Drivers and Impacts.....	155
5.3.2.2.1 Population Growth and Urbanization.....	155
5.3.2.2.2 Aquaculture and Agriculture.....	156
5.3.2.2.3 Coastal Protection Structures and Flood Control Walls.....	158
<b>6 Major Results and Discussion</b>	<b>162</b>
6.1 Modelling Urban Sprawl using Remotely Sensed Data.....	162
6.2 A Remote Sensing Approach to Environmental Monitoring in a Reclaimed Mine area.....	162
6.3 Satellite Image Fusion to Detect Changing Surface Permeability and Emerging Urban Heat Islands.....	163
6.4 Drivers of Mangrove Degradation at Regional to Global Levels.....	163



6.5 Contributions.....	164
6.6 Outlook and Concluding Remarks.....	165
Reference.....	170



## List of Tables

Table No	Title	Page No
2.1	A technical description of the Landsat TM and ETM+ imageries used in this study.....	70
2.2	Landuse and landcover (LULC) nomenclature.....	71
2.3	Description and formulae for spatial metrics computation.....	73
2.4	Landscape indices, entropy values and their changes in percent.....	80
2.5	Comparison of the LULC areas of three study periods, i.e., 1991, 2003 and 2016, with the predicted LULC areas of Chennai for 2027.	83
3.1	Description of Land-Use and Landcover (LULC) classes.....	95
3.2	Summary of the confusion matrix for the classified images of 2013–2016 (PA – Producer Accuracy; UA – User Accuracy). ....	97
3.3	Comparison of the land-use and land cover (LULC) types during 2013–2016.....	99
3.4	Vegetation productivity changes between 2013–2014, 2014–2015, and 2015–2016. Value ranges 0.42–1, 0.08–0.42, and –1–0.08 indicated highly, medium, and lowly productive vegetation, respectively, and the overall changes in their coverage are reported in bold.....	102
4.1	Landuse and landcover (LULC) classes definition.....	117
4.2	Change in the area coverage of the landuse and landcover (LULC) classes between 2007 and 2017.....	123
4.3	Accuracy assessment results for the landuse and landcover classification using fused images of 2007 and 2017.....	124
4.4	Changes in the coverage of soil permeability (indicated by soil-adjusted vegetation index (SAVI)) classes in Tirunelveli between 2007 and 2017.....	129
4.5	Areal average SAVI values for the LULC zones.....	129

4.6	Statistics of the area between 2007–2017 with corresponding changes in LST.....	132
4.7	Average land surface temperature (LST) in degrees Celsius by landuse and landcover cover (LULC) zones.....	132
4.8	Spearman correlation between soil-adjusted vegetation index (SAVI) and land surface temperature (LST) by landuse and landcover (LULC) zones. All correlation coefficients are statistically significant at $p \leq 0.01$ .....	134
5.1	List of the combination of mangrove relevant keywords and number of studies considered.....	141
5.2	23 Most mangrove-rich countries and their covered area changes from 2000 to 2012.....	146
5.3	Ramsar site mangrove loss during 2000 and 2012	147
5.4	Listed several drivers on mangrove studies covered in this paper N/A – Not available.....	148



## List of Figures

Figure No	Title	Page No
1.1	Interaction amongst humans, climate and environmental system in urban landscape.....	41
1.2	Interaction amongst geological changes and environmental system in mining landscape.....	46
1.3	Interaction amongst forest changes and environmental systems in coastal landscape.....	49
1.4	The relationship between increasing human population and different landscape changes and its consequences.....	54
1.5	Regional to global scale social-ecological impacts of anthropogenic landscape associated with different aspects, which threats to ecosystem and biodiversity.....	55
1.6	Thirty-Three global regions covered by the studies in this thesis to understand the impact of different types of landscape changes: Urbanization, Geological changes and Forest degradation.....	57
1.7	Different topics covered in this dissertation.....	59
1.8	Schematic diagram of the work-flow of this dissertation.....	61
2.1	The study area covering Chennai city and 10 km sub-urban buffer.....	69
2.2	Flow-chart for image processing, classification and accuracy assessment.....	72
2.3	Methodology applied for the prediction of urban sprawl extent and level for 2027.....	76
2.4	Landuse and landcover (LULC) maps for 1991, 2003, and 2016 in Chennai.....	79
2.5	Simulated LULC map for the year 2027.....	83
2.6	Urban sprawl, i.e., changes in urban extents between 1991–2027.....	84

3.1	Inundation and subsidence through geological changes in a mining-affected area. The changes observed in the surface level using remote sensing (RS) may indicate the geological changes at the subsurface level. The figure is created according to the description of subsidence in Brunn et al. (2002).....	89
3.2	Location of Kirchheller Heide and mining area. The maps were created using Google Maps.....	91
3.3	Methodology for the analysis of landscape dynamics and vegetation health (productivity) (NDVI: Normalized Difference Vegetation Index; ETM: Enhanced Thematic Mapper; SMA: Spectral Mixture Analysis; LULC: Land-use and Land cover).....	93
3.4	Classified land-use and landcover (LULC) maps of Kirchheller Heide in July 2013, 2014, 2015, and 2016.....	98
3.5	Changes in the extent and coverage of waterbodies in Kirchheller Heide during 2013–2016. (a) The location of waterbodies (A and B) in the red circle indicate the waterbodies with the highest (87.2%) growth and potential subsidence spots; (b) the dynamics of the extent of waterbodies A and B during the years 2013–2016; and (c) the changes in the area coverage of waterbodies A and B during 2013–2016.....	100
3.6	(a) NDVI map of the Kirchheller Heide mining area in July 2013, 2014, 2015, and 2016. Value ranges 0.42–1, 0.08–0.42, and –1–0.08 indicated highly, medium, and lowly productive vegetation, respectively (see b and Table 6 for details). The location of the waterbodies, which experienced abrupt growth, are in the black circles; (b) Area coverage in km <sup>2</sup> by vegetation productivity classes in 2013, 2014, 2015, and 2016.....	101
4.1	Geographic location and area of Tirunelveli city. The maps were generated using Google Maps.....	111
4.2	Methodological flow for landuse and landcover classification, surface permeability, surface temperature and urban heat islands emergence assessment. Fig. legends- DEM: Digital Elevation Model; LULC: Landuse and Landcover; ETM: Enhanced Thematic Mapper; SAVI: Soil-Adjusted Vegetation Index; LST: Land Surface Temperature; UHI: Urban Heat Island.....	114
4.3 (a)	Classified landuse and landcover (LULC) maps of Tirunelveli city in 2007.....	121

4.3 (b)	Classified landuse and landcover (LULC) maps of Tirunelveli city in 2017.....	122
4.4 (a)	Soil-Adjusted Vegetation Index (SAVI) (surface permeability) maps of the Tirunelveli city in 2007.....	127
4.4 (b)	Soil-Adjusted Vegetation Index (SAVI) (surface permeability) maps of the Tirunelveli city in 2017.....	128
4.5 (a)	Land Surface Temperature (LST) maps of the Tirunelveli city for 2007.....	130
4.5 (b)	Land Surface Temperature (LST) maps of the Tirunelveli city for 2017.....	131
4.6	UHI emergence potential map of Tirunelveli city for 2017.....	134
5.1	Studies covered in this review chapter in region wise.....	144
5.2	Mangroves covers assessment from different sources.....	145
5.3	Environmental Drivers in mangrove forest and its consequence.....	149



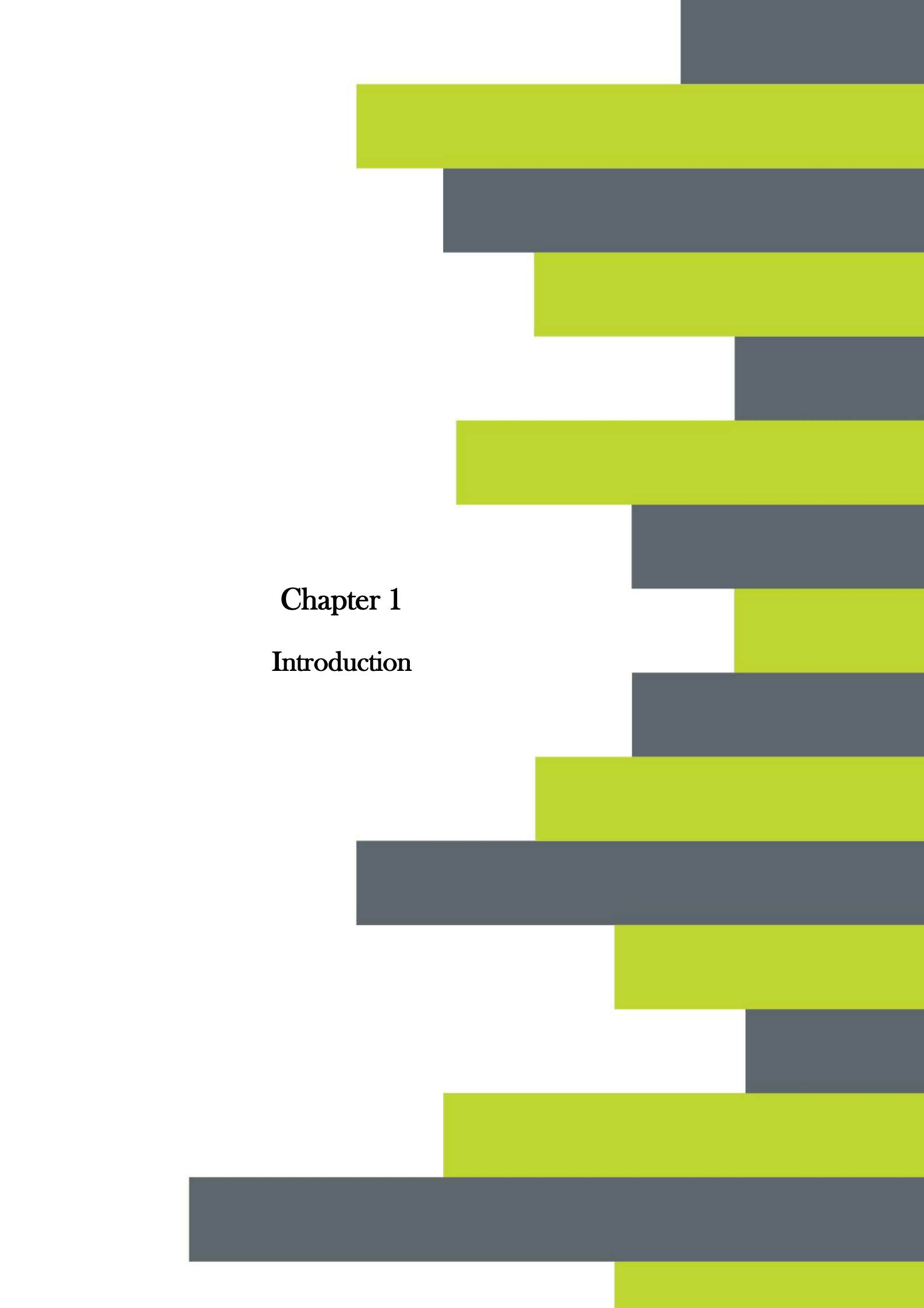


## Acronyms

<b>CART</b>	classification and regression tree
<b>CARDS</b>	Centre for Agriculture and Rural development studies
<b>CA</b>	Class Area
<b>CLUMPY</b>	Clumpiness Index
<b>Cu</b>	Copper
<b>DT</b>	Decision Tree
<b>DEM</b>	Digital Elevation Model
<b>DN</b>	Digital Number
<b>ETM</b>	Enhanced Thematic Mapper
<b>ENVI</b>	ENvironment for Visualizing Images
<b>EU</b>	European Union
<b>FRAC_AM</b>	Fractal Index Distribution
<b>Fe</b>	Iron
<b>GEE</b>	Google Earth Engine
<b>GPS</b>	Global Positioning System
<b>GIS</b>	Geographic Information System
<b>Hg</b>	Mercury
<b>IHS</b>	Intensity-Hue-Saturation
<b>InSAR</b>	Interferometric Synthetic Aperture Radar
<b>IRS LISS</b>	Indian Remote Sensing Satellite Resourcesat-1 - Linear Imaging Self-Scanning
<b>ISRO</b>	Indian Space Research Organization

<b>IPCC</b>	Intergovernmental Panel on Climate Change
<b>ISRO</b>	Indian Space Research Organization
<b>KC</b>	kappa coefficient
<b>LST</b>	Land Surface Temperature
<b>LPI</b>	Largest patch Index
<b>LASER</b>	Light Amplification by Stimulated Emission of Radiation
<b>LIDAR</b>	Light Detection and Ranging
<b>LULC</b>	Landuse and Landcover
<b>LULCC</b>	land use landcover changes
<b>LPS</b>	Leica Photogrammetry Suite
<b>Mg</b>	Magnesium
<b>Mn</b>	Manganese
<b>NRSC</b>	National Remote Sensing Centre
<b>NP</b>	Number of Patches
<b>NDVI</b>	Normalized Difference Vegetation Index
<b>PCA</b>	Principal Component Analysis
<b>PIF</b>	Pseudo-invariant features
<b>Pb</b>	Lead
<b>RQ</b>	Research Question
<b>RMS</b>	root mean square
<b>Rts</b>	Raster Time Series Analysis
<b>Rgdal</b>	Raster Geospatial Data Abstraction Library
<b>RE</b>	Renyi's Entropy

<b>RF</b>	Random Forest
<b>ROF</b>	Rotation Forest
<b>RS</b>	Remote Sensing
<b>PIF</b>	Pseudo-invariant features
<b>PA</b>	Producer Accuracy
<b>Rgdal</b>	Raster Geospatial Data Abstraction Library
<b>SMA</b>	Spectral Mixture Analysis
<b>UHI</b>	Urban Heat Islands
<b>SAVI</b>	Soil-Adjusted Vegetation Index
<b>SLC</b>	Scan Line Corrector
<b>SAVI</b>	Soil-Adjusted Vegetation Index
<b>Sn</b>	Tin
<b>TOA</b>	Top-of-Atmosphere
<b>TM</b>	Thematic Mapper
<b>US</b>	Urban Sprawl
<b>UNESCO</b>	United Nations Educational, Scientific and Cultural Organization
<b>UEPM</b>	urban extent prediction model
<b>USGS</b>	United States Geological Survey
<b>UTM</b>	Universal Transverse Mercator
<b>UHI</b>	Urban Heat Islands
<b>UA</b>	User Accuracy
<b>WGS</b>	World Geodetic System
<b>Zn</b>	Zinc



## Chapter 1

### Introduction

*"We won't have a society if we destroy the environment".*

*Margaret Mead*

# CHAPTER 1

## Introduction

---

### 1.1 Global Anthropogenic Landscape Changes

Everything that has developed modern human society is delivered by nature and, progressively, research determines the natural world's incalculable significance to our health, wealth, food and security [1]. The worldwide economic movement eventually depends on different services provided by the environment and nature, assessed to be valued around US\$125 trillion a year [1]. Mounting human population and exploding human consumption has substantially degraded 75% of Earth's land areas [2]. These lands that have either become wastelands, are contaminated, or have been deforested and transformed to agricultural land are also the main driving force behind the unparalleled environmental transformation we are witnessing today, through the augmented demand for water, land, and energy [2]. If this unsustainable growth continues, 95% of Earth's productive land areas might become degraded by 2050, which will force millions of people to migrate, as food production will break down in many places [3].

Productive land degradation, loss of biodiversity, and climate alteration are diverse aspects of the same principal challenge: the increasingly hazardous influence of our choices on the health of our natural environment and ecosystem [2]. There are three different types of landscape changes that have extensive impacts on the global climate and are interconnected with ecological and biophysical processes: Urbanization, geological changes, and forest degradation [4–7]. The growing threat of climate change rapidly increases due to the decline of biodiversity by overexploitation of species, deforestation, agriculture, and land transformation [8]. Climate change is distressing in all parts of the world: disrupting economies, affecting lives, altering the dynamics of entire species on the earth [9]. The Paris agreement in 2015 disclosed the importance of the global participation to reduce the rise in global temperature by 2 degrees Celsius [10]. Greenhouse gases are found to be one of the major reasons for the rising temperature and climate change [11]. Research evidenced that the forests including wetland forests help to reduce the emission of greenhouse gases [12].

Researchers are developing sophisticated new tracking and systematic tools to match commodities and their supply chains to certain influences on the ecosystem. Improving the transparency around these complex relationships may help to stop global climate change and biodiversity loss [1,8,13,14]. By 2020, ensure the conservation, restoration and sustainable use of terrestrial and inland freshwater ecosystems and their services, in particular forests, wetlands, mountains, and drylands, in line with obligations under international Paris agreements [15]. In order to achieve these targets, it is important to find the existing techniques and understand the gaps in analyzing urbanization process, geological changes, and forest degradation, which can help in landscape and climate change related planning.

## 1.2 Landscape Change and the Urbanization Process

Urbanization is a dynamic and complex progression playing out over various scales of space and time. Globally, in 2008 the urban human population outstripped the non-rural (villages and towns) population for the first time in history and it is projected that 70% of the global population will live in an urban region by 2050, with more than 50% of them intense in Asia [16]. The United Nations (UN) also predicts that the urban population will broaden upsurge from 3.3 billion to 4.9 billion worldwide by 2030 [17]. Almost all future population growth will take place in cities of the developing countries like India, in which the proportion of urbanization and peri-urbanization is faster than in developed countries [18]. Apparently, the area of urban landscape around the world is increasing on average twofold as fast as their populaces, principally in India and China [18]. Almost one-quarter of the global population resides within 100km of the coast and dwells less than 10m above mean sea level [19]. Even though urban landscape cover is comparatively small in the ratio of the total Earth surface, urban landscape modifications drive global environmental change [20]. Increasing physical changes in urban landscape is predominantly categorized by peri-urbanization, the development whereby outskirts both distant or near from the center of cities are converted into cosmopolitan regions [21]. This drives the conversion of productive land, wetland, forest and pastures to urban land includes industrialization and encroachments [22].

An understanding of the development of urbanization and peri-urbanization could support us in coping with evolving environmental problems associated with mounting urban living



[23]. Urban landscape changes have been investigated and examined from several social, cultural, economic and environmental perspective, extending from population density, to urban-rural disparities, to the loss of ecosystem and natural habitats, to bio-diversity, and accumulating emission of greenhouse gas [24–26]. The landscape changes in urban areas have extensive impacts on the global climate which are interconnected with ecological and biophysical processes [4]. The changes in climate induced desertification, deforestation, drought, and loss in biodiversity [27].

Urbanization in developing countries like India is predominantly taking place in an unplanned way, driving low-density growth and improvident use of environmental resources [28,29]. Thus, time series analysis on urban landscape changes has been considerably recognized as data needed in order to comprehend the interaction amongst humans, climate and environmental systems (Figure 1.1).

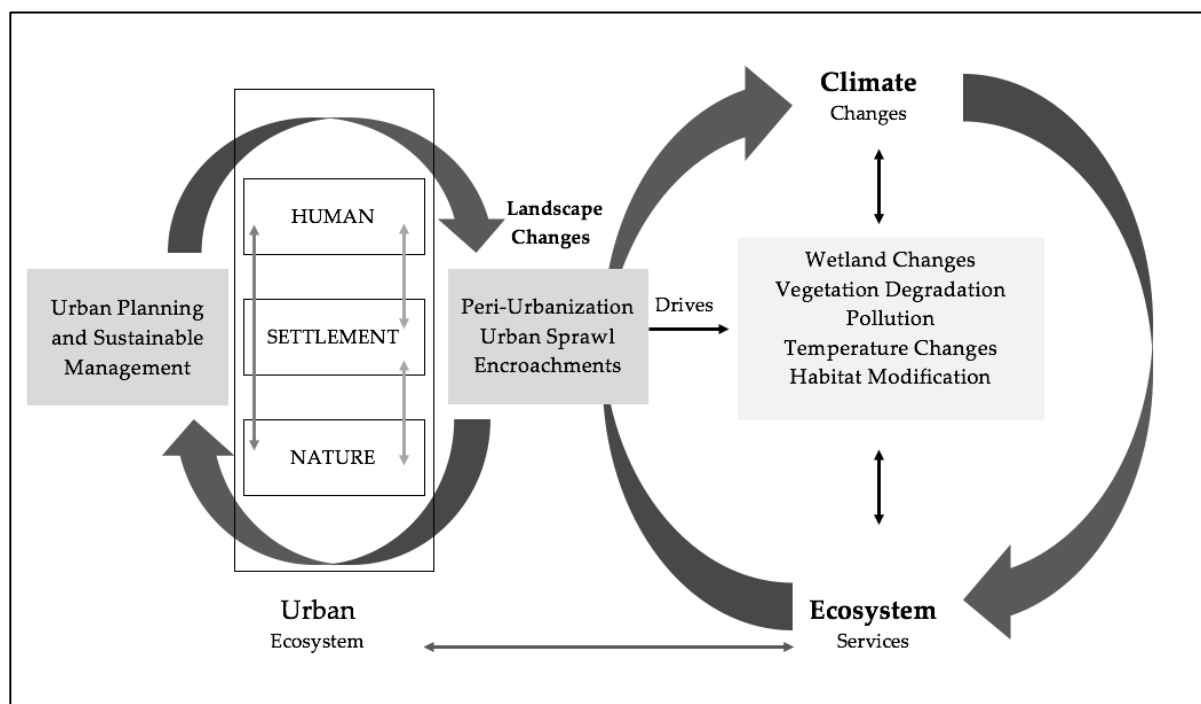


**Figure 1.1.** Interaction amongst humans, climate and environmental systems in urban landscape

In the last four decades, the development on Remote Sensing (RS)<sup>1</sup> technologies has evolved intensely to comprise a suite of sensors at a broad range and high-resolution imaging scales with probable interest and significance to urban planners and land administrators [30]. RS

data has been extensively used to measure urban growth, Urban Sprawl (US)<sup>2</sup>, geological movement and vegetation degradation with majority research using one or more geospatial images to deliver single portraits of landscape changes between different epochs [31]. Easy accessible RS data, the lessening in the price of data and increased <sup>1</sup>spectral, <sup>2</sup>spatial, <sup>3</sup>radiometric and <sup>4</sup>temporal resolution from <sup>5</sup>spaceborne-satellites and <sup>6</sup>airborne-platforms, have increased the impact of RS technology on urban management [31].

**1. Remote Sensing (RS)** — Remote sensing is the process of recording and monitoring earth objects or occurrence at far-away places. The sensors deployed in RS are not in physical contact with features on the earth while measuring its emitted and reflected radiation [32]. The RS process involves: i) Energy source of illumination, ii) Radiation energy interact with the atmosphere, iii) Radiation energy interact with the earth features/target, iv) Recording of energy by the sensor, v) Digital communication, reception, and processing, vi) Interpretation and investigation, vii) Applications. In RS, electromagnetic radiation acts as information carrier between a sensor at satellite or aircraft to the target, that collects information about features shape, size, and characteristics [32]. The two main categories of sensors that can be distinguished are active and passive sensors. The active sensor uses its own source of light energy, i.e., sensors emit radiation that is directed towards earth features to be researched. But in the case of a passive sensor relay, there are other sources of energy, e.g. sunlight [32]. RS facilitates to attain a wide-ranging area at a time, detect the area for a long dwelling time, receive time series information and enables to discover invisible information. This advantages support several applications, including vegetation monitoring, soil mapping, land cover change detection, disaster management, urban modelling, transport network analysis, ecosystem monitoring, and water resource management [32].

Current RS delivers combination and investigation of spatial data from ground-based, aerial and space-borne platforms, with an association to Geographic Information System (GIS)<sup>3</sup> data layers and functions, and evolving urban modeling competencies [33]. This has made RS a valuable data source of urban landscape information.

---

<sup>1</sup>**Spectral resolution** – Spectral resolution explains the ability of a sensor to define fine wavelength intervals [34].

<sup>2</sup>**Spatial resolution** – Spatial resolution defines how much detail in a photographic image is visible to the human eye [34].

<sup>3</sup>**Radiometric resolution** – Radiometric resolution of image defines the ability of the sensor to distinguish different grey-scale values [35].

<sup>4</sup>**Temporal resolution** – Temporal resolution of image defines the exact same area at the same viewing angle a second time is equal to this period [35].

**2. Urban Sprawl (US)** — The term Urban Sprawl describes the growth of urban population away from central city area into low-density sub-urban. It also refers to the movement of a human population from highly dense and occupied metropolises and towns to low dense housing development over further and further rural land [33]. This state triggers distribution of a city and its suburbs over the nearest and surrounding rural and undeveloped land. This process is also called sub-urbanization and relates to the environmental and social significances associated with this expansion [33]. In the European continent, the term “peri-urbanization” is frequently used to explain similar dynamics and occurrences. Urban areas and their suburbs are now reaching overcrowding associated with increasing human population, which makes it urgent to research the causes and the consequences on the environment. Some of the foremost environmental glitches related to sprawl are the loss of productive land, deforestation, habitat loss, and reduction in ecosystem services [33].

The available <sup>7</sup>Landsat satellite imagery from more than three decades and advanced modeling technologies open up new opportunities to map the spatial-temporal information about urban landscape [36]. New computational methods are also developed to attain urban landscape features and its characteristics from RS data such as urban growth, US, informal settlements, Urban Heat Island (UHI)<sup>4</sup>, surface permeability and other urban geographic features [36].

**3. Geographic Information System (GIS)** — A geographic information system is a computer-based system designed to digitally capture, collect, store, process, analyze, retrieve and manage large datasets that have location information on the earth surface elements [32]. The key word to this computer-system is Geography i.e., some part of the data used in this system is spatial. These advantages allow to map the spatial location and characteristics of real earth features and visualize the spatial connections among them, including political, topographic, physical, climatic, resource and network elements. And another part of GIS data is generally tabular known as attribute data that provides supplementary information about each of the earth spatial features [32]. These two combinations of data types enable to map the world features exact location, mapping quantities, mapping densities e.g. population densities, finding what is nearby, short route distance, mapping change (past, present and future condition of an area) [32].

---

<sup>5</sup>**Spaceborne satellite** – The satellite which are operating or travelling in space to obtain images of the earth's surface and atmosphere are called space borne satellite [37].

<sup>6</sup>**Airborne platforms** – Airborne platforms, downward or sideward looking sensors are mounted on an aircraft to obtain images of the earth's surface [38].

<sup>7</sup>**Landsat** — The Landsat program is the longest-running enterprise for acquisition of satellite imagery of Earth. There are several earth observation satellites launched includes Landsat 1, 2, 3, 4, 5, 6 and 7, and the recent one is Landsat 8 [36].

While existing research and models are focused on the targeted urban landscape changes in the developed part of the world, developing nations under severe landscape changes in urban regions associated with US, UHI, and vegetation degradation are still lacking due to economic constraints, comprising of large areas and scarce availability of spatial data on urban landscape degradation [33,39,40]. The dangers to whole ecosystems are still unidentified [31,41,42]. Thus, the implementation of urban management frameworks in rapid urban growth countries naturally depends on the large-scale evaluation of human and environmental stress of landscapes by filling data gaps. A novel method in monitoring urban landscape changes accounting for data scarcity is thus required that can also find new methods or platforms to handle large scale data and use them to analyze urban landscape changes and prediction of urban landscape degradation.

**4. Urban Heat Island (UHI)** — An Urban Heat Island is an urban area or town that is significantly warmer than its adjacent rural land due to anthropogenic activities. The main reason for the UHI consequence is from the changes in land surfaces for various human purposes [43]. The heat energy is produced from all the places that have heaps of human activity and lots of people. There are many reasons were identified for UHIs, e.g. when homes, factories, industries, shops, and other buildings are constructed close together [43]. The fabrication materials used for building construction are typically good at shielding or holding in heat [43]. These materials make the areas around settlements warmer, and these changes in heat waves decrease air quality by swelling the production of pollutants such as ozone, and reduces water quality as warmer waters run into watercourses and stimulate pressure on their local species that have adapted to sustain only in the cooler aquatic ecosystem [43].

### 1.3 Geological Changes Induced by Mining

Urbanization and Industrialization, together with demographic development, are driving mining activities. Mining products play a vital role in the global economy and are a considerable source of the prospering economy of the country by providing the raw materials including metals and coal for a wide spectrum of industrial and domestic purposes [44]. However, mining is essential to the development of industry and prompting energetic economy, also responsible for variety of environmental impacts such as landscape damage, vegetation degradation, land desertification, soil erosion, surface subsidence, surface and

groundwater pollution, futile water-body existence, sinkholes formation and ecosystem degradation [45–47]. These landscape changes may directly or indirectly cause vegetation failure in the mining area. This can lead to unhealthy vegetation extensively discharging carbon to the atmosphere, which deteriorates the overall carbon sink effect of the vegetation, including coastal and inland forest [48].

Regular studies and examining of geological changes in mining areas including subsidence is always needed to prevent related disasters and to support sustainable development [49]. Several studies on mining activities only focus on the consequences resulting from the removal of minerals from the ground, which means they only observed the transformation and ground movement present and post mining activity [49,50].

The extraction process and machines used to access the galleries produce irreversible variations of cohesion and compressing of the substrate above and kilometers around the mining surface even during and after the reclamation process [51,52]. These surface modifications result in changes in groundwater table dynamics, slow sinking of a ground surface and unexpected collapse of the ground [53]. The changes in ground water reach surfaces and form new waterbodies, these wetland changes directly affect the vegetation health, hydrological conditions, and ecological situation [54]. So, an extensive range of mining studies associated with landscape changes is always needed. The several subsidence surveying techniques such as electronic surveying and ground leveling is limited on high risk and vast area [49]. These types of field surveys are time consuming, expensive and labor-intensive.

It is significant to evaluate the health of vegetation and monitor the improvement of rehabilitation until the underground mines are refilled and reclaimed [55,56]. In addition to conventional field and laboratory measurements, which include sampling sites for analysis of soil surface condition, wetland changes, landscape integrity, vegetation health; RS and GIS have been widely used to understand and analyze the landcover changes relevant to hydrological dynamics and vegetation health and cover [57–59]. Particularly, these studies are useful for detecting transformation of forestland (deforestation), vegetation cover changes in

agriculture and farmland using several parameters. Similar to that, there are urban studies on nature and changes of hydrological dynamics and variations in flood dynamics derived from the landuse and landcover, maps of urbanization and watersheds models [60]. RS technology has intensive attention on monitoring the planted species and wetland during and after reclamation of mining areas [49]. Classifying and monitoring the condition of vegetation health on land surfaces in remote-sensing images is achieved by tonal signatures of vegetation on multispectral images [61]. Thus, time series analysis on mining landscape changes has been considerably recognized as data needed in order to comprehend the interaction amongst geological changes and environmental systems (Figure 1.2).

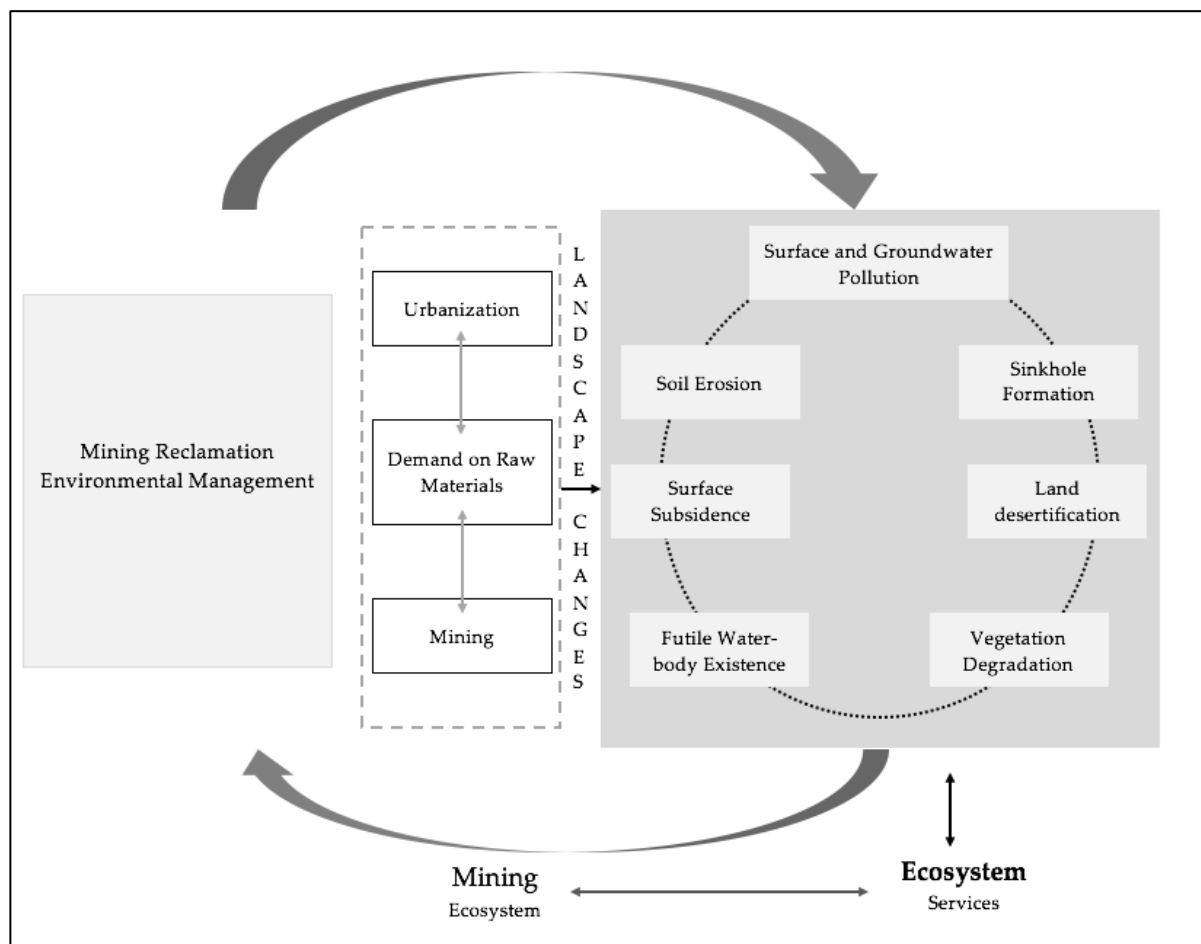


**Figure 1.2.** Interaction amongst geological changes and environmental systems in mining landscape

Comparatively, very few studies have systematically examined the implementation of RS and GIS to map and analyze the extent of post-mining surface through the different periods

[46,51,62]. The most successful studies on mining surface changes were obtained from LASER, SAR interferometry and LIDAR mapping [62–64]. But regional assessment of mining landscape degradation is inaccessible and dangers to whole ecosystems are still unidentified. Thus, the implementation of novel methods in monitoring mining landscape changes accounting for LIDAR, SAR and LASER data scarcity is thus required that can also find new methods to handle large scale data and use them to analyze geological changes in areas influenced by mining.

### 1.4 Forest Landscape Degradation

Forest degradation is a complex process in which the biological and natural prosperity of forests is permanently or temporarily weakened by some factor including climate and anthropogenic activities [65]. It has been estimated that globally some 2-billion-hectare area of forests are degraded with about half occurring in tropical countries [66]. While some 350 million ha of former tropical forests have been converted to other land uses, the remaining forests, owing to poor logging practices, have become severely degraded and are not in a good condition to deliver timber and other ecological services anytime in the foreseeable future [65].

Indeed, planted forests now make up 7 percent of the world's forest area and contribute over 40 percent of the global industrial wood and fiber supply [67]. To cut the forest degradation on a large scale, mangrove forests are the highly valued solutions for threatening climate changes [68]. They have valued at least 1,6 billion dollars in ecosystems services and sustain communities in many regions of the world by providing food, fire wood, shelter and sustainable tourism opportunities to local people [65]. Mangrove forests act as natural protection in case of storms and decrease erosion on coastal areas [69]. The huge volume of mangrove biomass disperses the energy of incoming waves and may greatly decrease the impact of hurricanes and tsunamis in coastal areas [70]. But global mangrove forest is undergoing an extensive deterioration of ecosystem health and loss of canopy cover has indicated that the degradation may be driven by:



- (i) anthropogenic activities, e.g. in situ encroachment, coastal LULC changes, US, exploitation of forest resources, water withdrawal and pollution in upstreams [71],
- (ii) climatic and associated geological changes, e.g. increased salinity driven by increasing temperatures [72] and
- (iii) natural disasters, e.g. tropical cyclones. Among them, tropical cyclones entail disruptive damages, whereas climatic changes and anthropogenic activities cause incremental degradation of the global mangrove forest [73].

The mangrove species in tropical environments are facing a major habitat degradation at an alarming rate, possibly even more rapidly than non-coastal tropical forests [74,75]. About 35% of the mangrove forest area has vanished during the past 20 years, and much of the leftovers is in a degraded state [76,77]. This is mainly due to climatic changes and human activities, which cause major alterations over the coastal ecosystem, mostly through deforestation, agriculture, aquaculture, and urban development [78–83]. Globally, there are many mangrove species identified at risk of extinction, which leads to a tremendous loss of several ecosystem functions, especially in Asia where over-exploitation of mangrove is reported [84,85].

The monitoring of the distribution and changes in mangrove populations at global and regional scales has been carried out with Remote Sensing (RS) methods [86–90] using different types of data, varying from airborne data to space borne images. These studies enabled the investigation of the human interference on mangroves through the analysis of landuse landcover changes (LULCC), at regional and global scales [91]. Additionally, research has been employed to identify several drivers on a regional level, which is geographically limited to small case studies [92–98]. However, such LULCC studies do not allow to detect the drivers of mangrove degradation at the global scale [99]. Identifying the global drivers of mangrove habitat loss is still challenging [100]. Thus, time series analysis on coastal landscape changes has been considerably recognized as data needed in order to comprehend the interaction amongst forest changes and environmental systems (Figure 1.3).



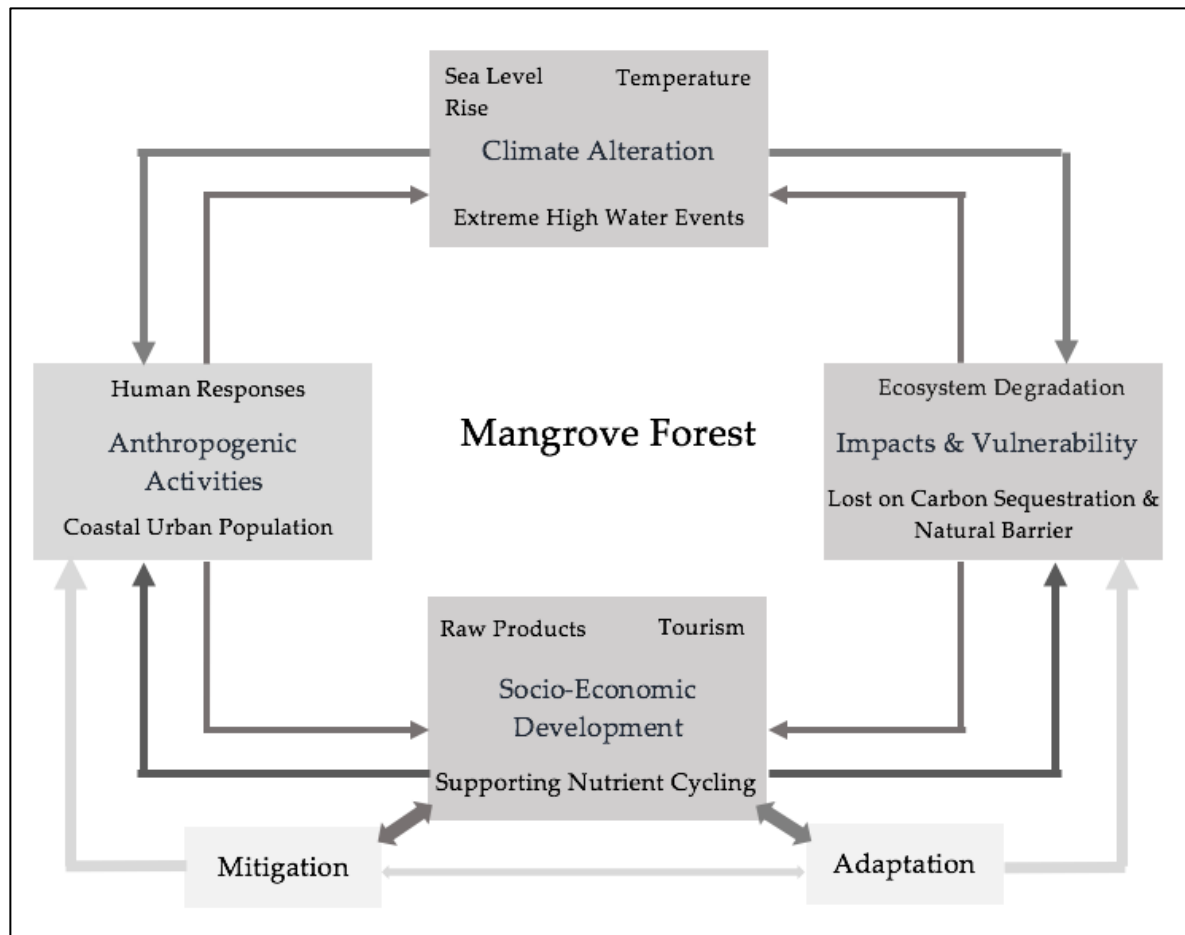


**Figure 1.3.** Interaction amongst forest changes and environmental systems in coastal landscape

## 1.5 Motivation

The pace, magnitude and spatial spread of human modifications of the Earth's land surface and its features are unprecedented. The modification of wetlands and vegetation are among the most important [101]. The key aspect of Earth system functioning and Ecosystem Services (ES)<sup>5</sup> are directly influenced by the alteration of biophysical attributes of the earth's surface (Landcover) and human purpose (Landuse) [102]. This influences the worldwide biodiversity, local and regional climate and ecosystem transformation, as well as to global climate warming [41]. The fluctuations in climate drives degradation of wetlands, inland and coastal vegetation and sea-level rise [103].

**5. Ecosystem Services (ES)** — Humans and other living beings have benefitted from the nature and environment in different ways for several millennia. But the modern science theory developed in the 1970s as ‘Environmental services’ was only further researched and renamed ‘Ecosystem Services’ in the mid-1980s [104]. Ecosystem services (ES) are benefits that living being generously gain from the biological nature and its environment without disturbing properly functioning ecology [104]. These ecosystems incorporate forest, aquatic, grassland and agroecosystems. The ecosystem provides valuable provisioning (e.g. aquaculture, food, fisheries, fuel, clean water, medicine, and textiles), regulation (e.g. shoreline protection, erosion control, and climate regulation), supporting (nutrient cycling, oxygen production, and nursery habitat), and cultural (recreation and tourism) ecosystem services with an important impact on human well-being [104]. Nowadays the policy makers and environmental scientist focused on assessing ecosystem services to study how the loss on ES drives degradation of human health, climate, carbon sequestration, atmosphere and environment [104].

Landuse and Landcover (LULC)<sup>6</sup> change is a locally pervasive and globally important biological trend. In the last three centuries, worldwide nearly 5.6 million km<sup>2</sup> of pasture, savanna and 1.2 million km<sup>2</sup> of timberland and forest have been converted to other land-uses [105]. Concurrently agriculture and fertile land has swelled by 1.2 million km<sup>2</sup> to uphold the food security of the world population [106]. The growth of human population as a driving force of biodiversity and environmental transformation because of the natural resources necessitated to endure the demand of 7.6 billion [107]. Much relative research offer statistical and spatial evidence which supports the claim that growth in population pushes to inland and coastal forest, and productive vegetation land clearance [31,101,108]. The destruction of 90% of the productive land aims to alleviate the scarcity of urban land to accommodate city population [109].

**6. Landuse and Landcover (LULC)** — The term Landuse and Landcover are frequently being used interchangeably but their real meanings are reasonably distinct. Landuse signifies how the land serves, i.e., how humans exploit the land, and of socio-economic action [102]. The most general classes in landuse are settlement and agriculture. The application of landuse include both baseline mapping and succeeding monitoring, subsequently periodic information is a prerequisite to estimate and measure the present and past amount of land utilization [102]. The year to year study understanding will aid in developing policies to balance land allocation, inconsistent uses, and urban progressive pressures. Problems driving Landuse research involve urban encroachment, removal of productive land, deforestation and pollution [102].

Landcover signifies the surface cover on the earth, i.e., physical material of the land surface [110]. According to the FAO, there are 14 landcover classes including manmade structures, woody crops, tree-covered area, herbaceous crops, shrubs, barren land, grassland, multiple or layered crops, sparsely natural green areas, mangroves, brackish water vegetation, coastal and inland waterbodies, permanent snow and glaciers [110]. This landcover monitoring is important for global climate studies, environmental monitoring, natural resource management, and other development plannings [110].

The destruction of productive land mostly proceeds in the outskirts of urban landscape to accommodate immigrants as well as to create employments by strengthening the industries [40]. This finally leads to US and the uneven development, through the conversion of suburban lands to built-up settlements [111]. US has influenced several environmental impacts, which include loss of productive urban and sub-urban land, aggregate soil, water and air pollution, abridged open spaces, greater energy and water consumption, damage to fragile land, cut-rate the diversity of species, ecosystem fragmentation, amputation of native vegetation, amplified runoff storm water and flooding [58,111,112]. In addition to that US triggers environmental injustice, whereby minority and poor immigrant groups suffer disproportionately from urban disinvestment or/and harmful land uses [105]. These results in removal/transfer of poor people and resources from inner city and inner-ring suburbs to more unsociable suburbs, and such handovers is implemented with unlawful control over land uses [33]. This directly threatens human health due to landfilling the toxic hazardous waste from city and inner suburbs to brownfields and least required areas, and draining the sewage and industrial waste into the watercourse environment [58].

The consequences of LULC and US not only prime landscape degradation but also affect several aspects of local, regional, and global environments, including changes in climatic parameters such as land and surface temperature, humidity and precipitation [113]. A primary impact of upsurge of built-up area and anthropogenic activities of urbanization decreases agriculturally fertile land, forest area and coastal wetlands, and upsurge of barren and impermeable surface area [58]. This leads to the secondary impact of shrinkage in wetlands and rise in Land Surface Temperature (LST) and UHI in and around cities [114]. So, the LULC data is needed in the analysis of environmental processes and associated problems

that must be understood if living conditions and standards are to be improved or maintained at sustainable conditions.

Information on the rate of change in the use of land resources and its impacts on temperature and vegetation are essential for proper planning, management and regularizing the use of such resources [115]. For estimating these spatiotemporal changes on LULC, UHI and US, traditional methods of monitoring spatio-temporal changes are based on field study combined with large scale aerial photography, which is time consuming and expensive [116]. RS has become an important tool applicable to developing and understanding the global, physical processes affecting the earth [117]. Recent development in the use of satellite data helps to take advantage of increasing amounts of geographical data available in conjunction with GIS to assist in interpretation of LULC, US, UHI and LST [118].

LST is disturbed due to changes in LULC and vegetation changes [119]. It is measurable continuously over space using RS methods which, in contrast to the conventional non-contiguous meteorological temperature measurements requires extrapolation [120]. Further RS enables the detection and analysis of the state of vegetation of the same area. However, with a few exceptions like LULC, such findings are scarce. The Soil Adjusted Vegetation Index (SAVI) and Normalized Differentiate Vegetation Index (NDVI) provide a fine estimate of vegetative cover and vegetative health conditions [121]. It has been widely used as an early warning on food security and ecological conditions [106]. SAVI can therefore be used as an indicator of climate change, and especially the rate of increase in LST which is one of the major components of LULC [121].

Human population plausibility boosts the extraction, production and consumption of industrial and domestic raw materials from mining and other natural resources to fabricate garments and produce sustenance, lumber, fuels, metals and medicinal good [49].

---

<sup>8</sup>*European Union (EU) – EU is a political and economic union of 28 member states that are located primarily in Europe [55].*

Mining is an important source of raw materials and minerals, e.g., metals, salt, and coal, for industrial and domestic usage [55,64]. Countries in the European Union <sup>8</sup>(EU) and Asia produce about 7% and 35% of the industrial and domestic commodities from mine-extracted resources respectively [53,122]. Mining industries also play a vital role in global to regional economies, e.g., in energy production and fuel supply [49].

Mining activities may lead to several geological changes, i.e., ground movements, collision with mining cavities, and deformation of aquifers. These changes may constitute an increase in the groundwater table, and thus a slow sinking of subsurface soils and an unexpected collapse, i.e., subsidence [55]. The extraction processes and machines used to access mine galleries may produce irreversible damage in soil cohesion and eventually compress soil substrates [47,49]. Consequently, groundwater may intrude the surface level, form new waterbodies, and cause inundation. This, in turn, leads to several adverse long-term environmental impacts from regional to global, such as vegetation degradation, soil erosion, flooding, sinkhole formation, and soil and water contamination [51,63], as well as to the damage of infrastructures [45].

The geological changes and associated environmental impacts may continue even after reclamations, if mines are not properly backfilled [53]. The greater changes in LULC, US, LST and vegetation dynamics due to increasing human population not only affect inland forest and wetland, but also directly influences coastal forest lands such as mangroves, peat swamps and riparian forest and threatens to ecosystem services [55,71,90,123] (Figure 1.4). Mangrove forests are among the greatest productive and biologically important ecosystems of the world because they provide significant and unique ecosystem properties and services to human society and marine and coastal systems [124]. Global mangrove forest is undergoing an extensive deterioration of ecosystem health and loss of canopy cover has indicated that the degradation may be driven anthropogenic activities or climate changes.

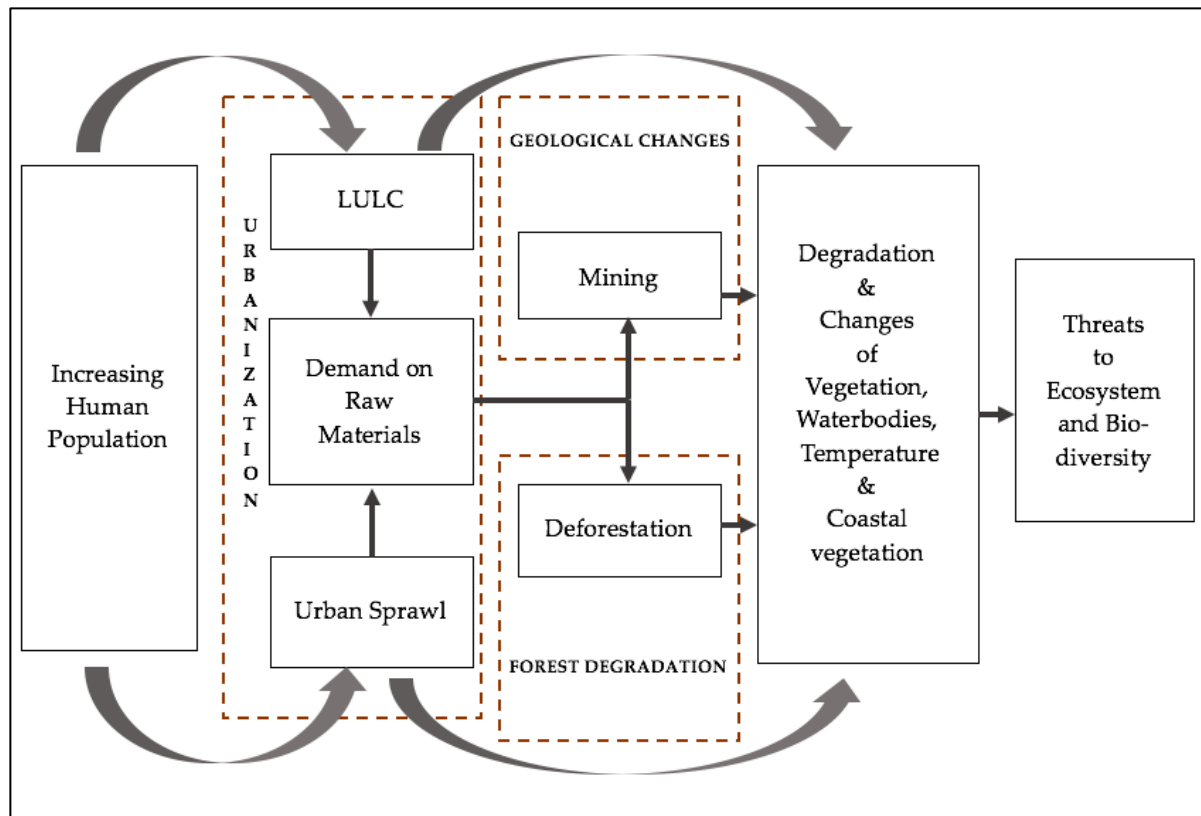


**Figure 1.4.** The relationship between increasing human population and different landscape changes and its consequences.

LULC is the common aspect that influences several ecological issues, environmental degradations, changes in land-atmosphere temperature, hydrological changes and ecosystem function at the global level [125,126]. Research on the drivers and progressions of LULC change has been key to developing models that can project and predict future LULC extent, level and patterns under different assumptions of socioeconomic, ecological and environmental situations. Figure 1.5 shows the regional to global scale social-ecological impacts of anthropogenic landscape associated with different aspects, which threatens ecosystems and biodiversity.

Thus, complexity of inland and coastal landscape degradation should be addressed using multidisciplinary methodology and conditions. Therefore, this dissertation aims to assess the impact of LULC associated with vegetation, temperature and wetland changes. To understand the relation among the landscape dynamics associated with anthropogenic activities at local to global level, we have selected thirty-three global study areas (Figure 1.5).

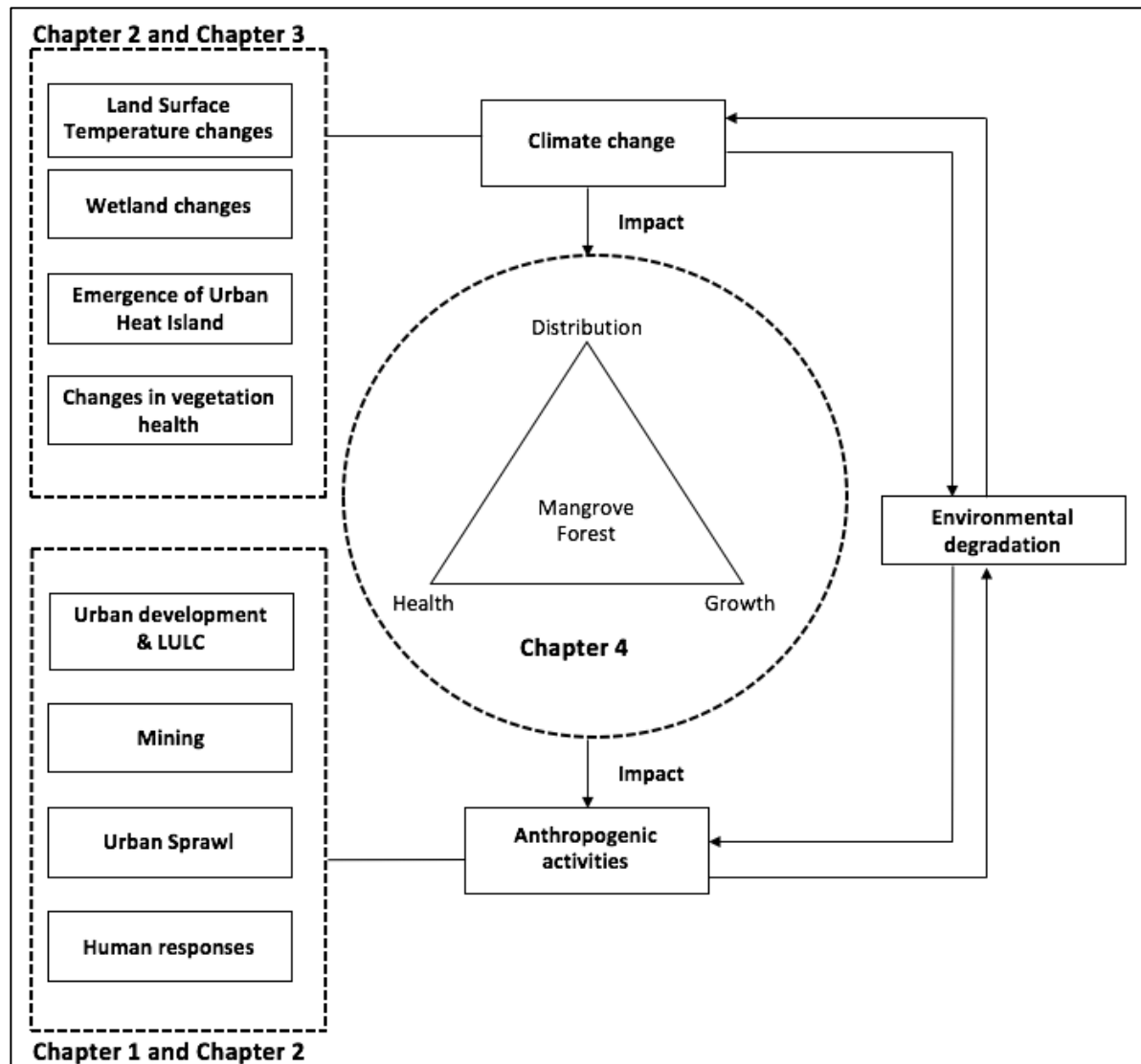


**Figure 1.5.** Regional to global scale social-ecological impacts of anthropogenic landscape associated with different aspects, which threats to ecosystem and biodiversity.

## 1.6 Research Hypotheses

Thus, it is fundamental to understand the connection between three different types of landscape changes: Urbanization, Geological changes and Forest degradation due to anthropogenic activities and climate changes. In order to understand the regional to global scale social-ecological impacts of anthropogenic landscape changes, this study used a RS approach. In this dissertation, there are four main motivating research questions (RQ):

**RQ1:** Can we estimate the extent and level, and model future extent and impact of urban growth and urban sprawl for congested fast growing urban landscape remotely?

**RQ2:** Do we quantify vegetation productivity dynamics and potential subsidence spots in the mining-influenced landscape by estimating the growth of wetlands?

**RQ3:** Do we identify the potential zones for Urban Heat Island emergence in fast growing sparse urban landscape associated with vegetation dynamics and Land Surface Temperature?

**RQ4:** How do the anthropogenic activities associated with environmental changes in different landscape drive global mangrove forest degradation?

### 1.7 Research objectives

The objectives of this dissertation are to understand the impact of different types of landscape changes: Urbanization, Geological changes and Forest degradation. We are interested in the quantification of regional to global scale social-ecological impacts of anthropogenic landscape changes by connecting the different aspects, which threats to ecosystem and biodiversity. Thus, four studies have been conducted using small and large scale dataset covering thirty-three global regions (Figure 1.6). The specific objectives are:

1. To quantify the changes in US extent, level and patterns using entropy and landscape metrics and predict the US extent and level using a land change model;
2. To examine LULC dynamics and identify the potential zones for UHI emergence using a SAVI-LST combined metric;
3. To examine the short-term LULC dynamics in the reclaimed mine area and quantify the emergence and growth of wetlands in the mining-influenced area and thus identify potential subsidence spots, i.e., spots exhibiting abrupt growth of waterbodies;
4. To examine the vegetation productivity dynamics as a surrogate of the ground water table fluctuation and ecological stress;
5. To identify the local and global drivers for degrading mangrove forest.



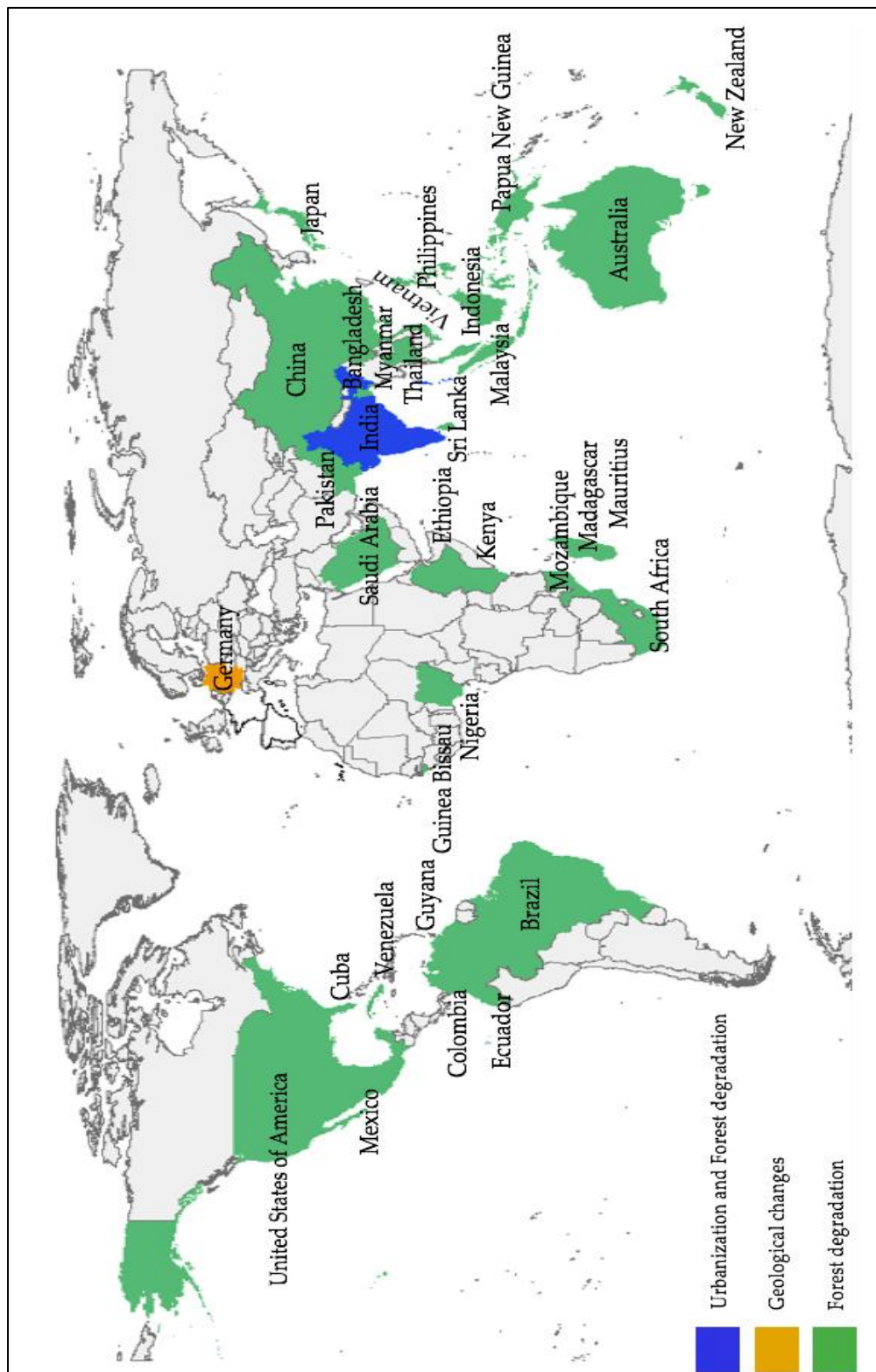


**Figure 1.6.** Thirty-Three global regions covered by the studies in this thesis to understand the impact of different types of landscape changes: Urbanization, Geological changes and Forest degradation.

## 1.8 Outline of the dissertation

We expect this dissertation will contribute to a better understanding of the impact and consequences of anthropogenic activities on different kinds of landscape changes: Urbanization, Geological changes and Forest degradation. Figure 1.7 shows the different topics covered in this dissertation. We developed four studies: an urban landscape dynamics associated with LULC and US in India, Asia context, a second identifying the consequences of mining associated with geological changes in Germany, Europe context, a third one relation between LULC and UHI emergence in growing towns, India circumstance and a fourth identifying the climatic and anthropogenic drivers caused mangrove degradation in global perspective.

**Chapter 1** presents a brief introduction and the motivation behind this dissertation, research hypothesis, research objective and methodology outline of the thesis.

**Chapter 2** addresses and quantifies the extent and level of US within a 10km suburban buffer of an Indian megacity, i.e., Chennai, Tamilnadu, using Landsat imageries from 1991, 2003 and 2016. We quantified: (1) the changes in US extent between 1991 and 2016; (2) the US level and patterns using entropy and landscape metrics; and (3) predicted the US extent and level for 2027 using a land change model.

**Chapter 3** identifies the subsidence zones and vegetation productivity degradation in a reclaimed mine area through the analyses of short-term landscape dynamics using RS and GIS techniques. We examined: (1) the short-term, i.e., during 4 years, LULC dynamics in the reclaimed mine area; (2) the emergence and growth of wetlands in the mining-influenced area and thus identify potential subsidence spots, i.e., spots exhibiting abrupt growth of waterbodies; (3) examine the vegetation productivity dynamics as a surrogate of the ground water table fluctuation and ecological stress.

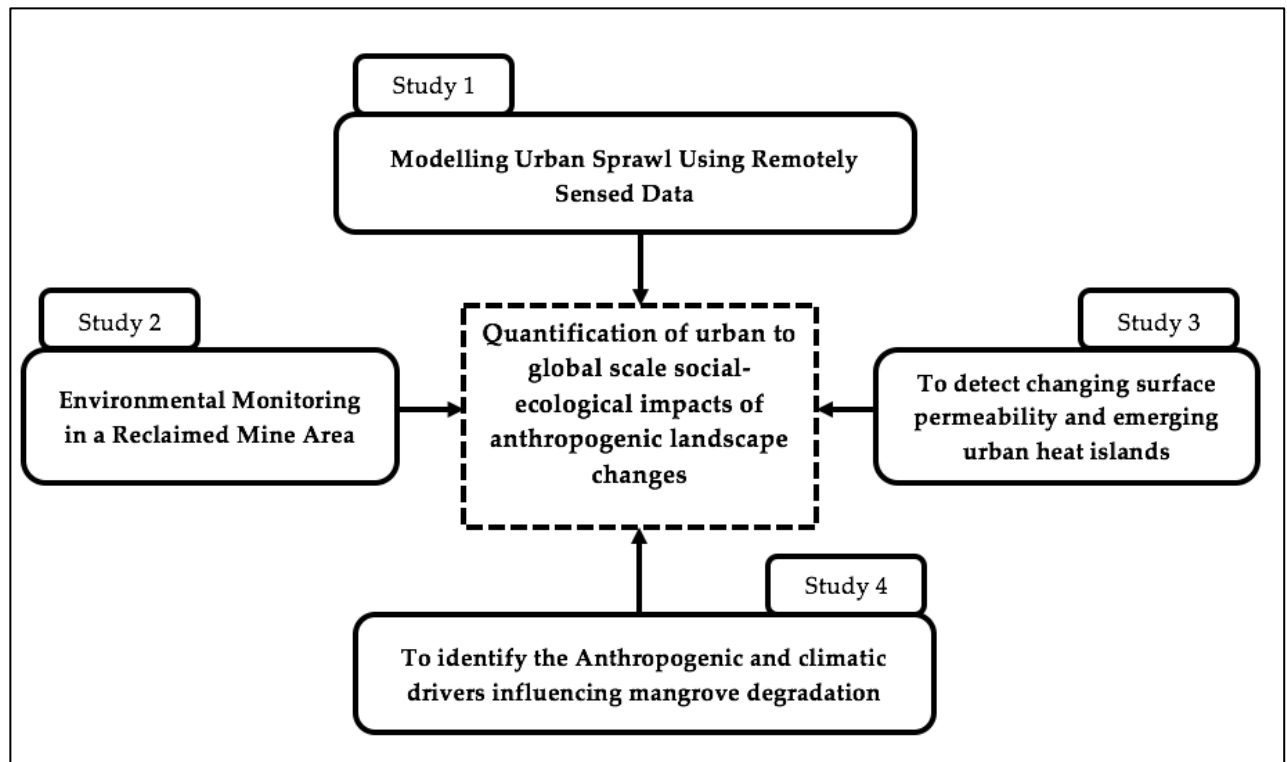


**Figure 1.7.** Different topics covered in this dissertation.

**Chapter 4** quantified the LULC, SAVI and LST changes, as well as the relationship between SAVI and LST changes, in a fast-growing city, i.e. Tirunelveli, Tamilnadu, India, during a 11 years period, i.e. between 2007 and 2017. We fused satellite imageries from two different sensors, i.e. IRS-LISSIII and Landsat-7 ETM+, to arrive at a combined high spatial resolution (23.5m of IRS P6-LISSIII) and high thermal band (30m of Landsat-7 ETM+) imageries for Tirunelveli. The objectives of our study are twofold: (1) To demonstrate the advantage of using fused imageries over non-fused single images through a comparison of image classification accuracies and (2) to identify the potential zones for UHI emergence using a SAVI-LST combined metric for Tirunelveli in 2017.

In **Chapter 5** we addressed up-to-date information on anthropogenic and environmental drivers of the mangrove degradation, and the causes of disturbance over its ecosystems. First we discussed the global spatial distribution and changes in the mangrove forest. Subsequently we discussed the different global and regional drivers on mangrove degradation.

**Chapter 6** presents the main research findings and conclusions corresponding to each research objective. The main contributions and innovation of methodical output of this

dissertation are deliberated followed by recommendations for future research to additional progress to the quantification of regional to global scale social-ecological impacts of anthropogenic landscape.

## 1.9 Research Methodology

The current dissertation is included in the GIS research body, and is centred on the landscape, wetland and vegetation spatial dynamics value literature. This study utilized RS spatial data to understand the local to global scale social-ecological impacts of anthropogenic landscapes (Figure 1.8). Since, RS techniques and GIS have shown clear advantages over conventional field monitoring and laboratory measurements for assessing long- to short-term landscape dynamics [15–17]. Particularly for large areas, where surveying using Global Positioning System (GPS), field surveying and ground levelling are time-consuming, expensive, and labor-intensive, RS and GIS provide prompt and efficient information on landscape changes, US and geological movement [4]. These techniques are also useful for detecting changes in vegetation productivity and cover and LST changes through LULC maps [17,18].

Multispectral satellite images allow for detecting gradual as well as abrupt changes in landscapes [19]. However, besides widespread application in monitoring general landscape dynamics, the application of RS and GIS in monitoring and assessing anthropogenic effects on landscapes and environment and in associated climate changes and vegetation productivity dynamics is limited [10–14,20]. Although high-resolution Light Amplification by Stimulated Emission of Radiation (LASER), Interferometric Synthetic Aperture Radar (InSAR), and Light Detection and Ranging (LIDAR) mapping have been sparsely applied in small areas, environmental impacts in large areas have rarely been investigated using RS and GIS techniques [21–27].

We used Landsat Thematic Mapper (TM) images with a 30m spatial resolution covering the temporal scenes from 1991 and Enhanced Thematic Mapper (ETM+) images with a 30m spatial resolution covering the temporal scenes from 2003, 2007, 2013, 2014, 2015, 2016 and 2017 and Indian Remote Sensing Satellite Resourcesat-1 - Linear Imaging Self-Scanning Sensor -3 (IRS LISS-III) images with 23.5 m spatial resolutions from June 2007 and June 2017.

In order to handle the huge volume of spatial data to delineate LULC classifications and other indices calculation, we have introduced R programming with geospatial data throughout this research. We have applied Random Forest (RF) and Rotation Forest (ROF) machine learning algorithm on the pre-processed TM and ETM+ images for several LULC classification to analyze landscape dynamics of different study area. We also presented Renyi's Entropy (RE) instead of common Shannon's entropy method to estimate the level, pattern and dynamics of US.

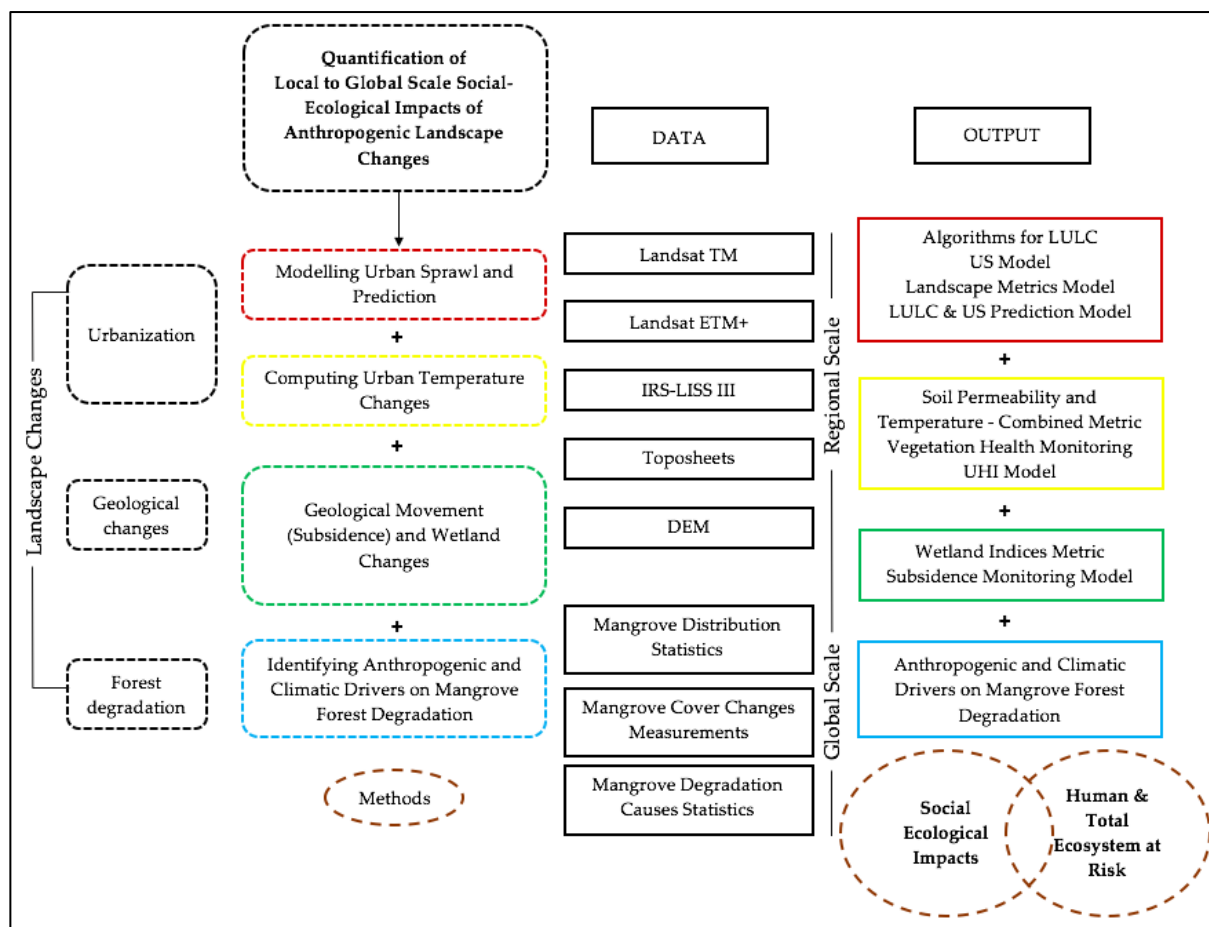


**Figure 1.8.** Schematic diagram of the work-flow of this dissertation

The practices of fused and non-fused imageries are not new; though they have rarely been compared for image classification accuracies in complex urban settings. Moreover, application of fused imageries for identifying UHIs in fast growing cities in developing countries is inadequate and scarce. So, we demonstrated the advantage of using fused imageries over non-fused single images through a comparison of image classification

accuracies and to understand the UHI emergence associated with SAVI-LST. The several Indices calculation such as Spectral Mixture Analysis (SMA), Soil-Adjusted Vegetation Index (SAVI), Normalized Difference Vegetation Index (NDVI) and Land Surface Temperature (LST) used in this research were obtained in the R environment. We also identified mangrove degradation drivers at regional and global levels resulted from decades of research data to understand the local to global scale social-ecological impacts of anthropogenic landscapes includes forest degradation (Figure 1.5).

### 1.10 Path of Research

This dissertation folds the findings of several research studies, reported in this dissertation separately by four chapters, including international journals and conferences with double blind review process, indexed in Institute for Scientific Information (IISI), Web of Science (WOS). The beginning of the research started at the NOVAIMS, Portugal, an initial literature review and proposal of a thesis framed here.

**The chapter 2**, Modelling Urban Sprawl Using Remotely Sensed Data was carried out with the help of delegates from the NOVA IMS – Universidade NOVA de Lisboa, Campus de Campolide, 1070-312, Lisbon, Portugal, Stockholm Resilience Centre, Stockholm University, Kraftriket 2B, SE-104 05 Stockholm, Sweden, Institute for Geoinformatics (IFGI), Westfälische Wilhelms-Universität, Heisenbergstraße 2, 48149 Münster, Germany, School of Humanities and Social Sciences, Nanyang Technological University, 14 Nanyang Drive Singapore 637332 and Tomsk State University, Lenin Avenue 36, 634050 Tomsk, Russia. The field survey and ground-truthing were carried out by visiting the study area during 2016-2017. Rajchandar Padmanaban (R.P.), and Dr. Pedro Cabral (P.C) have conceived the study. To maintain the high accuracy in classification, we employed third party to conduct accuracy assessment, thus Oraib Almegdadi (O.A.), and Wang Shunago (W.S) together with R.P conducted accuracy assessment and R.P conducted image processing and classification under the supervision of Avit.K.Bhowmik (A.K.B.), and P.C. R.P., and A.K.B. wrote the paper, P.C., Alexander Zamyatin (A.Z.), O.A., and W.S. revised the paper. The chapter 2 then published in the Entropy journal-ISSN 1099-4300 on 7<sup>th</sup> April, 2017. Entropy is an International and Peer-reviewed open access journal from Molecular Diversity Preservation International and



Multidisciplinary Digital Publishing (MDPI), Switzerland with an impact factor 2.305 (2017). The chapter later issued in the Stockholm Resilience Centre Newsletter as an article named “Swallowing valuable land - Rapid urban expansion leaves India mega city Chennai without essential ecosystem services” on May 10, 2017.

**The chapter 3**, A Remote Sensing approach to Environmental monitoring in a Reclaimed area was carried out during 2017 from NOVAIMS with the supervision of P.C and A.K.B. The field survey and ground-truthing carried out by visiting study area during 2017. R.P. and P.C. conceived the study. R.P. conducted image processing, classification accuracy assessment, and indices calculation under the supervision of A.K.B. and P.C. R.P. and A.K.B. wrote the paper, P.C. revised the paper. The chapter 3 was published in the International Journal of Geo-Information (IJG) - ISSN 2220-9964 on 8<sup>th</sup> December, 2017. IJG is an International and Peer-reviewed open access journal from the International Society for Photogrammetry and Remote Sensing (ISPRS), MDPI with an impact factor 1.723 (2017).

**The chapter 4**, Satellite image fusion to detect changing surface permeability and emerging urban heat islands in a fast-growing city was carried out during 2018 from NOVAIMS, with the supervision of P.C and A.K.B. The field survey and ground-truthing carried out by visiting the study area during 2018. R.P. and P.C. conceived the study. R.P. conducted image processing, fusion, classification, accuracy assessment, and indices calculation under the supervision of A.K.B. and P.C. R.P. and A.K.B. wrote the paper. A.K.B. and P.C. revised the paper. The chapter 4 was then published in Public Library of Science one (PLOSone) journal on January, 2019. PLOSone is a multidisciplinary open access journal from the Public Library of Science, United States with an impact factor 2.766 (2017). The chapter later issued in the Hindu Newsletter, a national daily in India as an article named “Urbanization of Tirunelveli city might warm it up” on January 20, 2019. The following chapter later published in the Stockholm Resilience Centre Newsletter as an article named “Hot in the City” on February 1, 2019.

**The chapter 5**, What drives mangrove degradation? was carried out during 2018 from NOVAIMS with the supervision of P.C and A.K.B. R.P. wrote the paper. A.K.B. and P.C.

revised the paper. The paper was presented in the National conference on Recent Innovations in Engineering, Science and Management (RJEM) 2018 sponsored by Indian Space Research Organization and organized by Department of Civil Engineering, Dr. N.G.P Institute of Technology, Coimbatore on September 28, 2018.



The background of the page features a series of horizontal bars of varying lengths and colors, including grey and lime green, arranged in a stepped, staircase-like pattern on the right side.

## Chapter – 2

### Modelling Urban Sprawl Using Remotely Sensed Data

*“Will urban sprawl spread so far that most people lose all touch with nature? Will the day come when the only bird a typical American child ever sees is a canary in a pet shop window? When the only wild animal he knows is a rat – glimpsed on a night drive through some city slum? When the only tree he touches is the cleverly fabricated plastic evergreen that shades his gifts on Christmas morning”.*

***Frank N. Ikard***

## Chapter 2

# Modelling Urban Sprawl Using Remotely Sensed Data

---

### 2.1 Introduction

A rapid global increase in human population has triggered the migration of rural poor towards the cities for a better standard of living, education and income [115]. By 2030 the world's population is expected to increase by 72% with a 175% upsurge in urban areas (>100,000 inhabitants) [126]. The migrant rural poor often encroach the cheap suburban peripheries [61,127] and, consequently, the cities expand to accommodate immigrants as well as to create employments by intensification of industries [61]. This eventually leads to urban sprawl (US) and the uneven development, through the conversion of suburban lands to built-up settlements [33].

US entails adverse impacts on ecosystem services by diminishing agricultural lands, water bodies and forests [128]. US has also been associated with increasing risks from environmental externalities, such as energy crisis, biodiversity loss and floods [109]. Particularly, in developing countries like India, where 60% of the total population (approximately 70 million) are predicted to live in urban areas by 2030, US may entail disastrous impacts on ecosystem and biodiversity [16]. The quantification of the extent and level of US are thus essential for Indian cities to support sustainable planning, policies and efficient design of cities [42]. However, with a few exceptions, such studies are scarce for India [21,78,113,129–131].

Globally, remote sensing imageries and techniques showed considerable potentials for urban growth and US analysis [21,78,129–131]. Landuse and landcover classes (LULC) are important indicators for understanding the connections between environment and human activities [57,111], which can be efficiently obtained from satellite imageries through image classification. These are particularly useful for countries like India, where ground monitoring data are scarce and inaccessible [111]. Moreover, the availability of remotely sensed data from multiple dates enables to carry out studies on multitemporal urban modeling [57,101,111,132–

138]. The extent of urban areas can be automatically identified from satellite imagery using machine learning algorithms [139]. Change detection analysis can be carried out through the use of transition matrices, which measure the changes between two LULC maps from different periods of time. They, in turn, help to quantify the extent of US through the differences between urban extent across multiple temporal periods [57]. In addition, the spatial and physical characteristics of urban features, urban patterns and their forms may be quantified using several landscape metrics [135]. These metrics can be derived from thematic maps computed from remotely sensed data [136]. Furthermore, Entropy values, includes Shannon's Entropy, which are widely used to characterize and identify the degree of spatial dispersion and concentration of urban areas [22,140–146], can also be computed from remotely sensed images and effectively used to quantify the level of US [143].

In this study, we quantified the extent and level of US within a 10 km suburban buffer of an Indian megacity, i.e., Chennai, Tamilnadu, using Landsat imageries from 1991, 2003 and 2016. We quantified: (1) the changes in US extent between 1991 and 2016; (2) the US level and patterns using entropy and landscape metrics; and (3) predicted the US extent and level for 2027 using a land change model.

## 2.2 Study Area

Chennai is the capital city of Tamilnadu state, India, and the gateway of south India (Figure 2.1). The geographical location of Chennai spans between 13.04° N 80.17° E with an elevation between 6 m and 60 m above the mean sea level. It covers an area of about 42,600 ha [137]. This is India's fourth largest city, with a total population of 8,233,084 according to the 2011 India census [137], which has doubled during in the last two decades [131]. Chennai is also one of the principal business hubs of India with an unprecedented expansion of industries and infrastructures [147]. With several United Nations Educational, Scientific and Cultural Organization <sup>9</sup>(UNESCO) world heritage sites, Chennai is one of the main tourist hubs [131].

---

<sup>9</sup>UNESCO – UNESCO is an International collaboration agency of the United Nations <sup>10</sup>(UN) based in Place de Fontenoy, Paris, purpose is to contribute to security and peace by through scientific, educational, and cultural reforms in order to spread world-wide respect for the rule of law, human rights, and justice [148].

The suburban periphery of the city represents a unique biodiversity hotspot. The coastal area (Marina beach) at the East represents a unique mangrove ecosystem [149], whereas the dense forest at the West represents a rare composition of tropical flora and fauna [150].

The city of Chennai is one of the fastest growing urban areas in the world during the last three decades [131]. This has resulted in an uncontrolled US with negative consequences regarding air pollution, housing scarcity, overcrowding, encroachment, slums, unregulated disposal of waste, increasing water scarcity and pollution [151]. The US has also lead to various adverse environmental impacts, such as higher energy exploitations, disturbance of species diversity, increasing flood risk, and ecosystem fragmentation [152].

The spatial trend of US in Chennai is towards two peripheral districts, i.e., Tiruvallur (Northwest Chennai) and Kanchipuram (Southwest Chennai) [21]. Consequently, we selected an area constituting 82,488.16 ha, which covers the geographic extent of the Chennai city and a 10 km suburban buffer, i.e., Tiruvallur and Kanchipuram districts, to study US.

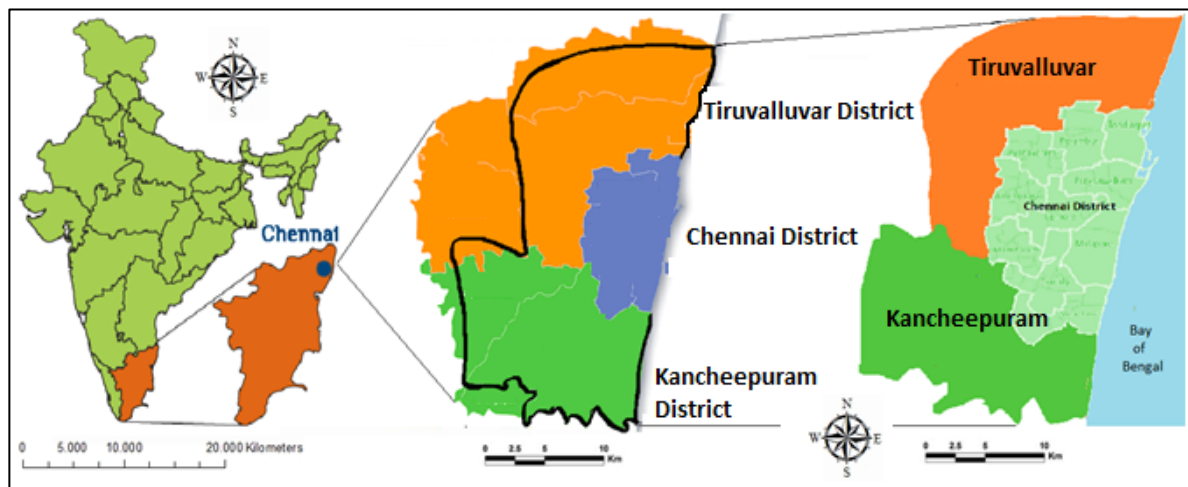


**Figure 2.1.** The study area covering Chennai city and 10 km sub-urban buffer.

<sup>10</sup>**United Nation (UN)** – UN is an intergovernmental organization located at Manhattan, New York, United States of America purpose to uphold intercontinental amity, security and well-being among nations, accomplish world-wide cooperation and be a centre for harmonizing the action of nations [148].

## 2.3 Materials and Methods

### 2.3.1 Data and Pre-Processing

We used Landsat Thematic Mapper <sup>11</sup>(TM) and Enhanced Thematic Mapper plus <sup>12</sup>(ETM+) images with a 30-m spatial resolution covering the temporal scenes from 1991, 2003, and 2016 (Table 2.1). The images were freely downloaded from the United States Geological Survey <sup>13</sup>(USGS) portal [153] in <sup>14</sup>GeoTIFF format and georeferenced using the World Geodetic System <sup>15</sup>(WGS) 1984 coordinate reference system. The data were initially geo-corrected and rectified, and cropped to the study area (Figure 2.1). The image pre-processing was performed using ENvironment for Visualizing Images <sup>16</sup>(ENVI) software package (5.1) [154,155].

**Table 2.1.** A technical description of the Landsat TM and ETM+ imageries used in this study.

Date	Sensor	Path/Row
25 August 1991	Landsat-5 TM	142/51
9 May 2003	Landsat-7 ETM+	142/51
4 July 2016	Landsat-7 ETM+	142/51

### 2.3.2 Landuse and Landcover (LULC) Mapping, and Accuracy Assessment

We applied a Random Forest (RF) machine learning algorithm on the pre-processed TM and ETM+ images for LULC classification [156] (Figure 2.2). The RF algorithm in <sup>17</sup>R involves the following steps:

---

<sup>11</sup>**Thematic Mapper (TM)** – The Thematic Mapper is a progressive, multispectral scanning, Earth resources satellite sensor designed to attain higher spatial resolution, sharper spectral separation, enhanced geometric fidelity and greater radiometric accuracy in satellite images [157].

<sup>12</sup>**Enhanced Thematic Mapper Plus (ETM+)** – The Enhanced Thematic Mapper Plus (ETM+) is multispectral scanning radiometer capable of providing high-resolution imaging information of the Earth's surface. It detects spectrally-filtered radiation in the visible and near-infrared (VNIR), Short-wavelength infrared (SWIR), Long-wavelength Infrared (LWIR) and panchromatic bands (Black and White) [157].

1. Create the stack for the available raster data;
2. Create n-tree bootstrap samples from the raster data;
3. Apply an unpruned classification grown for each of the bootstrap samples according to the Digital Number <sup>18</sup>(DN) values of the raster data;
4. Create N number of polygons according to the DN raster values;
5. Assign different color bands to the several classes;
6. Display the unsupervised classification.

In a next step, the spatially-cohesive features of the classified images were homogenized using a segmentation algorithm and the regions with the maximum homogeneity were delineated [20]. The regions with five distinct LULC classes (Table 2.2) were delineated for 1991, 2003 and 2016 by providing the minimum and maximum threshold values of pixels obtained from the RF, and the population thresholds for pixels corresponding to a LULC class [101]. We used the RF package in R for the classifications of LULC [158]. The classified image homogenization and delineation of LULC regions were performed using the ENVI (5.1) feature extraction tool [60,155].

**Table 2.2.** Landuse and landcover (LULC) nomenclature.

No	LULC Classes	Land Uses Included in the Class
1	Water bodies	Rivers, reservoir, lakes, streams, open water, and ponds
2	Urban	Roads, airports, and built-up areas
3	Agriculture	Agriculture lands and plantations
4	Bare land	Dry lands, non-irrigated lands, ready for construction, and real estate plots
5	Vegetation	Forests and shrubs

<sup>13</sup>**United States Geological Survey (USGS)** – USGS is a fact-finding scientific organization of the Federal Government of the United states has four main science disciplines concerning geology, hydrology, biology and geography. USGS researchers publish their work and make the data available from the different satellite and airborne sensors in the web portal (<https://earthexplorer.usgs.gov/>) [159].

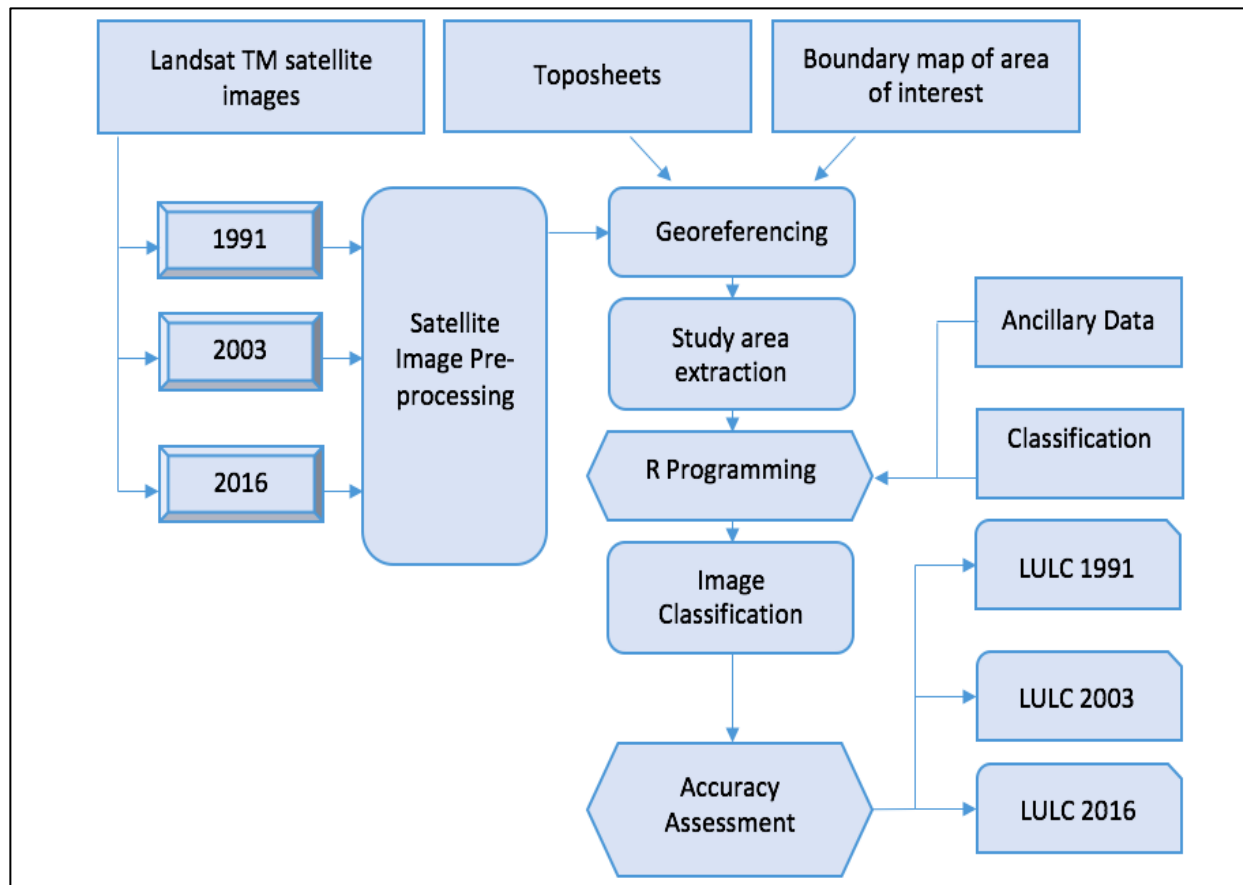


**Figure 2.2.** Flow-chart for image processing, classification and accuracy assessment.

The accuracy of the image classification was assessed using the kappa coefficient <sup>19</sup>(KC) [143,145]. We compared the classified images with the ground truth data obtained from <sup>20</sup>Google-Earth image of 2016 and the landuse and landcover map of 2005 from the Indian Geo-platform of Indian Space Research Organization <sup>21</sup>(ISRO) - <sup>22</sup>Bhuvan (<http://bhuvan.nrsc.gov.in>) [21]. Subsequently, a <sup>23</sup>confusion-matrix and KC were calculated using <sup>24</sup>eCognition-Developer (8.7) for each of the classified images of the three years [160].

<sup>14</sup>**GeoTIFF** – GeoTIFF is one of the image format public domain metadata (a set of data that defines and gives info about other data) standard which allows georeferencing (Georeferencing is the procedure of assigning real-world coordinates to each pixel of the raster) information to be embedded within a TIFF (Image) file [161].

<sup>15</sup>**World Geodetic System (WGS)** – World Geodetic System a reference frame for the earth for use in geodesy and navigation. It includes a standard coordinate system for the world [162].

<sup>16</sup>**ENvironment for Visualizing Images (ENVI)** – ENVI is image analysis software tool is used by remote sensing scientists, GIS specialists, and image analysts to obtain meaningful information from satellite or aerial imagery to make better decisions [163].



### 2.3.3 Quantification of Extent and Level of Urban Sprawl (US)

#### 2.3.3.1 Extent of US

We calculated six landscape metrics to quantify the extent of US between 1991 and 2027 in the Chennai city (see Table 2.3 for details on the landscape metrics) [160]. These metrics quantify the spatial characteristics and pattern of the classified LULC areas using three levels, i.e., the patch level, class-area level and landscape level. The landscape metrics were computed in the freely available <sup>25</sup>FRAGSTATS software package (4.2) [164].

**Table 2.3.** Description and formulae for spatial metrics computation.

Landscape Metrics	Formula	Description	Range
Class Area Metrics (CA)	$CA = \sum_{j=1}^n a_{ij} \left( \frac{1}{10000} \right)$ $a_{ij} = \text{area in m}^2 \text{ of patch } ij.$	Total amount of class area in the landscape	CA > 0, without limit
Number of Patches (NP)	$NP = n_i$ $n_i = \text{total number of patches in the area of patch type } i \text{ (class).}$	Number of patches of landscape classes (Built up and non-built-up)	NP ≥ 1, without limit
Largest patch Index (LPI)	$LPI = \frac{\max_{j=1}^n (a_{ji})}{A} (100)$ $a_{ij} = \text{area in m}^2 \text{ of patch } ij \text{ and } A = \text{landscape area in total (m}^2\text{)}$	Percentage of the landscape included by the largest patch	0 < LPI ≤ 100
Clumpiness Index (CLUMPY)	$Clumpy = [(G_i - P_i) / P_i \text{ for } G_i < P_i \& P_i < 5, \text{ else } G_i - P_i / 1 - P_i]$ $g_{ii} = \text{number of like joins among pixels of patch type, } i \text{ based double-count process and } g_{ik} = \text{number of like joins among pixels of patch type, } k \text{ based double-count process, } P_i =$	Measure the clumpiness of patches in urban areas	-1 ≤ CLUMPY ≤ 1

	amount of the landscape occupied by patch type		
Fractal Index Distribution (FRAC_A)	$AM = \sum_{j=1}^n [x_{ij} (a_{ij} / \sum_{j=1}^n a_{ij})]$ <p><math>a_{ij}</math> = area in m<sup>2</sup> of patch <math>ij</math>.</p>	To measure area weighted mean patch fractal dimension	$1 \leq FRAC\_AM \leq 2$
Contagion	<p><i>Contag</i></p> $= [1 + \sum_{i=1}^m \sum_{k=1}^m [(p_i) \{g_{ik} / \sum_{k=1}^m g_{ik} \} \{ \ln(p_i) [g_{ik} / \sum_{k=1}^m g_{ik} ] / 2 \ln(m) \}] 100]$ <p><math>p_i</math> = amount of the landscape employed by patch type (<math>i</math>) class and <math>g_{ik}</math> = number of like joins among pixels of patch type, <math>i</math> and <math>k</math> based double-count process, <math>m</math> = number of patch classes (types) existing in the landscape</p>	Defines the heterogeneity of a landscape	Percent < <i>Contagion</i> ≤ 100

### 2.3.3.2 Level of US

Renyi's Entropy (RE) [165,166] was calculated to estimate the level of US between 1991 and 2016. First, we aggregated the classified LULC map into two classes, i.e., built-up and non-built-up. Then, the total number of patches ( $N$ ) for the built-up and non-built-up areas and their corresponding perimeters ( $P_i$ ) were computed. Finally, a  $H$  order entropy value  $H$  as calculated using (1), where  $\alpha \geq 0$  and  $\alpha \neq 0$ :

$$H_\alpha = \frac{1}{1-\alpha} \ln \sum_{i=1}^N P_i^\alpha \quad (1)$$

The RE values ( $H_\alpha$ ) varied from 0 (indicating very dense distribution of aggregated classes) to 1 (indicating dispersed distribution across the study area) [166]. The changes in RE values for the built-up patches during three decades, i.e., 1991–2016, represented the change in the US level (i.e., dispersion of urban areas) for the Chennai city, Tamilnadu.

### 2.3.4 Prediction of Urban Extent for 2027

The prediction of future urban extent was performed using the Land Change Modeler available in the <sup>26</sup>TerrSet (formerly IDRISI) software (18.3) [103]. The land change model was calibrated to predict the extent of Chennai for 2016 using a four-step procedure: (1) quantification of urban change between 1991 and 2003; (2) transition modelling between 1991 and 2003; (3) urban extent prediction for 2016; and (4) validation using the classified LULC for 2016 as reference data (Figure 2.3).

---

<sup>17</sup>**R** – R is a programming language and free software environment for statistical computing and graphics supported by the R Foundation for Statistical Computing. The R language is widely used among statisticians and spatial and non-spatial data miners for developing statistical software, spatial model, forecasting and data analysis [167].

<sup>18</sup>**Digital number (DN)** – Digital number in remote sensing arrangements, a variable assigned to a pixel, regularly in the form of a binary integer in the range of 0–255 (i.e. a byte). A single pixel may have several digital number variables corresponding to different bands recorded in the satellite or airborne images [168].

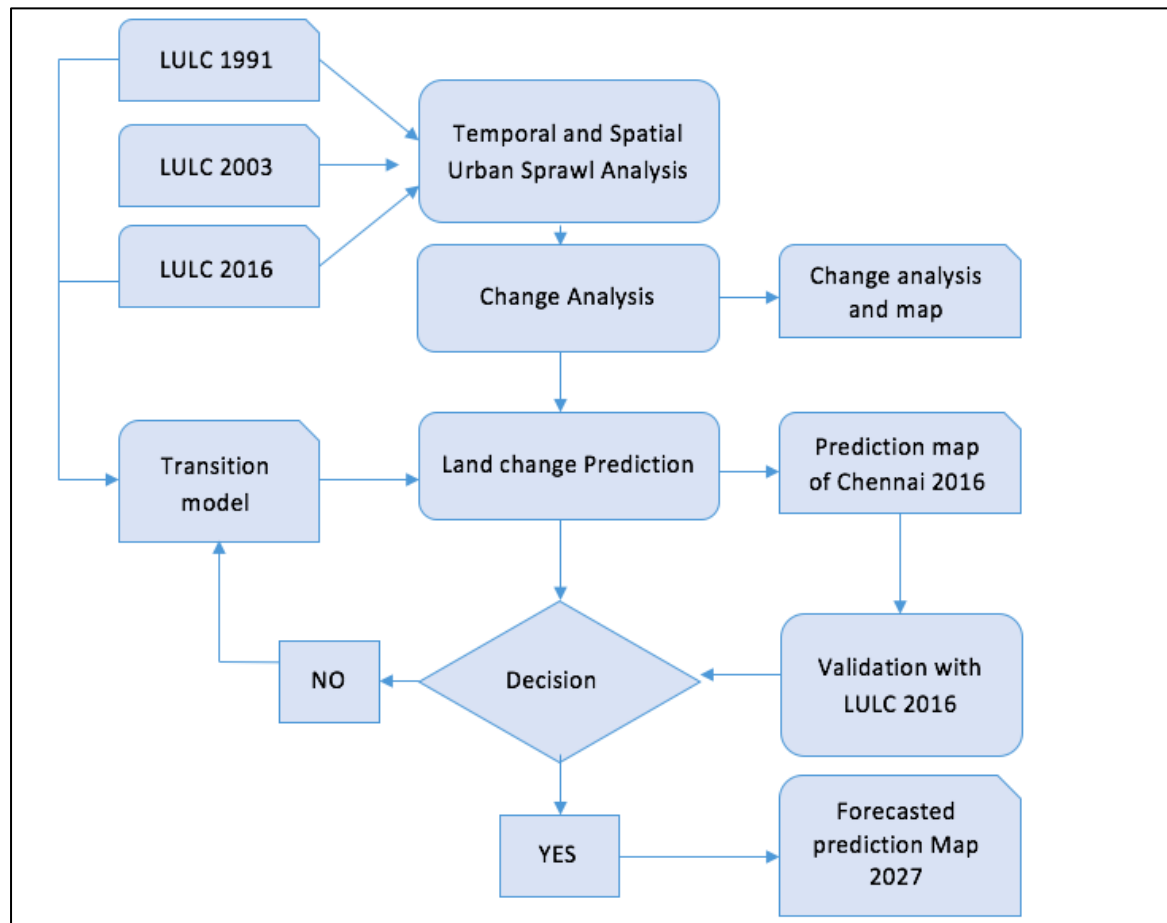


**Figure 2.3.** Methodology applied for the prediction of urban sprawl extent and level for 2027.

LULC change analysis was conducted using the LULC maps for 1991 and 2003 as primary inputs [103]. The land changes between 1991 and 2003 were quantified and the losses and gains among the LULC classes were obtained.

<sup>19</sup>**Kappa coefficient** - Kappa coefficient in Remote Sensing is frequently used to test interrater reliability (accuracy) of two or more raster data set [169].

<sup>20</sup>**Google Earth** – Google earth is a digital application that renders a 3Dimension (3D) representation of Earth based on satellite imagery[170].

<sup>21</sup>**Indian Space Research Organisation (ISRO)** – The Indian Space Research Organisation is the space agency of the Government of India mission of bringing space to the service of the common man, to the service of the Nation. ISRO provides various applications and services: broadcasting, weather forecasting, communications, disaster management, and navigation [171].

Then, a change map between 1991 and 2003 using a multilayer perception neural network algorithm was computed. This included constraints and factors used in the urban extent prediction. Next, a change map was generated for the period 2003–2016 using the computed changes between 1991 and 2003. Subsequently, a change probability grid for the 2003–2016 period was obtained. In a final step, we calibrated the urban extent prediction model (UEPM) using a Markov Chain, which combined the change map with a change probability grid for the period 2003–2016.

The urban extent of Chennai was predicted for 2016 applying the UEPM. The predicted urban extent was compared with observed LULC map for 2016 using Kappa variations, i.e.,  $K_{location}$  and  $K_{quantity}$  [172–176]. If acceptable values for these kappa variations are obtained, then we proceed to 2027 simulation [177]. The calibrated and validated UEPM was applied to predict the urban extent of Chennai for 2027 using the urban extent for 2016 as baseline and combining the change map and change probability grid between 2016 and 2027 computed using the procedure described above. The year 2027 was selected for our prediction because we wanted to use a 10-year horizon for this study. The transition probabilities used in the modeling process were obtained using the period 1991–2003 which is very similar to the period from 2016–2027 used in the prediction.

---

<sup>22</sup>**Bhuvan** – Bhuvan, is a web mapping service provided by ISRO which permits researches and students to explore a 2 Dimension (2D) and 3 Dimension (3D) representation of the surface of the Earth. It also provides free satellite data, Landuse and Landcover map of India, climate and environment data products, disaster management support and services, ocean services and online map creation platform [178].

<sup>23</sup>**Confusion matrix** – Confusion matrix is a table that is regularly used to define the performance of a classification model (LULC) on a set of test data for which the true values are known [179].

<sup>24</sup>**eCognition Developer** – eCognition is the image analysis software tool used in the geology, geography and earth science discipline to develop rules sets for the programmed and automatic analysis of remote sensing data [180].

## 2.4 Results and Discussion

### 2.4.1 The Extent and Patterns of US between 1991 and 2016

The LULC maps of three different periods show that the study area has experienced a remarkable land cover change between 1991 and 2016 (Figure 2.4). From 1991 to 2016 the growth of urban, i.e., built-up, areas were more than three-fold, i.e., an increase of about 37,919.81 ha (Table 2.4). This transformation influenced several classes, especially the agriculture and vegetation land, which decreased by about 3802.70 ha (4.61%) and 9923.32 ha (12.03%), respectively.

The bare land exhibited the highest amount of decrease, i.e., 30.3% and thus indicate that the growth of urban areas were accommodated mostly by diminishing bare lands. The water bodies increased by 1451.79 ha between 1991 and 2003, but decreased slightly between 2003 and 2016 (about 651.65 ha).

These results confirm that the urban areas in Chennai are extending toward the peripheral region of Kanchipuram (South Chennai) and to the Thiruvalluvar (North Chennai) district area, and thus a substantial US. Although, the US was mostly accommodated by the loss of bare lands, this growth has greatly impacted the landscapes with the loss of valuable vegetation and agriculture lands.

---

<sup>25</sup>**FRAGSTATS** – FRAGSTATS is a computer software program designed to compute a wide variety of landscape metrics for categorical map patterns [164].

<sup>26</sup>**TerrSet** – TerrSet (formerly IDRISI) is an incorporated remote sensing and geographic information system (GIS) software developed by Clark Labs at Clark University for the investigation and presentation of digital geospatial information for efficient and responsible decision making for equitable resource allocation, sustainable resource development and environmental management [181].

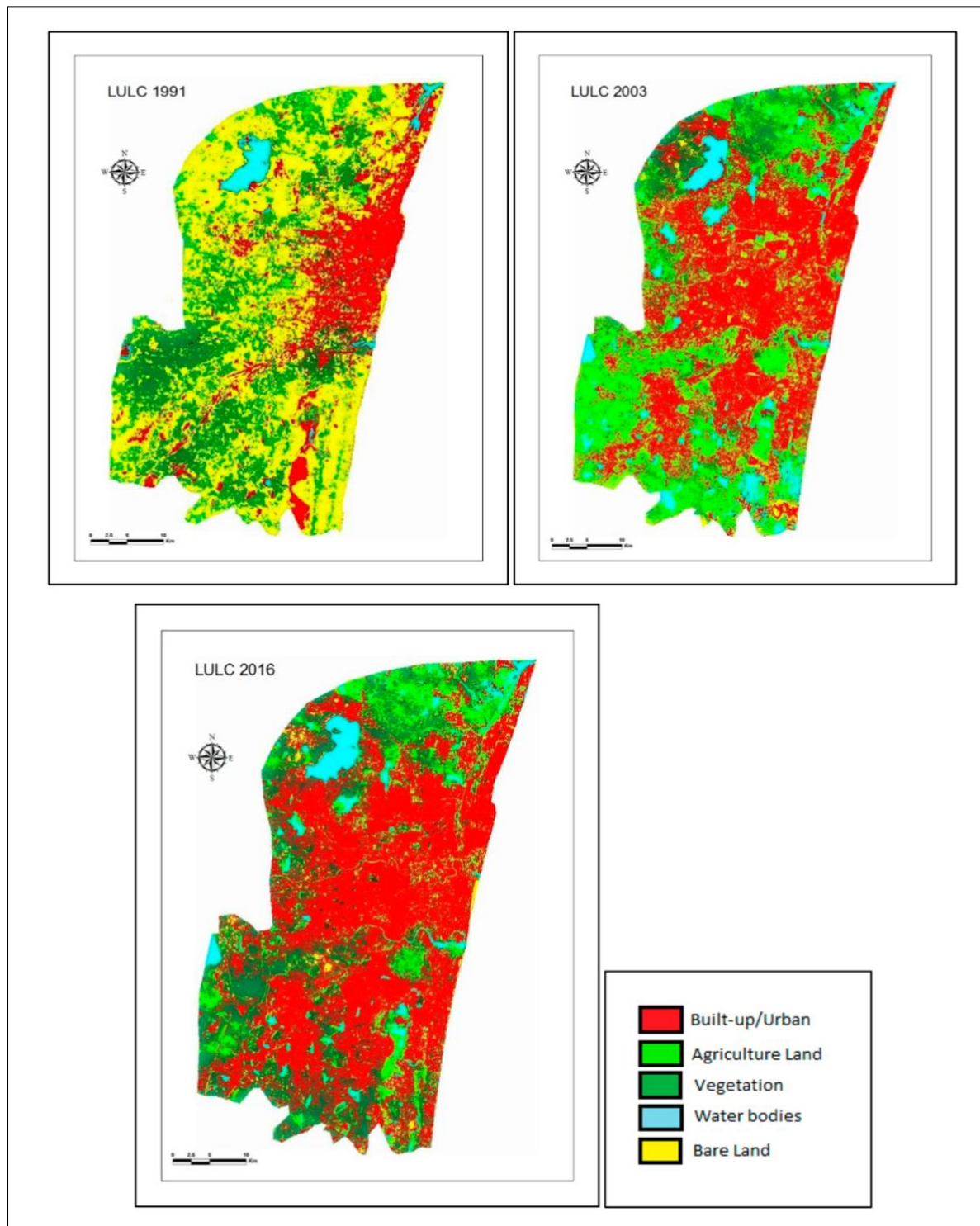


**Figure 2.4.** Landuse and landcover (LULC) maps for 1991, 2003, and 2016 in Chennai.

**Table 2.4.** Landscape indices, entropy values and their changes in percent.

Metrics	Year			Changes in Urban Structure		
	1991	2003	2016	$\Delta\% = 1991-2003$	$\Delta\% = 2003-2016$	$\Delta\% = 1991-2016$
CA	20,110.6	39,965.5	58,030.4	98.72	45.20	188.5
	1	1	2			
NP	289	354	477	22.49	34.74	65
LPI	2.14	4.87	6.78	127.57	39.21	216.8
Clumpy	-1	0.6	0.8	160	33.33	180
FRAC_A						
M	1.12	1.27	1.83	13.39	44.09	63.3
CONTAG	72.32	68.43	71.24	6.66	4.10	1.4
Renyi's	0.4	0.5	0.9	24.9	80	125

The Chennai coastline has also experienced a remarkable urban growth between 1991 and 2016 (Figure 2.4). Almost all the coastline of the study region was covered by urban settlements by 2016 by an alarming rate of conversion of the mangrove forest area (Figure 2.4). These results are in line with [182,183], which demonstrated negatively impacted mangrove forests and the Savukku plantations in the periphery of Chennai. This vegetation provides important ecosystem services, such as protection from Tsunami, cyclones, and other ecological disasters [77]. As a result, we anticipate environmental externalities and biodiversity loss for Chennai, such as habitat loss for native species including the Great Indian Horned Owl, spotted deer, mongooses, bonnet monkeys, and golden jackals [151].

Additionally, the degradation of forest may lead to an increase in city temperature and air pollution levels [120,184], e.g., recent studies have revealed Chennai as one of the highly air polluted cities in India [185].

The obtained KC for the LULC maps of 1991, 2003, and 2016 were 0.92, 0.97, and 0.92, respectively. These values indicate a high accuracy level for landuse and landcover classification [39,101].



The landscape metrics indicate that the urban class area (CA) has increased by 98.72% and 45.20% between 1991 and 2003, and 2003 and 2016, respectively (Table 2.4). The NP for urban settlements has shown an associated increase of 22.49% and 37.74% between 1991 and 2003 and 2003 and 2016, respectively. These values indicate a high level of land fragmentation.

The LPI increased by 127% between 1991 and 2003. This high value due to the large urban patches indicates a compact urban growth for the centre, but fragmented and dispersed urban growth in the fringe areas, i.e., US. LPI continued to increase from 2003 to 2016 (39.21%), confirming the continuation of US process for Chennai.

The CLUMPY in 1991 was -1, showing a maximally disaggregated urban patch. However, these values were 0.6 and 0.8 in 2003 and 2016, respectively, indicating an aggregation or clumpiness of urban patches. Likewise, FRAC\_AM increased between 1991 and 2003 as a result of contained urban growth with reasonable shape complexity (the values for this metric were marginally greater than 1). Nevertheless, the FRAC\_AM value between 2003 and 2016 was 1.83 (increased by 44.09%), indicating that the landscape had a higher range of urban growth and more dispersed urban sprawl than the 1991–2003 period. The decrease in the CONTAG value between 1991 and 2003 indicates a high fragmentation of the landscape. However, this value increased slightly between 2003 and 2016 (4.10%) showing that the fragmented urban area has become denser than the 1991–2003 period.

### ***2.4.2 Change in US Level***

The Renyi's entropy value for the Chennai was 0.4 in 1991, indicating rather moderately aggregated urban settlements, i.e., negligible US level. However, in 2003 the entropy value reached the threshold value of 0.5, indicating the initiation of dispersion, i.e., US, in Chennai [143,174]. In 2016, the entropy value was 0.9, which indicates a very high level of US in the periphery of Chennai. This high level of US in 2016 may directly relate to the haphazard encroachment of the urban fringe. This, in further, relates to the rapid population growth and land scarcity in the city centre, which were claimed to be the major reasons behind the US in the peripheral districts of Chennai [128].

The high level of US adds strain to urban infrastructure, such as sewage water disposal and waste management, and directly lead to urban water and soil pollution [78]. Recent studies showed that the threat of pollution of the Cooum river [78] and the coastal zones in Chennai have been increased towards 2016 due to the uncontrolled discharge of untreated sewage wastes from domestic and commercial activities, which may be linked to the high level of US observed in our study [146]. Moreover, the high level of US hampers waste management, e.g., 0.71 kg of daily garbage per capita in Chennai are currently incinerated at Perungudi and Kodungaiyu dump yards [146]. This creates severe soil and air pollution, and causes several health hazards, including respiratory disorders and cancers, for the city residents [147].

### ***2.4.3 US Extent and Level Prediction for 2027***

The obtained  $K_{location}$  and  $K_{quantity}$  for comparison between the modelled and classified LULC for 2016 were 84% and 81%, respectively. These values indicate a high level of accuracy for the calibrated UEPM for urban extent prediction for 2016 in Chennai [22,175,176,186].

The predicted LULC for 2027 is shown in Figure 2.5. It shows an increase in the projected urban area of 12,805.58 ha (22.06%) from 2016 (Table 2.5). The vegetation and agriculture classes are predicted to decrease to 3961.66 ha (66.29%) and 701.35 ha (87.44%), respectively. This is associated with a transition of 4883.09 ha agricultural lands and 7792.9 ha vegetation areas to urban areas, between 2016 and 2027 (Figure 2.6 and Table 2.5). The increase of bare land i.e., 1570.12 ha (57.31%) will occur as a consequence of the transitions from vegetation, water bodies, and agriculture land (Table 2.5). Thus, the bare land will increase at the expense of vegetation and agricultural lands and will potentially lead to the loss of important ecosystem services.

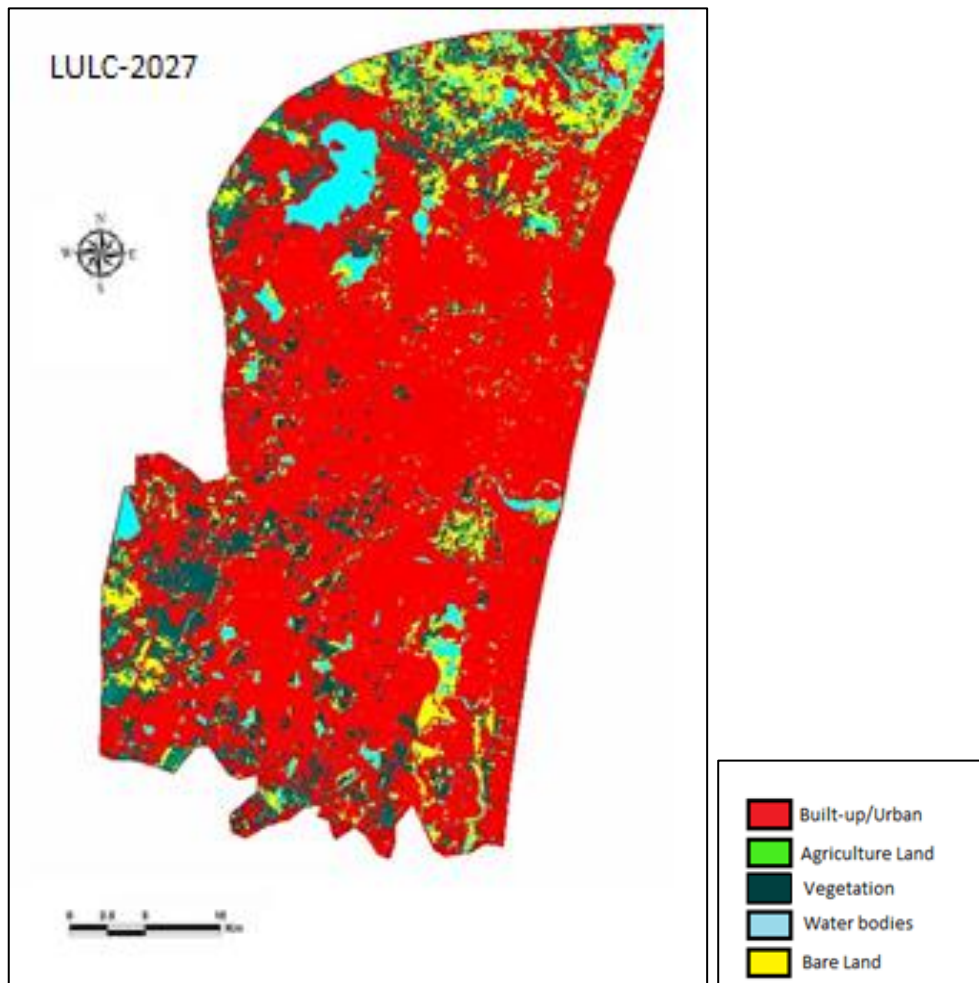


**Figure 2.5.** Simulated LULC map for the year 2027.

**Table 2.5.** Comparison of the LULC areas of three study periods, i.e., 1991, 2003 and 2016, with the predicted LULC areas of Chennai for 2027.

Land-Use Class	1991	2003	2016	2027	Forecasted LULC in	
					2027	
					ha	%
Built-up/urban	20,110.61	39,965.51	58,030.42	70,836.76	12,805.58	22.06
Agriculture	9387.15	22,857.47	5584.44	701.35	-4883.09	-87.44
Vegetation	21,677.89	9296.41	11,754.56	3961.66	-7792.9	-66.29
Water bodies	5320.48	6772.27	6120.62	5420.62	-700	-11.43
Bare land	25,992.02	3596.48	998.10	1570.12	572.02	57.31
Total	82,488.16	82,488.16	82,488.16	82,488.16	-	-

The urban areas covered 70.35% of the total landscape in 2016, which is predicted to increase to 85.87% in 2027 (Figure 2.6). The Renyi's entropy value of the predicted urban area in 2027 is expected to be 1.7, which is above the range value of 1 [143], indicating a tremendous level of US. Overall, the extent and level of US for the coming 12 years is expected to increase at an alarming rate and cause degradation of urban ecosystem services.

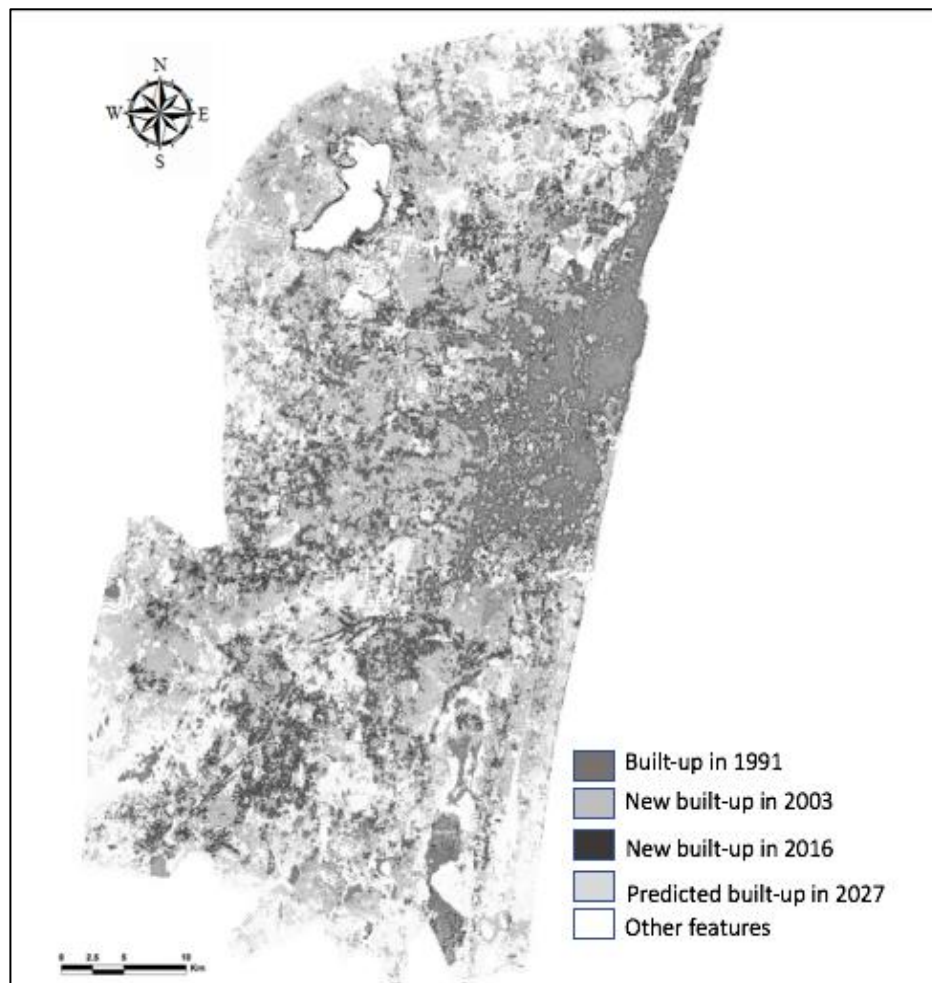


**Figure 2.6.** Urban sprawl, i.e., changes in urban extents between 1991–2027.

## 2.5 Concluding Remarks

We found fragmented urban growth in the outskirts of Chennai city, with the transformation of vegetation cover and agriculture land into built-up settlements. This alarming extent and level of US will have adverse impacts on the natural resources and land of Chennai. The combined application of geographic information systems, remote sensing, urban change modelling, landscape metrics and entropy measures proved to be a useful and efficient

approach for our assessment and modelling US for the Chennai city. Consequently, this study contributes with indicators and metrics to monitor this US in Chennai. It also provides relevant information for sustainable urban growth and efficient urban planning as well as for mitigation of environmental impacts in Chennai. To conclude, our study provides quantitative measures for urban planning and management authorities for mitigating social-ecological consequences of US and preventing loss of urban ecosystem services.



## Chapter – 3

### A Remote Sensing Approach to Environmental Monitoring in a Reclaimed Mine Area

*“The mining industry might make wealth and power for a few men and women, but the many would always be smashed and battered beneath its giant treads”.*

***Katharine Susannah Prichard***

## Chapter 3

### A Remote Sensing Approach to Environmental Monitoring in a Reclaimed Mine Area

---

#### 3.1 Introduction

Mining is an important source of raw materials and minerals, e.g., metals, salt, and coal, for industrial and domestic usage [44,53]. Countries in the European Union (EU) produce about 7% of the industrial and domestic commodities from mine-extracted resources [53]. Mining industries also play a vital role in global to regional economies, e.g., in energy production and fuel supply [44].

Mining activities may lead to several geological changes, i.e., ground movements, collision with mining cavities, and deformation of aquifers (Figure 3.1). These changes may constitute an increase in the groundwater table, and thus a slow sinking of subsurface soils and an unexpected collapse, i.e., subsidence [53]. The extraction processes and machines used to access mine galleries may produce irreversible damage in soil cohesion and eventually compress soil substrates [46,53]. Consequently, groundwater may intrude the surface level, form new waterbodies, and cause inundation. This, in turn, leads to several adverse long-term environmental impacts, such as vegetation degradation, soil erosion, flooding, sinkhole formation, and soil and water contamination [45,53,187], as well as to the damage of infrastructures [47,53]. The geological changes and associated environmental impacts may continue even after reclamations, if mines are not properly backfilled [49,50,122]

Regular landscape management and monitoring at the surface level are crucial for the prevention of subsidence and development of early warning systems in a reclaimed mine area (Figure 3.1). These are also vital for environmental protection, as well as for mitigation of the aftermaths from mining activities [53]. Particularly, monitoring short-term landscape dynamics, i.e., changes in the extent of waterbodies and vegetation, may provide important information about long-term geological changes such as subsidence, sinkhole formation, and changes in water table dynamics and associated effects on the environment [47]. In addition,



changes in the productivity of vegetation is an important indicator for assessing the geological changes in an active and reclaimed mine area [51,52]. Productivity of vegetation may surrogate ecological health as well as growth of water bodies and plant stress [53].

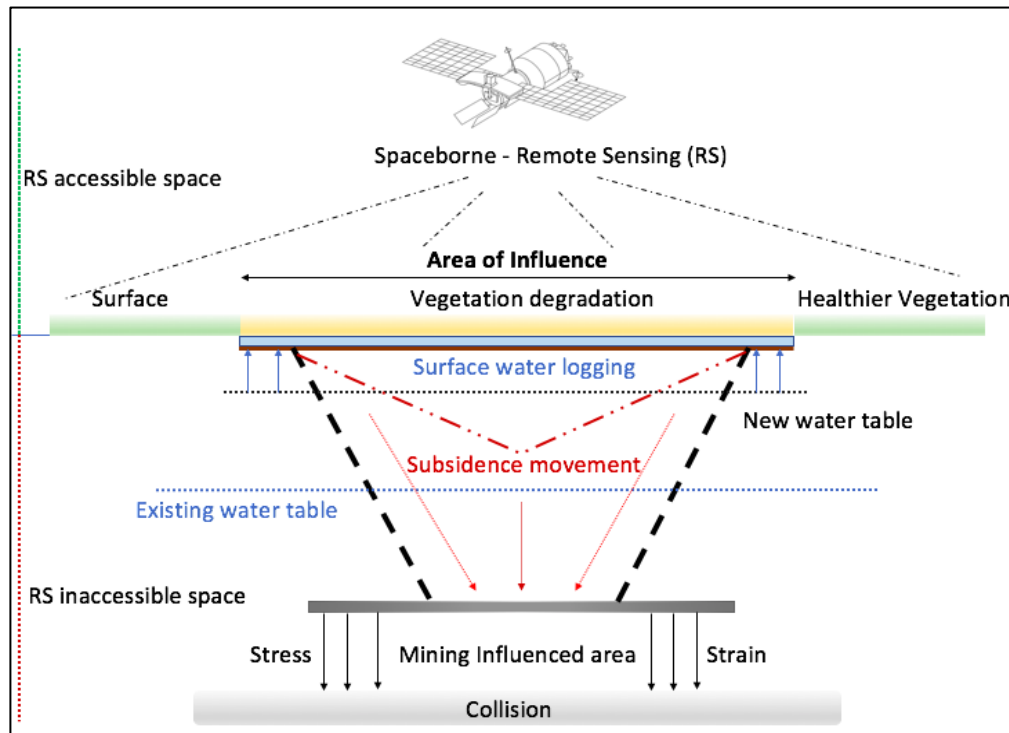


**Figure 3.1.** Inundation and subsidence through geological changes in a mining-affected area. The changes observed in the surface level using remote sensing (RS) may indicate the geological changes at the subsurface level. The figure is created according to the description of subsidence in Brunn et al. (2002) [46].

Remote Sensing (RS) techniques and Geographic Information Systems (GIS) have shown clear advantages over conventional field monitoring and laboratory measurements for assessing long- to short-term landscape dynamics [54–56]. Particularly for large areas, where surveying using Global Positioning System<sup>27</sup>(GPS) and ground levelling are time-consuming, expensive, and labor-intensive, RS and GIS provide prompt and efficient information on geological changes and subsidence[46]. These techniques are also useful for detecting changes in vegetation productivity and cover and flood dynamics through land-use and landcover maps [57]. Multispectral satellite images allow for detecting gradual as well as abrupt changes in landscapes [26]. However, besides widespread application in monitoring general landscape dynamics, the application of RS and GIS in monitoring and assessing mining effects on

landscapes and environment and in associated geological changes and vegetation productivity dynamics is limited [59,122]. Although high-resolution Light Amplification by Stimulated Emission of Radiation <sup>28</sup>(LASER), Interferometric Synthetic Aperture Radar <sup>29</sup>(InSAR), and Light Detection and Ranging <sup>30</sup>(LIDAR) mapping have been sparsely applied in small areas, environmental impacts in large mine reclamation areas have rarely been investigated using RS and GIS techniques [60–63,188].

This study aims to identify the subsidence zones and vegetation productivity degradation in a reclaimed mine area through the analyses of short-term landscape dynamics using RS and GIS techniques. The specific objectives were:

- (1) To examine the short-term, i.e., during 4 years, land-use and landcover (LULC) dynamics in the reclaimed mine area;
- (2) To quantify the emergence and growth of wetlands in the mining-influenced area and thus identify potential subsidence spots, i.e., spots exhibiting abrupt growth of waterbodies; and
- (3) To examine the vegetation productivity dynamics as a surrogate of the ground water table fluctuation and ecological stress.

### 3.2 Study Area

The study area, “Kirchheller Heide” (in English “Kirchhellen Heath”), is located in western Germany, surrounded by the towns of Bottrop and Huxe in the North, Oberhausen in the South, Gladbeck in the East, and Dinslanken in the West (Figure 3.2). The mining reclamation area lies between 51°34'53" N and 6°51'50" E and covers an area of about 57.74 km<sup>2</sup>. This site is one of the recreation areas for 7.5 million residents of the Kirchheller Heide and Ruhr district [44,46].

---

<sup>27</sup>**Global Positioning System (GPS)** – Global Positioning System is a satellite centred radio navigation installed and maintained by the United States government and operated by the United States Air Force. It is a worldwide navigation satellite system facilitate to provide geolocation (exact location on the earth) and time information to a GPS receiver (Eg. Mobile) [189].

<sup>28</sup>**Light Amplification by Stimulated Emission of Radiation (LASER)** – A laser is an instrument that emits light through a process of optical amplification based on the stimulated emission of electromagnetic radiation [190].

The area was a major industrial region dominated by 229 coal and steel mines from the second half of the 19th to the end of the 20th century, which produced approximately 400,000 tons of coal per year [44,46]. The coal was extracted from this area from depths up to 1500 m using the <sup>31</sup>longwall-mining method [53]. This mining method creates cavities in the ground and rock formation, which may result in surface subsidence and changes in the ground water table [59]. Moreover, 88.9% of production area was not properly backfilled when it was reclaimed during the 1990s [44,46]. Improper backfilling often leads to surface and sub-surface level depressions, while the magnitude of depressions depends on the length of long walls and the dip and width of the mined area [44,46]. Usually, such depressions and surface movements start six months after reclamation and gradually result into subsidence, surface area inundation, and vegetation degradation [53]. Hence, Kirchheller Heide was chosen to study potential occurrence of subsidence, inundation, and vegetation degradation caused by mining activities [44].

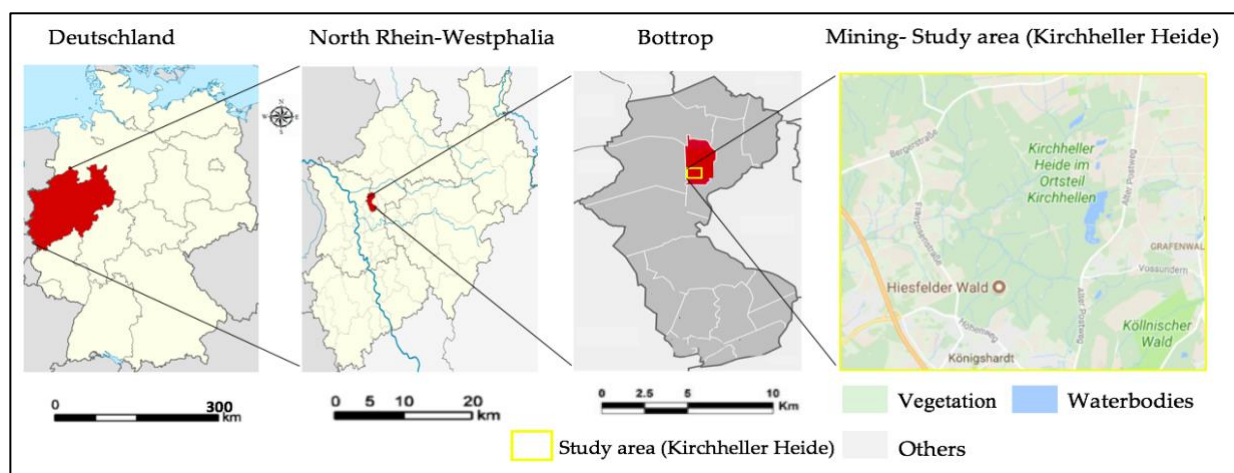


**Figure 3.2.** Location of Kirchheller Heide and mining area. The maps were created using Google Maps.

<sup>29</sup>**Interferometric Synthetic Aperture Radar (InSAR)** – INSAR is a technique is used to generate maps of surface digital elevation, using differences in the phase of the waves retuning to the satellite [123].

<sup>30</sup>**Light Detection and Ranging (LIDAR)** – LIDAR is a surveying method that measures distance to a target by illuminating the target with pulsed laser light and measuring the reflected pulses with a sensor [191].

<sup>32</sup>GMES4Mining team and EU-project <sup>33</sup>MINEO have monitored the wetland and vegetation dynamics in Kircheller Heide until 2012 [44]. These monitoring programs have detected incidences and passive impacts of surface flooding and subsidence using ground monitoring and air-borne hyperspectral images [44]. However, this monitoring was tedious, lengthy, and stopped after October 2012, largely because hyperspectral sensors could not cover the area in a continuous mode, i.e., mono-temporal, and hence, continuous monitoring was impossible [192,193]. Consequently, we aim to quantify landscape dynamics as well as to identify potential subsidence zones and vegetation degradation in Kircheller Heide after 2012, i.e., during 2013–2016, using imageries from sensors that continuously captured images of the area at a regular (yearly) interval, i.e., Landsat ETM+.

### 3.3 Materials and Methods

#### 3.3.1 Satellite Data

We used four Landsat Enhanced Thematic Mapper plus (ETM+) imageries covering the dates of 22 July 2013, 25 July 2014, 03 July 2015, and 30 July 2016, with 30 m spatial resolution. The imageries covering four years were chosen to study short-term landscape dynamics. To be consistent with seasonal variations and the vegetation productivity analysis, we selected images covering the frost-free growing season of Germany. This season starts in May (Spring) and ends in September (Fall/Autumn) [44]. To be further consistent with vegetation proportion, we selected images of July (growing season), which recorded consistent precipitation level varying between 28.2 and 34.4 L per m<sup>2</sup> during 2013–2016 [194]. Landsat ETM+ data were freely downloaded from the United States Geological Survey (USGS) gateway [133].

---

<sup>31</sup>**Longwall mining** – Longwall mining is a form of underground coal mining where a long wall of coal is mined in a single slice (typically 0.6 – 1.0 m thick). The longwall panel (the block of coal that is being mined) is typically 3 – 4 km long and 250 – 400 m wide [195].

<sup>32</sup>**GMES4Mining** – GMES4Mining is a Research and Development project supported with funds from the EU and Federal State of North Rhine-Westphalia, Germany aims to support particular tasks within the different phases of a mining life cycle. This team also monitors vegetation health, surface subsidence, floods and other environmental hazards in mining influenced area [53].

### 3.3.2 Image Processing

We followed a four-step procedure for investigating the landscape dynamics and vegetation productivity in Kirchheller Heide (see Figure 3.3). First, the satellite images were ortho-rectified and geo-corrected using the available “geoshift” and “georef” functions of the “Landsat” package in R studio [196–198]. Then, we geo-referenced the images using Universal Transverse Mercator (UTM) coordinate system [199]. The ETM+ images were cropped to the study area using a 10 km buffer around the mining area. To enhance the separability of the mining area from other land-use and landcover types, we applied the Tasseled Cap transformation for each imagery based on digital numbers (DN) [199].

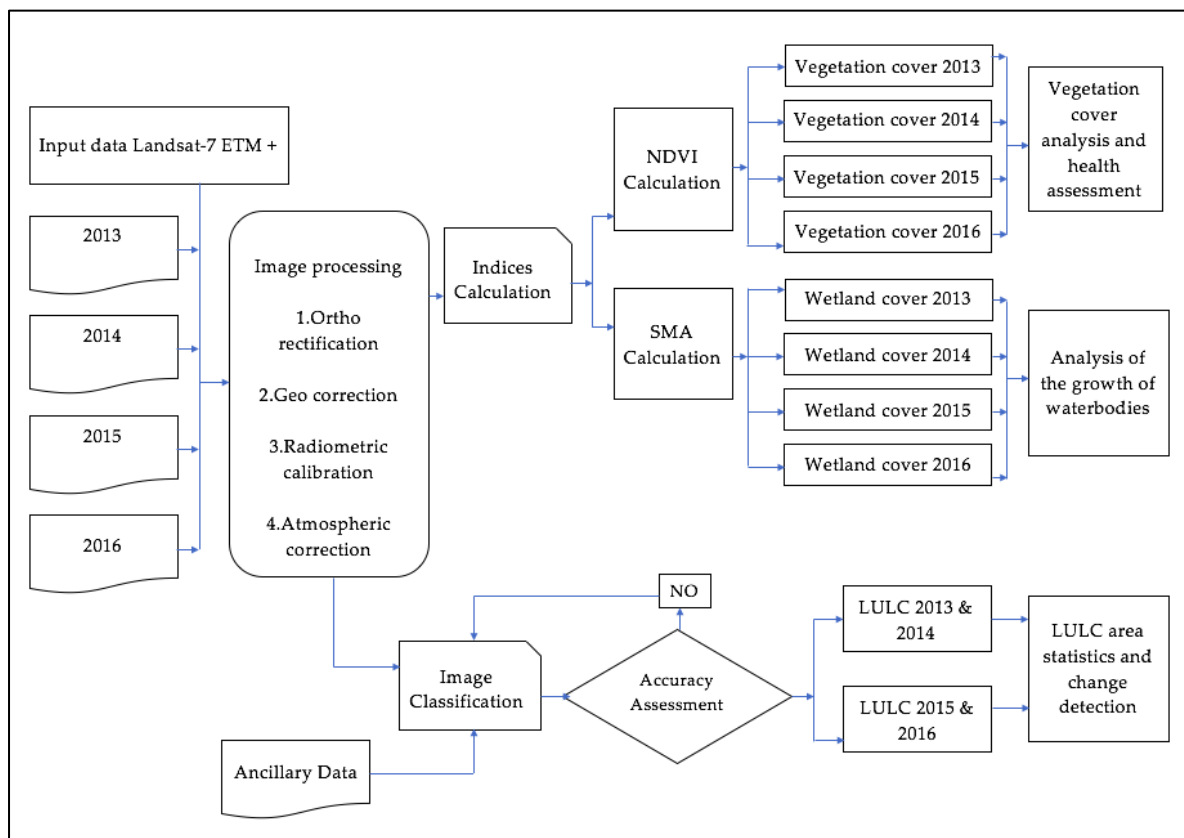


**Figure 3.3.** Methodology for the analysis of landscape dynamics and vegetation health (productivity) (NDVI: Normalized Difference Vegetation Index; ETM: Enhanced Thematic Mapper; SMA: Spectral Mixture Analysis; LULC: Land-use and Land cover).

<sup>33</sup>**MINEO** – MINEO The project MINEO aims at developing Earth Observation (EO) based methods and tools for assessing and updating environmental status and impact in European mining areas [53].

We were cautious about the scan line error that occurred in the Landsat 7 ETM+ sensor in 2003 and subsequently affected the produced imageries in 2003 and following years [200]. To fill the data-gap, i.e., Not Available (NA) values, in the imageries that occurred due to this scan line error, we applied Landsat 7 Scan Line Corrector (SLC)-off Gap function [197]. The SLC-off images were further rectified by mosaicking as suggested by USGS [197], and the residual gaps were filled using histogram correction [35,201]. Scan line error correction was performed in ERDAS Imagine (version 8.7) [202].

We first distributed and stored the Landsat images in a common radiometric scale to detect and quantify changes in the landscape of Kirchheller Heide, particularly for waterbodies and vegetation. For this purpose, we converted digital number (DN) integer values (0–255) to at-satellite radiance values using the available parameters in the ETM+ metadata (radiometric calibration), i.e., Top-of-Atmosphere (TOA) radiance [35]. We also applied atmospheric correction to overcome the mismatch between surface reflectance and at-sensor reflectance. The cloud, snow, aerosol, and cirrus were first identified and classified, and then were removed using absolute atmospheric correction, i.e., Dark Object and Modified Dark Object Subtraction Method. To ensure the homogeneity of reflectance values for the analysis of vegetation dynamics, invariant features in images across 2013–2016 were identified using the Pseudo-invariant features (PIF) function and subsequently corrected using a major axis regression. The radiometric and atmospheric corrections were conducted employing an atmospheric simulation model available in Landsat and RStool packages available in the R library [158,203–205].

### ***3.3.3 Land-Use and Landcover Classification and Accuracy Assessment***

We analyzed the overall surface level landscape dynamics over the four years using an unsupervised image classification technique. The images were classified for 2013, 2014, 2015, and 2016 into five land-use and landcover (LULC) classes (Table 3.1). We applied a Random Forest (RF) classification technique that optimizes the proximities among data points [206,207]. The RF classification algorithm constitutes the following steps:

1. Draw n-tree bootstrap model from the satellite imageries;
2. For each bootstrap model: grow unpruned classification according to the DN values;

3. Generate N number of polygons according to the DN values;
4. Choose five classification land-use classes;
5. Display land-use classification.

The LULC classification was performed in R [208] using Classes and Methods for Spatial Data (Sp), Raster Geospatial Data Abstraction Library (Rgdal), Raster, and Random forests packages [204–207].

**Table 3.1.** Description of Land-Use and Landcover (LULC) classes.

No	LULC Classes	Land Uses Involved in the Class
1	Settlement	Urban built-up and roads
2	Dense vegetation	Forests, gardens and shrubs
2	Waterbodies	Rivers, lakes, ponds, open water and streams
3	Agriculture	Farms and Agriculture parcels
4	Bare land	Non-irrigated properties and Dry lands

The accuracy of image classification was evaluated by comparing the classified LULC maps with reference Google Earth images from 2013 to 2016 of the study area obtained from Google Earth Engine (GEE) platform [209]. We produced a set of 75 random points and extracted those values for four different study periods. Then, the selected random point values were identified from GEE and compared to the LULC maps. We used the kappa coefficient to quantify the accuracy of the classified images using ERDAS Imagine (version 8.7) [210]. The user and producer accuracies were also calculated through a confusion matrix [187]. A kappa coefficient of more than 0.8 indicates a satisfactory accuracy of classified images, i.e., classified images are analogous to the reference data [169,211–214].

### **3.3.4 Wetland Coverage and Surface Flooding**

The dynamics of wetland coverage as well as the extent of surface flooding were assessed to identify potential subsidence zones. We applied a SMA on the Landsat imageries to track the



changes in wetland coverage and identify the emergence of waterbodies [215]. SMA delivers pixel estimates for water extent delineated from other landcover pixels based on available radiometric data in imageries [215] (Equations (1) and (2)). Hence, the RF classification was expanded to the SMA for an accurate and precise examination of wetland dynamics, delineated from other LULC classes.

$$DN_i = \sum_j F_j DN_{i,j} + r_i \quad (1)$$

$$\sum_j F_j = 1 \quad (2)$$

where,  $DN_i$  is the measured value of a mixed pixel in band  $i$ ;  $DN_j$  is the measured value of each endmember (wetland pixel);  $F_j$  is the fraction of each endmember; and  $r$  is the root mean square (rms) residual that accounts for the difference between the observed and modeled values [212]. Thus, waterbodies and their extent were delineated from other landcover classes for each year during 2013–2016. We calculated the total and individual area coverage of waterbodies in each year, as well as identified if any waterbody emerged. SMA calculation and changes in waterbodies were analyzed using R packages SP, Rgdal, Raster, and Raster Time Series Analysis (rts) [203,216,217].

### 3.3.5 Vegetation Productivity and Coverage

We calculated the Normalized Difference Vegetation Index (NDVI) for the quantification of vegetation productivity during 2013–2016 using Equation (3) [218]:

$$NDVI = (NIR - Red) / (NIR + Red) \quad (3)$$

where, NIR = Near Infrared Band value and R = Red Band value recorded by the Landsat ETM+ imageries [219]. Photosynthesis is the main function of plants, which is directly associated with electromagnetic energy [220–222]. The spectrum of visible region strongly absorbed by green vegetation and reflects in the NIR region [73,121,223]. NDVI performed the NIR and R band-ratio to describe the relative density of vegetation greenness. Thus, we integrated plant ecological functions with available radiometric data of mining area associated with the principles of electromagnetic spectrum.



We classified the obtained NDVI values into 10 raster zones based on natural breaks to distinguish among different stages of vegetation productivity and coverage, i.e., value ranges 0.42–1, 0.08–0.42, and –1–0.08 indicated high productivity (dense canopies), medium productivity, and low productivity (mostly bare land and water) vegetation, respectively. We calculated the changes in the area coverage of each raster zone during 2013–2016 and thus quantified the dynamics in vegetation productivity and coverage. NDVI calculation and changes in vegetation productivity were analyzed using R packages SP, Rgdal, Raster, and rts [203].

### 3.4 Results and Discussion

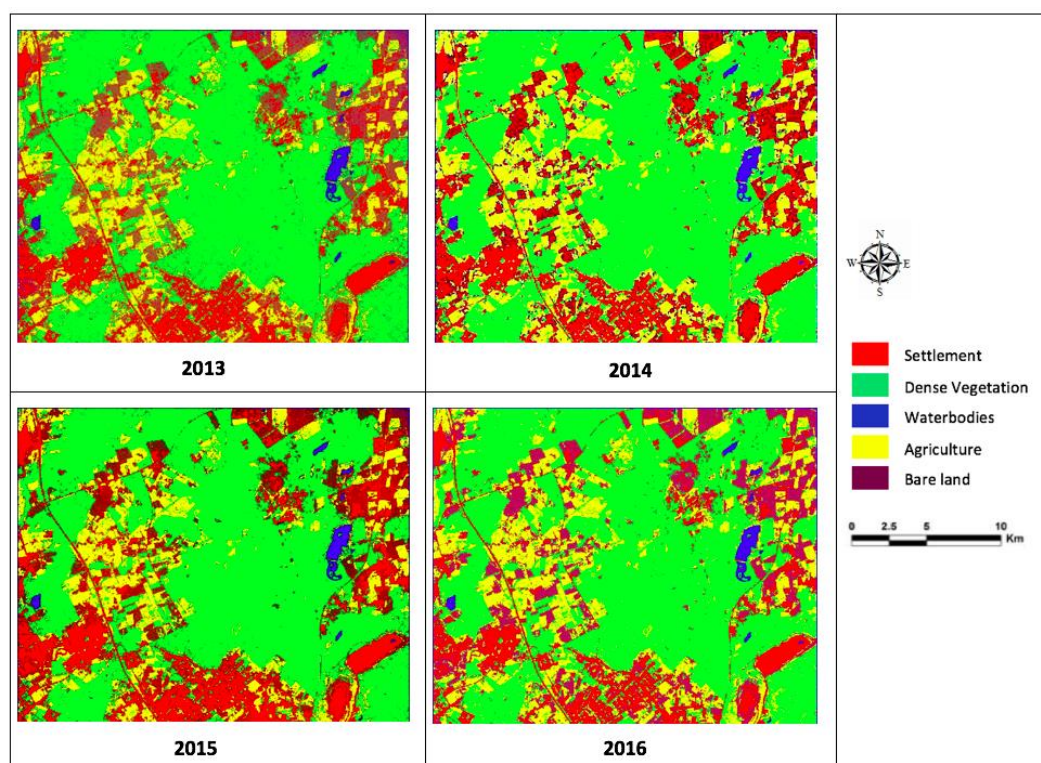
#### 3.4.1 Landscape Dynamics during 2013–2016

Figure 3.4 displays the LULC maps of Kirchheller Heide mining area obtained for July 2013, 2014, 2015, and 2016 using RF classification in R. We obtained an overall accuracy value of more than 85% for the classified LULC maps of all years with kappa coefficient values of more than 0.84 (Table 3.2). These values indicate a satisfactory accuracy of the classified LULC maps.

**Table 3.2.** Summary of the confusion matrix for the classified images of 2013–2016 (PA – Producer Accuracy; UA – User Accuracy).

LULC Classes	2013		2014		2015		2016	
	PA	UA	PA	UA	PA	UA	PA	UA
Settlement	87.02	82.21	86.01	82.12	88.22	79.71	92.02	88.19
Dense Vegetation	83.05	83.85	82.14	85.34	81.76	81.96	83.14	87.02
Agriculture land	86.78	91.76	83.21	94.21	83.45	92.12	88.46	96.75
Water bodies	86.95	91.35	81.11	89.55	87.65	88.76	82.11	85.88
Bare land	91.21	84.12	88.54	79.32	89.31	83.66	81.43	83.23
Kappa	0.87		0.84		0.86		0.85	

The classified LULC maps exhibit a 19.9% increase in the coverage of waterbodies between 2013 and 2016 with an annual growth rate of 6.5% (Table 3.3, Figure 3.4). This increase in the coverage of waterbodies was associated with a 5.43% decrease in the coverage of dense vegetation and 25.6% increase in the bare land area (Table 3.3, Figure 3.4). The coverage of agricultural land also exhibited a 3.2% decrease, whereas the settlement coverage increased by 5.45%. The increase in the coverage of waterbodies may relate to the subsidence and changes in ground water table in the surface level [49]. This subsidence may have led to collision with non-stowed mining cavities, groundwater intrusion, and caused surface flooding, which, in turn, affected and caused the decrease in the coverage of dense vegetation and agricultural lands. These results are in line with [53], which showed the relation between surface landscape dynamics and subsurface geological changes. The observed increase in the coverage of bare land may also indicate the vegetation damage caused by the subsidence and surface flooding [122].



**Figure 3.4.** Classified land-use and landcover (LULC) maps of Kirchheller Heide in July 2013, 2014, 2015, and 2016.

**Table 3.3.** Comparison of the land-use and land cover (LULC) types during 2013–2016.

LULC Classes	Area in Km <sup>2</sup>				Differences (km <sup>2</sup> )	Differences (%)
	2013	2014	2015	2016	2013–2016	2013–2016
Settlement	12.70	13.04	13.25	13.40	0.69	0.05
Dense vegetation	30.78	30.27	29.72	29.10	–1.67	–0.05
Waterbodies	0.29	0.31	0.32	0.35	0.06	0.20
Agriculture	9.24	9.16	9.02	8.95	–0.29	–0.03
Bare land	4.74	5.03	5.75	5.95	1.21	0.26

### 3.4.2 Emergence and Growth of Waterbodies

The SMA did not identify any emergence of waterbodies in Kirchheller Heide during 2013 – 2016 (Figure 3.5a). However, we observed an abrupt growth (0.06 km<sup>2</sup>) in the coverage of two waterbodies within the four years (Figure 3.5a). The increase in the coverage of these two waterbodies (waterbodies A and B) accounted for 87.2% of the total growth the coverage of waterbodies in Kirchheller Heide, with an annual growth rate of 29% (Figure 3.5 b,c). Waterbodies A and B exhibited a 67% and 90% growth, respectively, in their coverage during 2013–2016 (Figure 3.5c). Hence, the locations of waterbodies A and B may have been the potential subsidence spots that led to surface sink, collapse, and groundwater intrusion, entailing an increase in the coverage of those waterbodies [46].

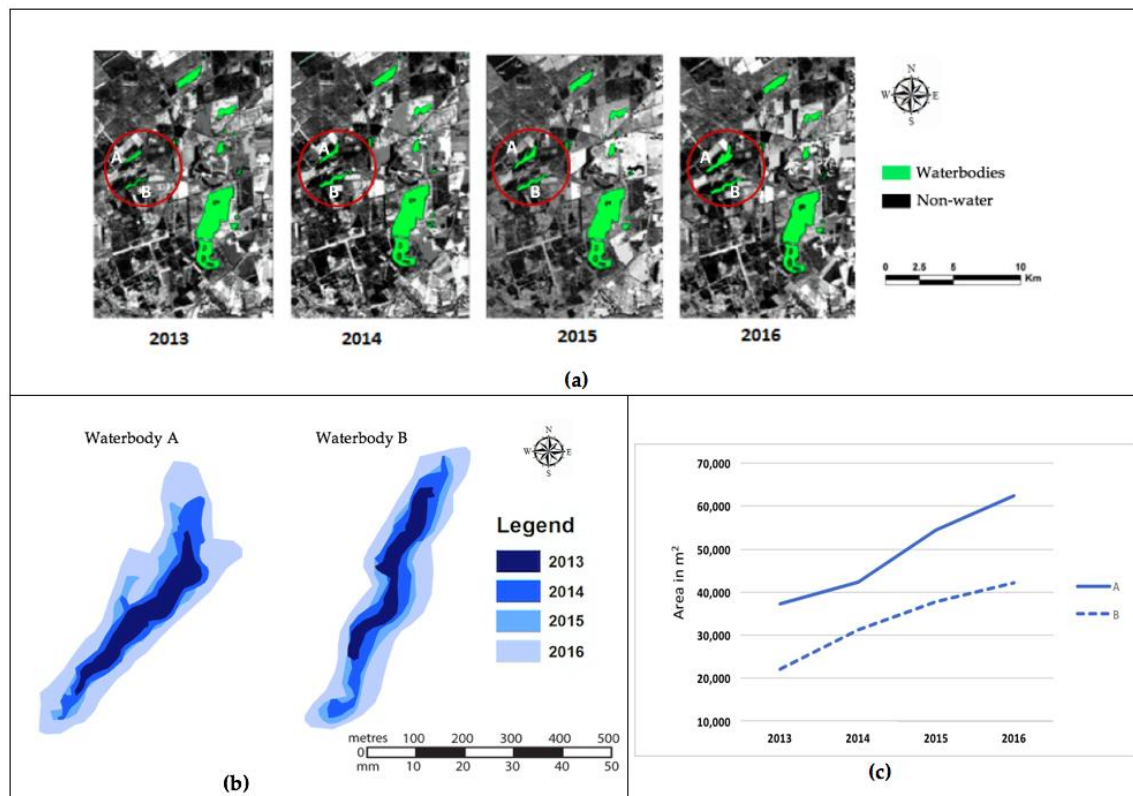
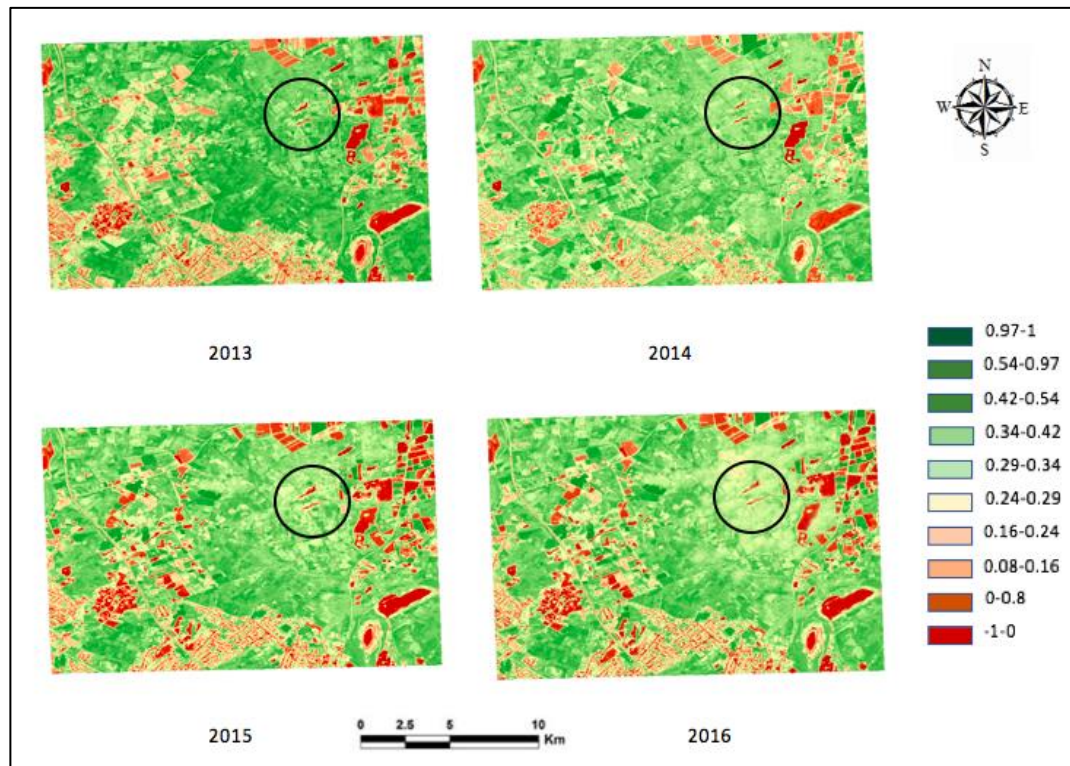


**Figure 3.5.** Changes in the extent and coverage of waterbodies in Kirchheller Heide during 2013–2016. (a) The location of waterbodies (A and B) in the red circle indicate the waterbodies with the highest (87.2%) growth and potential subsidence spots; (b) the dynamics of the extent of waterbodies A and B during the years 2013–2016; and (c) the changes in the area coverage of waterbodies A and B during 2013–2016.

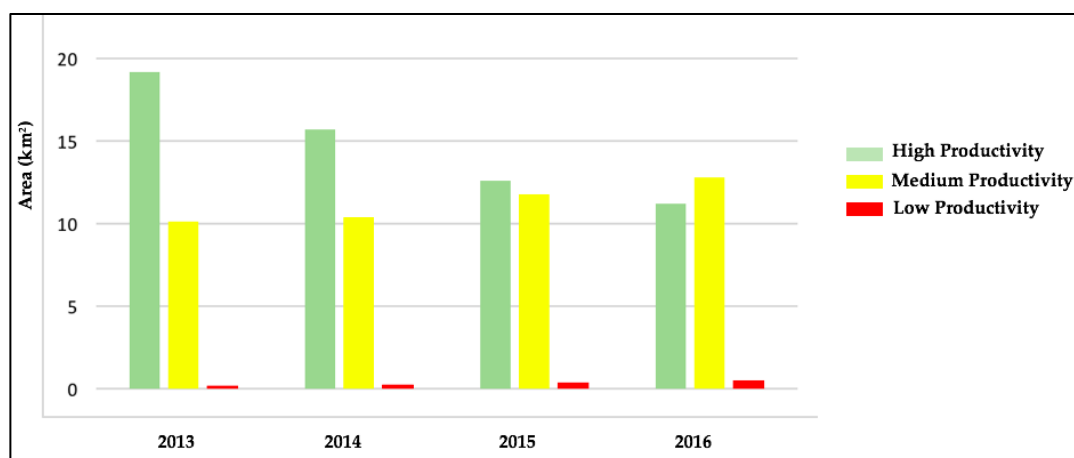
### 3.4.3 Vegetation Productivity

We observed a substantial decrease in the area coverage of highly productive vegetation, which was associated with an increase in the area coverage of medium and lowly productive vegetation (Figure 3.6, Table 3.4). The area around the waterbodies, which experienced the abrupt growth, was with the highest decrease in NDVI values between 2013 and 2016, i.e., the average NDVI values decreased from 0.61 to 0.29 (Figure 3.6). A total of 58.5% degradation in the productive vegetation mostly occurred in the neighborhood of waterbodies and along the water courses in the east (Figure 3.6, Table 3.4). Overall, the total area coverage under highly productive vegetation decreased from 56.5 to 28.3% with an annual rate of  $-9.5\%$ , whereas the area coverage under medium and lowly productive vegetation increased from 14 to 76% with an annual rate of  $15.5\%$  between 2013 and 2016 (Table 3.4).





(a)



(b)

**Figure 3.6.** (a) NDVI map of the Kirchheller Heide mining area in July 2013, 2014, 2015, and 2016. Value ranges 0.42–1, 0.08–0.42, and –1–0.08 indicated highly, medium, and lowly productive vegetation, respectively (see b and Table 6 for details). The location of the waterbodies, which experienced abrupt growth, are in the black circles; (b) Area coverage in km<sup>2</sup> by vegetation productivity classes in 2013, 2014, 2015, and 2016.

Our results indicate an overall degradation of vegetation productivity with substantial loss of vegetation productivity along the water course in the east of Kirchheller Heide (Figure 3.6, Table 3.4). This degradation of productivity was likely entailed by the increase in the groundwater table and consequent intrusion into the surface level (Figure 3.6) [3].

The variation in vegetation productivity can also be caused by confounding ecological variables, e.g., phenological characteristics (differences between growing characteristics across years). However, we controlled for the dominant drivers of seasonal variations, i.e., chose images from frost-free growing season in Germany, and precipitation level, i.e., between 28.2 and 34.4 L per m<sup>2</sup> in July during 2013–2016, while selecting the imageries [194]. Moreover, ours is a short-term study and hence, excludes variation in plant phenological characteristics, which is usually long-term and gradual. Furthermore, the major decrease in vegetation productivity was observed for the area neighboring the waterbodies that experienced the abrupt growth. Consequently, we argue that the increase in the groundwater table caused by the subsidence is the dominant cause for the degradation of vegetation productivity in Kirchheller Heide. Increasing groundwater table led to surface flooding as well as to soil erosion, which directly influenced the vegetation productivity, as observed in the extent of NDVI values (Figure 3.6) [53].

**Table 3.4.** Vegetation productivity changes between 2013–2014, 2014–2015, and 2015–2016. Value ranges 0.42–1, 0.08–0.42, and –1–0.08 indicated highly, medium, and lowly productive vegetation, respectively, and the overall changes in their coverage are reported in bold.

Vegetation Productivity Classes	NDVI Values	Changes in Area Coverage % (km <sup>2</sup> )		
		From 2013 to 2014	From 2014 to 2015	From 2015 to 2016
<b>Highly Productive</b>	0.97–1	–6% (0.55)	–8% (0.36)	–12% (0.27)
	0.54–0.97	–45% (7.56)	–67% (6.49)	–78% (4.36)
	0.42–0.54	–34% (11.25)	–62% (8.84)	–79% (4.85)

	0.42–1	–28% (19.36)	–45.66 (15.69)	–56% (9.48)
	0.34–0.42	62% (5.30)	71% (6.07)	74% (6.33)
	0.29–0.34	35% (3.20)	42% (3.83)	67% (6.11)
<b>Medium</b>	0.24–0.29	51% (29.00)	64% (3.64)	72% (4.10)
<b>Productive</b>	0.16–0.24	35% (8.00)	38% (0.87)	42% (0.96)
	0.08–0.16	21% (0.60)	29% (0.83)	44% (1.25)
	0.08–0.42	40% (12.80)	48% (15.24)	59% (18.75)
	0–0.08	12% (0.18)	61% (0.29)	86% (0.55)
<b>Lowly</b>	–1–0	16% (0.21)	57% (0.34)	66% (0.56)
<b>Productive</b>	–1–0.08	14% (0.39)	59% (0.63)	76% (1.10)

### 3.5 Outlook

We applied freely available Landsat imageries to study short-term landscape dynamics in the mine-reclaimed Kirchheller Heide, and identified two potential subsidence spots that may be under risk of collapse and overall degradation and damage of vegetation (Figure 3.5). Thus, our results inform environmental management and mining reclamation experts about land surface and vegetation loss because of subsidence. Environmental management authorities in Kirchheller Heide should prioritize the indicated subsidence areas for further surface and subsurface investigation, as well as for remediation and mitigation. The potential biodiversity and ecosystem impacts of subsidence should also be investigated.

In general, our study proves the virtue of RS and GIS for monitoring short-term geological changes and thus for predicting long-term environmental impacts in reclaimed mine areas. Thus, we urge the importance of including RS and GIS monitoring in environmental conservation and management projects in addition to field monitoring [63,122]. Our approach is also useful for identifying ecological stress, and surface erosion and inundation, and thus may provide important metrics for ecological restoration and infrastructure provision [46,187].

Our study also emphasizes the need for proper backfilling and management of reclaimed mine areas [63,122]. Environmental regulations mostly address the direct impacts of mining activities and insufficiently address the long-term impacts of post-mining activities [46,187]. We recommend that environmental management should take advantage of satellite imageries and RS and GIS techniques [50]. The reclaimed mine areas should be regularly monitored for the identification of subsidence and surface collapses.

Field observation and survey data should complement the applied RS techniques with freely available satellite data to validate our results [44]. The results should also be compared with the SAR analyses and monitoring [3,8]. Future studies should apply higher spatial resolution (e.g., 5 m) satellite imageries, e.g., <sup>34</sup>Quickbird and LIDAR images, for the identification of subsidence extent and magnitude in reclaimed mine areas [3,4]. RS-based monitoring could also result in surface metrics for quantification of geological changes in reclaimed mine areas.

High- and hyperspectral and temporal satellite imageries may provide landscape dynamics with higher precision than in our study [2–8]. For example, a comprehensive monthly variation analysis may provide precise information on the emergence and dynamics of subsidence zones when compared to yearly analysis, as subsidence occurs abruptly at the surface level [8]. Moreover, images with higher coverage of bands may identify subsidence spots that are not observed through the growth of waterbodies, e.g., sink holes and landslides [4–8]. We particularly recommend the usage of high- and hyperspectral and temporal resolution imageries collected in continuous mode for monitoring immediately after reclamation, when urgent surface and subsurface level investigation, as well as proper remediation through backfilling to avoid surface level collapse, are needed.

---

<sup>34</sup>**Quickbird** – Quickbird was a high-resolution commercial earth observation satellite [224].





## Chapter – 4

Satellite image fusion to detect changing surface permeability and emerging urban heat islands in a fast-growing city

*“To truly transform our economy, protect our security, and save our planet from the ravages of climate change, we need to ultimately make clean, renewable energy the profitable kind of energy.”*

***Barack Obama***

## Chapter 4

### Satellite Image Fusion to Detect Changing Surface Permeability and Emerging Urban Heat Islands in a Fast-growing City

---

#### 4.1 Introduction

Rapid urbanization has been globally a dominant driver of ecosystems and environmental degradation in the recent decades [31]. United Nations projected that two-thirds of the global population will live in urban areas by the year 2050 [17]. This will entail major landuse and landcover changes in urban areas, which will directly impact urban ecosystem services through a loss of agricultural and forested lands, and an increase of barren and impermeable built-up surface areas [58]. Loss of vegetation and increasing built-up surface areas may eventually affect climatic variability and thus lead to an increase in surface and air temperatures in urban areas [102,113,225].

Urban forests and vegetation control surface and air temperatures through shading and evapotranspiration [226]. According to the United States Environmental Protection Agency <sup>35</sup>(USEPA), shaded surfaces are, on average, 11–25°C cooler than unshaded surfaces, while evapotranspiration reduces peak summer temperatures by 1–5°C [3]. In contrast, impermeable built-up surface areas have a higher solar radiation absorption, and a greater thermal capacity and conductivity than the non-built-up areas [226,227]. Consequently, urban areas exhibit higher surface and air temperatures than surrounding rural areas [228]. Rapid urbanization and consequent expansion of impermeable built-up surface areas may thus lead to the emergence of urban heat islands (UHI), which have severe consequences for urban ecosystems and humans [22,57,101,225].

---

<sup>35</sup>United States Environmental Protection Agency (USEPA) – USEPA is the Environmental Protection Agency is an independent agency of the United States federal government for environmental protection [229].

Monitoring the rate and extent of urbanization and consequent decrease in surface permeability and emergence of UHI provide essential information for averting their adverse impacts on urban residents and ecosystems [230]. Particularly, in fast growing cities like Tirunelveli, India, which are experiencing rapid and abrupt expansion due to extensive rural-urban migration and urban sprawl, UHI can emerge spontaneously through the loss of vegetation and expansion of impermeable surfaces [231]. Hence, they require detailed and continuous monitoring of landuse and landcover (LULC) changes. Emergence of UHI can be controlled and prevented through proper urban planning, management and regulations of landuse zones that are informed by detailed and continuous LULC change monitoring [115]. Monitoring anthropogenic LULC changes may also provide quantification of environmental processes and respective sustainable living standards in urban areas [114].

Remote sensing provides important tools for detailed and continuous monitoring of LULC changes in fast growing cities as well as for assessing expansion of impermeable surfaces and detecting emergences of UHI [10,11]. Remote sensing tools demonstrate clear advantage for monitoring and estimating spatiotemporal changes of LULC over conventional methods that are based on time consuming and expensive field studies combined with large scale aerial photography [116]. Hence, remote sensing techniques have been widely applied for assessing LULC changes, surface permeability and temperature, and detecting emergence of UHIs, in several regions of the world, e.g. Egypt [11], Eritrea [13], Germany [14] and Vietnam [19]. Particularly, the advent of high quality satellite imageries from multiple sensors for a certain location enables the fusion of those imageries to arrive at a combined image for that location [232]. Such combined images are substantially more detailed than images from individual sensors as they fuse images with diverse spatial and spectral resolutions and thus enable the detection of a diverse range of objects, which are often undetected through single sensor derived images [40,233–236]. However, monitoring of surface permeability and UHI emergence mostly involve time consuming and expensive field studies and single sensor derived aerial and satellite imageries.

Fused remotely sensed imageries provide important metrics for the quantification of LULC changes, surface impermeability and consequent increase in surface temperature in urban areas as well as for the assessment of the relationship between changes in surface permeability and surface temperature [10–12]. For instance, the Soil Adjusted Vegetation Index (SAVI) quantifies changes in vegetation cover and health in relation with soil moisture, saturation and color [121]. Hence, it has been widely used as an important proxy for surface permeability and also as an early warning metric for food security and ecological health [237]. Moreover, Land Surface Temperature (LST) is a metric for measuring the temperature of the interface between the earth's surface and the atmosphere [115,238], which is often shaped by LULC and, particularly, vegetation cover [119]. Fused remotely sensed imageries provide considerably quicker continuous measurement of LST when compared with the conventional extrapolation of non-contiguous meteorological station measurements [120]. LST is also an important metric for the identification of the emergence and propagation of UHI [239]. Calculated SAVI can indicate climate change impacts in urban areas and hence, is associated with the changes in LST [121]. In general, areas with higher SAVI typically exhibit lower LST and vice-versa, given constant soil moisture and evapotranspiration capacity of the surface [27]. Overall, understanding the patterns of LULC, SAVI and LST changes, and their associations using fused remotely sensed imageries may provide quick and precise information crucial for urban ecosystem zoning and UHI control in fast growing cities like Tirunelveli [240,241].

This study quantified the LULC, SAVI and LST changes, as well as the relationship between SAVI and LST changes, in a fast-growing city, i.e. Tirunelveli, Tamilnadu, India, during a 11 years period, i.e. between 2007 and 2017. We fused satellite imageries from two different sensors, i.e. IRS-LISSIII and Landsat-7 ETM+, to arrive at combined high spatial resolution (23.5m of IRS P6-LISSIII) and high thermal band (30m of Landsat-7 ETM+) imageries for Tirunelveli. The objectives of our study are twofold: (i) To demonstrate the advantage of using fused imageries over non-fused single images through a comparison of image classification accuracies and (ii) to identify the potential zones for UHI emergence using a SAVI-LST combined metric for Tirunelveli in 2017.

## 4.2 Study Area

Tirunelveli is one of the largest and oldest municipal corporations at Tirunelveli district in Tamilnadu state of India with a total population of 473,637 according to the 2011 census [242]. The city lies between 8°44' and 9°30' of the Northern latitude, and 77°05' and 78°25' of Eastern longitude with an altitude of 47m above the mean sea level (Figure 4.1). Tirunelveli is situated on the East bank of Thamirabarani River, the major water course for domestic usage, power generation and irrigation in Tirunelveli and other neighboring cities (Tuticorin, Sankarankovil and Valliyur) [127].

The climate of Tirunelveli is dominantly tropical and receives rainfall in all seasons throughout a year [240]. The average annual rainfall during 2010-2016 was 947.6mm [243], with a contribution of 555.08mm and 189.6 mm rain from the North-East and South-West Monsoons, respectively. The average annual surface temperature of the city varies between 24.4°C and 34.6°C, with the lowest winter (November to February) and highest summer (March to June) temperatures of 27.1°C and 30.4°C, with an average precipitation of 127.7mm and 74.5mm, respectively [243].

Tirunelveli experienced a rapid and extensive urbanization and urban sprawl during the last two decades [231]. The city population has doubled during this time, which depicts Tirunelveli as one of the fastest growing cities in the India [241]. As a principal business hub of Southern India, Tirunelveli experienced a substantial immigration of people from neighboring cities and rural areas in search for better standard of lives, income and employments [231]. This has caused an uncontrolled expansion of the city and associated adverse effects on the city land, water and air [244]. According to the Centre for Agriculture and Rural development studies (CARDS), the rapid urbanization driven conversion of agriculture lands in Tirunelveli and surrounding districts have adversely impacted the region's food security [106,245].

---

<sup>36</sup>*Centre for Agriculture and Rural development studies (CARDS) – CARDS is a Non-Government Organization committed to reaching all parts of the rural society especially farming community and participates actively towards improving the quality of life of rural masses by addressing technical, economic policy issues related to the development of agriculture and rural society in India [246].*

The rapid urbanization also entailed rapid industrialization leading to the establishment of more than 25 large-scale industries such as cement factories, cotton yarn manufacturers, calcium carbide production plants, sugar factories, cotton seeds oil refinery plants, brick factories, paper and flour mills, and several hundreds of small-scale industries. This, in turn, led to air pollution, water scarcity, degradation of vegetation, ecosystems fragmentation, floods and droughts [247].

We selected an area of 104.2 km<sup>2</sup> covering the central area and periphery of Tirunelveli city (Figure 4.1). According to CARDS, this area has undergone the highest LULC conversion in Tirunelveli district between 2007 and 2017 [245]. Hence, we chose the years 2007 and 2017 for assessing LULC zones, SAVI and LST in Tirunelveli, as well as for quantifying their changes and detecting UHI emergence in our study.

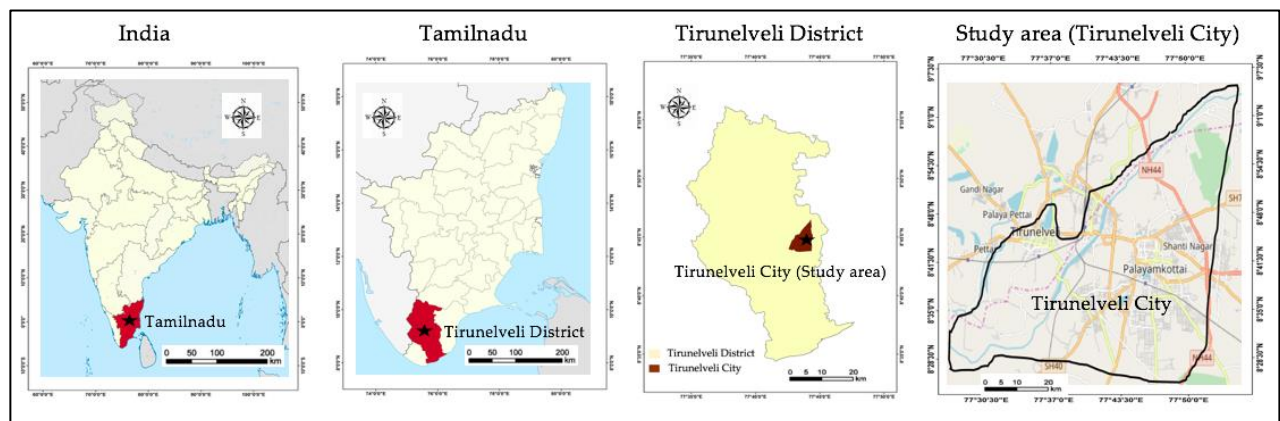


**Figure 4.1.** Geographic location and area of Tirunelveli city. The maps were generated using Google Maps.

<sup>37</sup>**United States Geological Survey (USGS)** formerly simply **Geological Survey**) – USGS is a scientific agency of the United States government study the landscape of the United States, its natural resources, and the natural hazards that threaten it [248].

## 4.3 Materials and Methods

### 4.3.1 Data

We used Landsat Enhanced Thematic Mapper (ETM+) and Indian Remote Sensing Satellite Resourcesat-1 - Linear Imaging Self-Scanning Sensor -3 (IRS LISS-III) images with 30 m and 23.5 m spatial resolutions, respectively, from June 2007 and June 2017. Freely available Landsat satellite data were downloaded from United States Geological Survey <sup>37</sup>(USGS) gateway in GeoTiff format [249]. IRS-LISSIII data was purchased from the National Remote Sensing Centre <sup>38</sup>(NRSC), Indian Space Research Organisation (ISRO) in GeoTiff format [171].

Daytime images from 11<sup>th</sup> June (summer) were chosen for both years to obtain the least cloud coverage possible as well as to control for the seasonal homogeneity in plant phenology for LULC classification, and SAVI and LST calculation, and thus to exclude impacts of seasonal variation of plant phenology [159]. Landsat ETM+ and IRS-LISSIII were georeferenced using the World Geodetic System (WGS) 1984 and then projected to the Universal Transverse Mercator <sup>39</sup>(UTM) coordinates [163,250]. The data has been geo-corrected and cropped to the study area (Figure 4.1).

### 4.3.2 Image Pre-Processing

We first pre-processed the Landsat ETM+ and IRS-LISSIII images, separately, for 2007 and 2017 (Figure 4.2). Triangulation and Digital Elevation Model <sup>40</sup>(DEM) were generated for IRS-LISSIII images from each year to examine the land dynamics and prime variations [179]. Triangulation process for IRS-LISSIII was performed by fitting a second order polynomial in <sup>41</sup>Leica Photogrammetry Suite (LPS) [251]. Then DEMs were generated using built-in image matching techniques [252]. DEMs were further edited using the built-in pit removal technique in LPS, where the abrupt elevational changes were identified [144]. The final DEMs of 2007 and 2017 were further orthorectified for LULC classification and analysis (Figure 4.2).

---

<sup>38</sup>**National Remote Sensing Centre (NRSC)** – NRSC is one of the centres of the Indian Space Research Organisation manages data from aerial and satellite sources [171].



The Landsat ETM+ images were first geometrically corrected and orthorectified using the “georef” and “geoshif” functions of the “Landsat” package in R [205]. Then the orthorectified images were checked for scan line errors that occurred in the Landsat 7 ETM+ sensor from 2003 onward and consequently, influenced our images from 2007 and 2017 [197]. The missing data occurred due to scan line error were filled with the Landsat 7 Scan Line Corrector (SLC)-off Gap function in ERDAS Imagine (version 8.7) [35,163]. The SLC-off images were further rectified by mosaicking as recommended by USGS, and the residual gaps were filled using the histogram correction technique [197].

We performed radiometric and atmospheric corrections of the orthorectified and SLC-off Landsat ETM+ images. First, we transformed Digital Number (DN) integer values (0–255) in Landsat ETM+ images to at-satellite radiance values using the ETM+ radiometric calibration of Top-of-Atmosphere (TOA) radiance [35]. Then, we applied atmospheric correction to minimize the mismatch between surface reflectance and at-sensor reflectance [44]. The cloud, aerosol, and cirrus were identified and classified, and removed using Dark Object and Modified Dark Object Subtraction method [44]. Finally, to ensure the homogeneity of reflectance values for the analysis of surface permeability, invariant features in images from 2007 and 2017 were identified using the Pseudo-invariant features (PIF) function and subsequently corrected using a major axis regression [35]. The radiometric and atmospheric corrections were conducted in R environment [205].

### 4.3.3 Image Fusion

The pre-processed IRS-LISSIII and Landsat 7 images were combined using the “Ehlers” image fusion technique [253,254]. Ehlers fusion works based on an Intensity-Hue-Saturation (IHS) transformation coupled with adaptive filtering in the Fourier domain to prevent the fused image from color distortion, which frequently occurs in conventional statistical or color transformation fusion methods (see [255] for details on Ehlers image fusion techniques). To avoid loss of information and further minimize color distortion, we also used all bands from IRS-LISSIII and Landsat ETM+ for the fusion process. The image fusion was performed using the “panSharpen” function of the “RStoolbox” package in R [256]. We maintained 30m resolution in fused images for further classification and indices calculation.

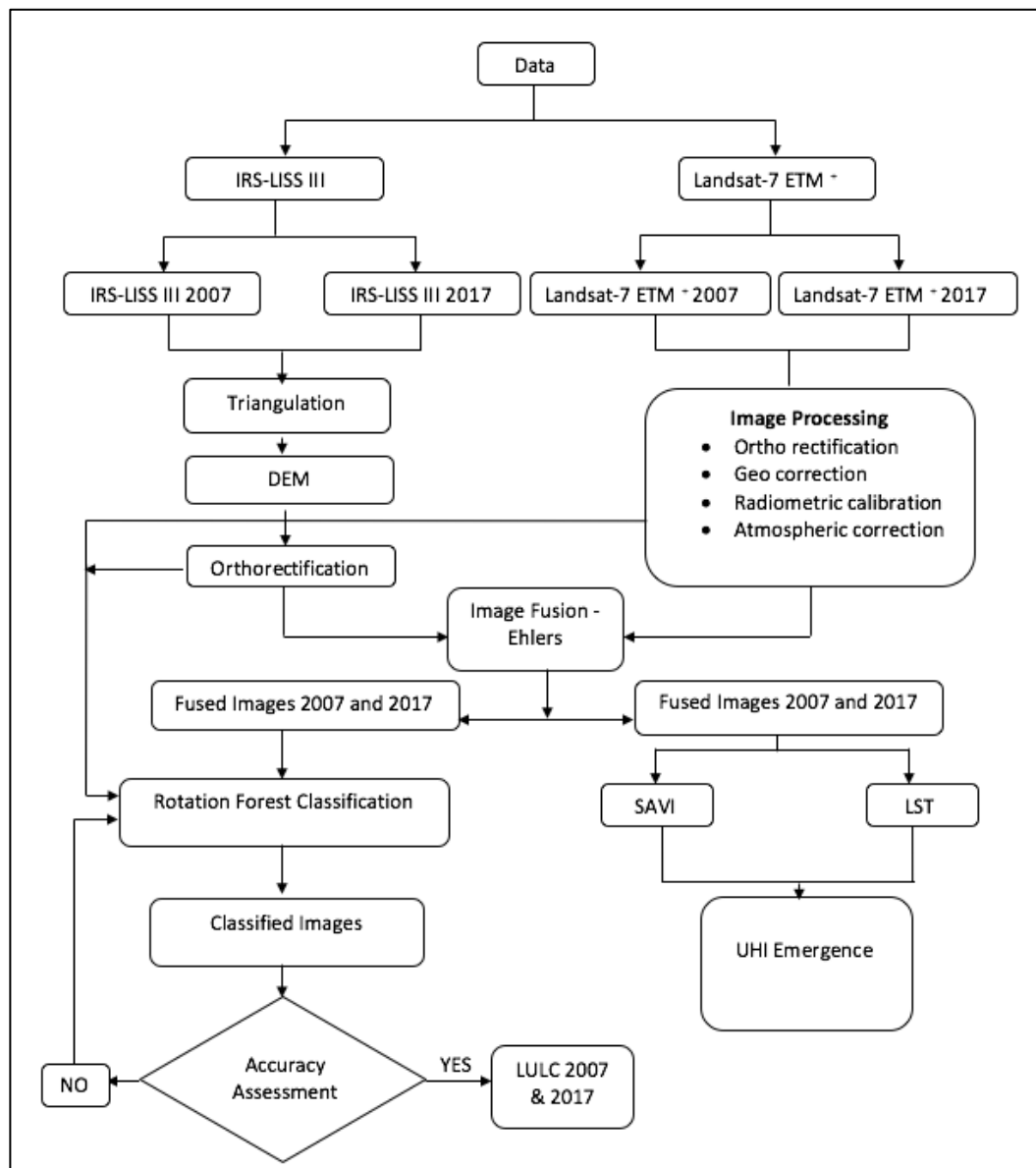


**Figure 4.2.** Methodological flow for landuse and landcover classification, surface permeability, surface temperature and urban heat islands emergence assessment. Fig. legends- DEM: Digital Elevation Model; LULC: Landuse and Landcover; ETM: Enhanced Thematic Mapper; SAVI: Soil-Adjusted Vegetation Index; LST: Land Surface Temperature; UHI: Urban Heat Island.

<sup>39</sup>**Universal Transverse Mercator (UTM)** – UTM coordinate system is a standard set of map projections with a central meridian for each six-degree wide UTM zone [257].

<sup>40</sup>**Digital Elevation Model (DEM)** – DEM is a 3Dimesnional representation of a terrain's surface [179].

#### 4.3.4 Image Classification

We classified the fused images using a Rotation Forest (ROF) machine learning algorithm [258]. Previous studies have demonstrated the higher accuracy levels of ROF than other available methods for fused and non-fused image classification, such as GentleAdaBoost and Random Forest [259]. ROF is based on an ensemble construction and is associated with a Decision Tree (DT), where each classifier is individually constructed [258]. The DT classifier is constructed following a five-fold process: (1) a K subset is randomly split from the feature set. The split subset are intersecting and disjoint, while we chose the disjoint subsets for a high diversity of features; (2) a Principal Component Analysis (PCA) is applied to each of the subsets to identify the variability information in the data; (3) undefined LULC classes are categorized; (4) the regular buoyancy for each class is computed; and (5) the label for each class is allocated to the one with the maximum buoyancy value [258].

We delineated eight LULC classes from the fused images of 2007 and 2017 using RF with the built-in DT classifier (see Table 4.1 for LULC classes definition). The delineation process includes the following steps in R [258] for training the DT classifier and image classification:

1. Build the stack for the fused raster data;
2. Divide the feature data set d into K feature subsets, each subset holds  $M=n/K$  number of feature;
3. Let  $F_{i,j}$  be the jth,  $j=1,...,K$ , subset of features for  $L_i$ , and  $X_{i,j}$  be the features in  $F_{i,j}$  from X;
4. Select new training set from  $X_{i,j}$  randomly using a bootstrap algorithm;
5. Transform  $X_{i,j}$  to get the coefficient  $m_{i,j},..., m_{i,j}$ , the size of  $m_{i,j}$  is  $M * 1$ ;
6. Implement the following sparse rotation matrix  $R_i$ , which is systematized with the above coefficients.

$$R_i = \begin{bmatrix} m_{i,1}, \dots, m_{i,1} & 0 & \dots & 0 \\ 0 & m_{i,2}, \dots, m_{i,2} & \dots & 0 \\ \vdots & \vdots & \ddots & \vdots \\ 0 & 0 & \dots & m_{i,k}, \dots, m_{i,k} \end{bmatrix} \quad (1)$$

7. Rearrange matrix  $R_i$  to  $R_i^a$  with respect to the initial feature set;
8. Train the classifiers in a parallel style;

9. Compute the confidence of the given data  $\chi$  for each landuse class by an average combination method:

$$\mu_K(\chi) = \frac{1}{L} \sum_{i=1}^L \gamma_{i,k}(\chi R_i^a), K = 1, \dots, c \quad (2)$$

Where  $\gamma_{i,k}(R_i^a)$  is the probability produced by  $L_i$

10. Allocate  $\chi$  to the landuse class with the highest confidence.
11. Transform the raster LULC classes into homogenized vector polygons. We selected the classification and regression tree (CART) transformation method, which is based on a decision tree algorithm and Gini index.

$$\text{Gini}(t) = \sum_{i=1}^c p_{wi} (1-p_{wi}) \quad (3)$$

Where  $c$  is the number of LULC classes and  $p_{wi}$  is the probability of class  $w_i$  at node  $t$ .

$$p_{wi} = \frac{n_{wi}}{N} \quad (4)$$

Where  $N$  is the total number of training set samples and  $n_{wi}$  is the number of samples of class  $w_i$

12. Extract the DN values of polygon classes derived from CART;
13. Generate numbers of polygons cohering to the DN values;
14. Allocate color bands to the LULC classes.

We also applied the above image classification algorithm on the non-fused IRS-LISSIII and Landsat ETM+ images of 2007 and 2017 to compare the image classification accuracies between the fused and non-fused images.

---

<sup>41</sup>**Leica Photogrammetry Suite (LPS)** – LPS is a software application for performing photogrammetric operations on imagery and extracting information from imagery [144].

**Table 4.1.** Landuse and landcover (LULC) classes definition.

No	LULC Classes	Definition
1	Barren land	Dry lands and non-irrigated
2	Crop land pasture	Agriculture lands, grazing area, coconut and banana farm
3	Fallow land	Non-plowed, dry farming area and real estate plots
4	Forest	Deciduous forest
5	Scrubs	Bushes and shrubbery
6	Urban	Roads, temples, and built-up areas
7	Water bodies	Rivers, lakes, open water, and ponds
8	Wetland	Marsh, bog, fen and swamp

#### 4.3.5 Accuracy Assessment

We assessed and compared the accuracy of classification between the fused and non-fused images of 2007 and 2017 [160]. Cartographic map of 2007 and classified Google Earth images of 2017 (as cartographic map wasn't available) of the Tirunelveli city obtained from BHUVAN, ISRO India and Google Earth Engine (GEE), respectively, were used as reference images (ground truth) for the accuracy assessment of the classified LULC maps and comparison between the fused and non-fused images [260]. 75 Random pixels were generated from the classified LULC data and LULC values were extracted for those pixels for 2007 and 2017. Then, the LULC values were identified for the same pixels in the referenced images and compared with the LULC values of classified images. We employed the kappa coefficient as the accuracy indicator [160]. A kappa coefficient of more than 0.8 indicates a satisfactory accuracy of LULC maps, i.e., classified images are satisfactorily analogous to the reference data [261]. Kappa coefficients were computed for the classified fused and non-fused images in ERDAS Imagine (version 8.7) and compared. We also computed the producer and user accuracies of image classification through a confusion matrix [160].

#### 4.3.6 Surface Permeability Assessment

We computed Soil-Adjusted Vegetation Index (SAVI) to assess the changes in surface permeability in Tirunelveli between 2007 and 2017. Generally, SAVI indicates vegetation

coverage and health with respect to soil moisture, saturation and color, and thus accounts for the high variability of built-up and non-built-up land cover in urban areas [121,262]. SAVI also controls for the influence of soil brightness in Normalized Difference Vegetation Index (NDVI) and thus, minimizes soil brightness-related noise in vegetation coverage estimation [263]. Since coverage, brightness and health of vegetation are strongly associated with surface permeability, SAVI provides an important proxy for the identification of impermeable surfaces, particularly in urban areas [237]. We calculated SAVI using equation (5) [264].

$$SAVI = \frac{(NIR - RED)}{(NIR + RED + L)} * (1 + L) \quad (5)$$

Where, RED is the reflectance of the band 3 (RED band) and NIR is the reflectance value of the near infrared band (Band 4). L is the soil brightness correction factor. For dense vegetation and highly permeable surface areas, L=0 and for vegetation scarce and impermeable surface areas, L=1 [263]. Due to high dynamics of vegetation and built-up coverage in Tirunelveli (urban areas in general), L was set to 0.5 [264].

SAVI was computed for each pixel of the fused images from 2007 and 2017. We delineated five raster zones based on natural breaks in SAVI values of the pixels to distinguish among degrees of surface permeability, e.g. 0.54–1 and –1–0.08 zones indicated highly permeable surface with high density healthy vegetation and impermeable surface with low density unhealthy or no vegetation (mostly barren and fallow land, and built-up surfaces), respectively. We computed the area coverage of each soil permeability zone in 2007 and 2017 and calculated percentage changes in their coverage between 2007 and 2017. Areal average and standard deviation of SAVI were also computed for each LULC class in 2007 and 2017.

#### ***4.3.7 Land Surface Temperature Measurement***

We calculated Land Surface Temperature (LST) index for each pixel of the fused images from 2007 and 2017 to measure the radiative skin temperature of the surface and its features, which depends on the optical brightness and reflectance of the surface (Albedo) [27]. Generally, bare soil and built-up settlements with low SAVI exhibit high Albedo whereas dense vegetation with high SAVI exhibits low Albedo and hence, low radiative skin temperature [265]. Thus,

LST indicates climatic variability across vegetation and urban settlements associated with the degree of surface permeability [266]. LST for each pixel was calculated using equation (6) according to the Landsat user's hand book, in which the digital number (DN) of thermal infrared band is converted into spectral radiance ( $L\lambda$ ) [213,267].

$$L\lambda = \{LMAX - LMIN \div QCALMAX - QCALMIN\} * DN - 1 + LMIN \quad (6)$$

Where,

$LMAX$  = the spectral radiance that is scaled to  $QCALMAX$  in  $W/(m^2 * sr * \mu m)$

$LMIN$  = the spectral radiance that is scaled to  $QCALMIN$  in  $W/(m^2 * sr * \mu m)$

$QCALMAX$  = the maximum quantized calibrated pixel value (corresponding to  $LMAX$ ) in DN  
= 255

$QCALMIN$  = the minimum quantized calibrated pixel value (corresponding to  $LMIN$ ) in DN  
= 1

Raster maps of the LST index were computed for 2007 and 2017 from the fused satellite images and compared to assess changes in surface radiant temperatures in Tirunelveli between 2007 and 2017. To be coherent with SAVI classes, we delineated five LST raster zones based on natural breaks and computed their area coverage in 2007 and 2017. The average and standard deviation of LST for each LULC class were also computed. We also quantified the association between surface permeability and temperature through a Spearman raster correlation analysis between SAVI and LST for entire Tirunelveli also for the classified LULC zones.

#### ***4.3.8 Emergence Potential for Urban Heat Islands***

We quantified the emergence potential of Urban Heat Islands (UHI) in Tirunelveli using a combined metric computed from LST and SAVI in 2017 [230]. Generally, impermeable surface areas with lower SAVI exhibit higher solar radiation absorption, and a greater thermal capacity and conductivity, and consequently exhibit higher potential for UHI emergence, and vice-versa [25,227]. Moreover, areas with high surface temperature (LST) exhibit higher number of daily high degree-hours and lower differences between daily maximum and minimum temperatures, and thus also exhibit higher potential for UHI emergence, and vice-versa [268]. Hence, we first coded the five SAVI and LST classes from 1 to 5 in descending and

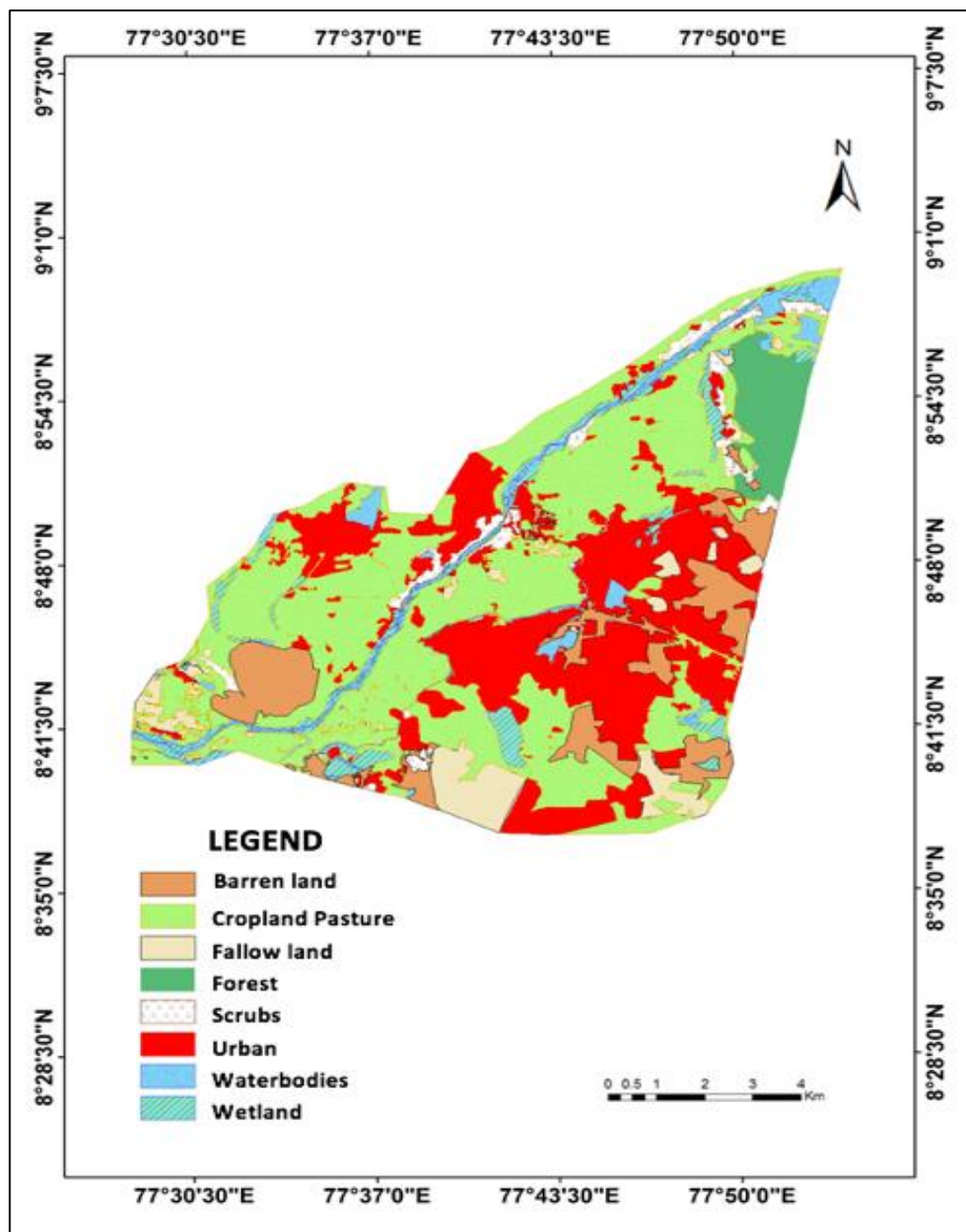
ascending orders, respectively. Subsequently, we sum aggregated the recoded SAVI and LST class values for each pixel to compute the combined metric for UHI emergence potential. Pixels with higher combined UHI metric value indicated higher potential for UHI emergence and vice-versa. Finally, we delineated the zones with high UHI emergence potential in Tirunelveli.

## 4.4 Results and Discussion

### 4.4.1 Landuse and Landcover Changes

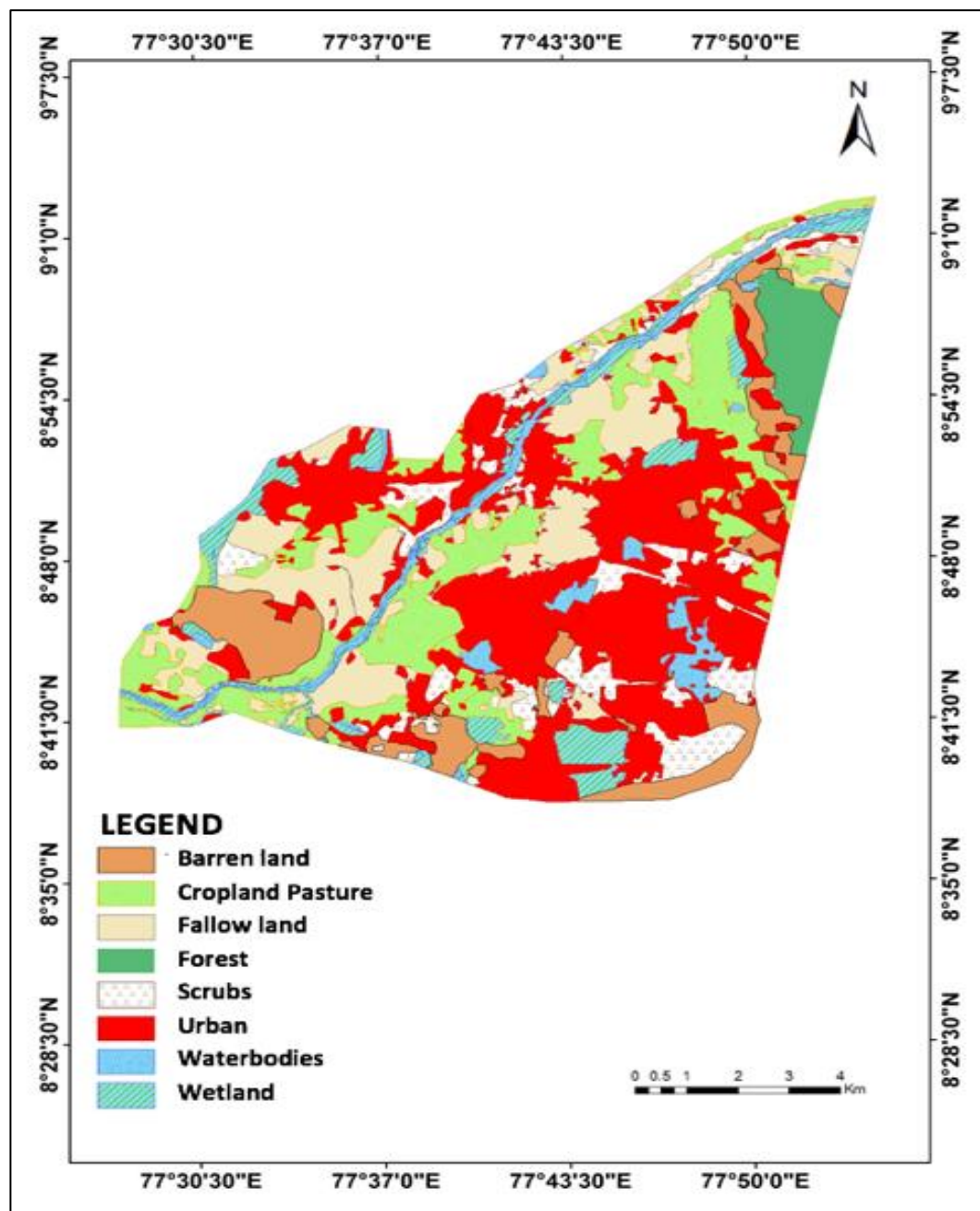
The LULC maps of 2007 and 2017 show that the Tirunelveli city has undergone a rapid urbanization at an average rate of 4% between 2007 and 2017, with a 32% total increase in the coverage of urban built-up areas (Figure 4.3, Table 4.2). Fertile cropland pastures have been substantially converted (59% decline between 2007 and 2017) into fallow lands (mostly real estate plots, 178% increase between 2007 and 2017) and fallow lands (transitioning into built-up areas, 6% increase between 2007 and 2017). Forested areas in the North-eastern part of the city decreased by 12% whereas the bushes and shrubbery covered infertile areas increased by 164% throughout the city between 2007 and 2017. The Western riparian part of the city has undergone the most expensive LULC conversion from cropland pasture to fallow lands and built-up areas (Figure 4.3), which is in line with the findings of CARDS [245]. Although the wetland and waterbodies showed an aggregate increase by 35% between 2007 and 2017, forest cover and vegetation exhibited substantial decrease and conversion into urban areas (Figure 4.3, Table 4.2). These results are in line with [58], which estimated a rapid urbanization and urban sprawl in the Tirunelveli city between 2007 and 2017.





(a)

Figure 4.3. Classified landuse and landcover (LULC) maps of Tirunelveli city in 2007



(b)

**Figure 4.3.** Classified landuse and landcover (LULC) maps of Tirunelveli city in 2017

**Table 4.2.** Change in the area coverage of the landuse and landcover (LULC) classes between 2007 and 2017.

Classes	2007 (km <sup>2</sup> )	2017 (km <sup>2</sup> )	Change (%)
Barren land	10.07	10.69	6.15
Cropland pasture	45.42	18.43	-59.42
Fallow land	5.79	16.11	178.23
Forest	1.78	1.56	-12.35
Scrubs	3.37	8.89	163.79
Urban	27.85	36.73	31.88
Water bodies	3.84	4.25	10.67
Wetland	6.08	7.54	24.01
<b>Total</b>	<b>104.2</b>	<b>104.2</b>	

We obtained kappa coefficient values of 0.84 and 0.83 with an overall accuracy value of 86% and 85% for the LULC classification for 2007 and 2017, respectively, using fused images (Table 4.3). In contrast, the average kappa coefficient and overall accuracy values for LULC classification using non-fused images for 2007 and 2017 were considerably lower, i.e. 0.72 and 0.75, 71% and 74%, respectively. Hence, the accuracy of LULC classification using fused images was considerably higher than the LULC classification using non-fused images because of the substantially higher spatial resolution and number of bands available in fused images than non-fused images [236]. These results are also in line with [235].

**Table 4.3.** Accuracy assessment results for the landuse and landcover classification using fused images of 2007 and 2017.

Classes	2007		2017	
	Producer	User	Producer	User
	Accuracy	Accuracy	Accuracy	Accuracy
Barren land	82.01	83.12	87.12	86.20
Crop land and pasture	84.15	87.14	82.56	83.21
Fallow land	82.34	89.16	87.32	92.35
Forest	84.15	90.12	84.51	87.18
Scrubs	88.11	84.21	83.15	82.13
Urban	91.32	89.34	88.29	96.07
Waterbodies	85.21	87.43	79.45	81.32
Wetland	89.01	91.03	84.56	89.04
Overall accuracy	85.75		84.62	
Kappa	0.84		0.83	

#### 4.4.2 Changes in Soil Permeability and Surface Temperature

We observed a substantial decrease (58% on average) in the area coverage of permeable surfaces (SAVI values 0.08-1) while a substantial increase (33% on average) in the area coverage of impermeable surfaces (SAVI values -1-0.08) in Tirunelveli between 2007 and 2017 (Figure 4.4 and Table 4.4). The riparian zone at the Western part of Tirunelveli, which experienced the most extensive LULC conversion (Figure 4.3), also undergone the highest decline in highly and medium permeable surfaces (SAVI values 0.34-1) with dense vegetation between 2007 and 2017, i.e., the average SAVI value decreased from 0.54 to 0.08 (Figure 4.4). In general, the highly (SAVI 0.54-1) and medium (0.34-0.54) permeable zones undergone the highest decline, i.e. more than 87%, in Tirunelveli between 2007 and 2017 (Figure 4.4 and Table 4.4). Conversely, impermeable surface zones (SAVI values -1-0.08) exhibited a substantial increase, mostly around the built-up Southeastern part of Tirunelveli.

Generally, we observed high areal average SAVI values, i.e. high surface permeability, for the LULC zones with vegetation cover, e.g. cropland and scrubs, in contrast to the low SAVI values for built-up LULC areas, e.g. urban and barren land (Table 4.5). The average SAVI values for all LULC zones decreased between 2007 and 2017 apart from the Wetlands (Table 4.5). The highest average changes in SAVI values were observed for the barren and fallow lands (Table 4.5). Fallow land also represents the LULC class that has undergone the highest transition (178%) into real estate plots and built-up areas, i.e. urbanization (Table 4.2). This indicates that the extensive urbanization has adversely affected the soil permeability in Tirunelveli between 2007 and 2017, which is in line with [262]. Although the area coverage by water bodies has increased by 11% between 2007 and 2017 (Table 4.2), the permeability of the surface beneath also decreased for this LULC class (Table 4.5), indicating marginal or no improvement of soil permeability through anthropogenic development of water courses [263].

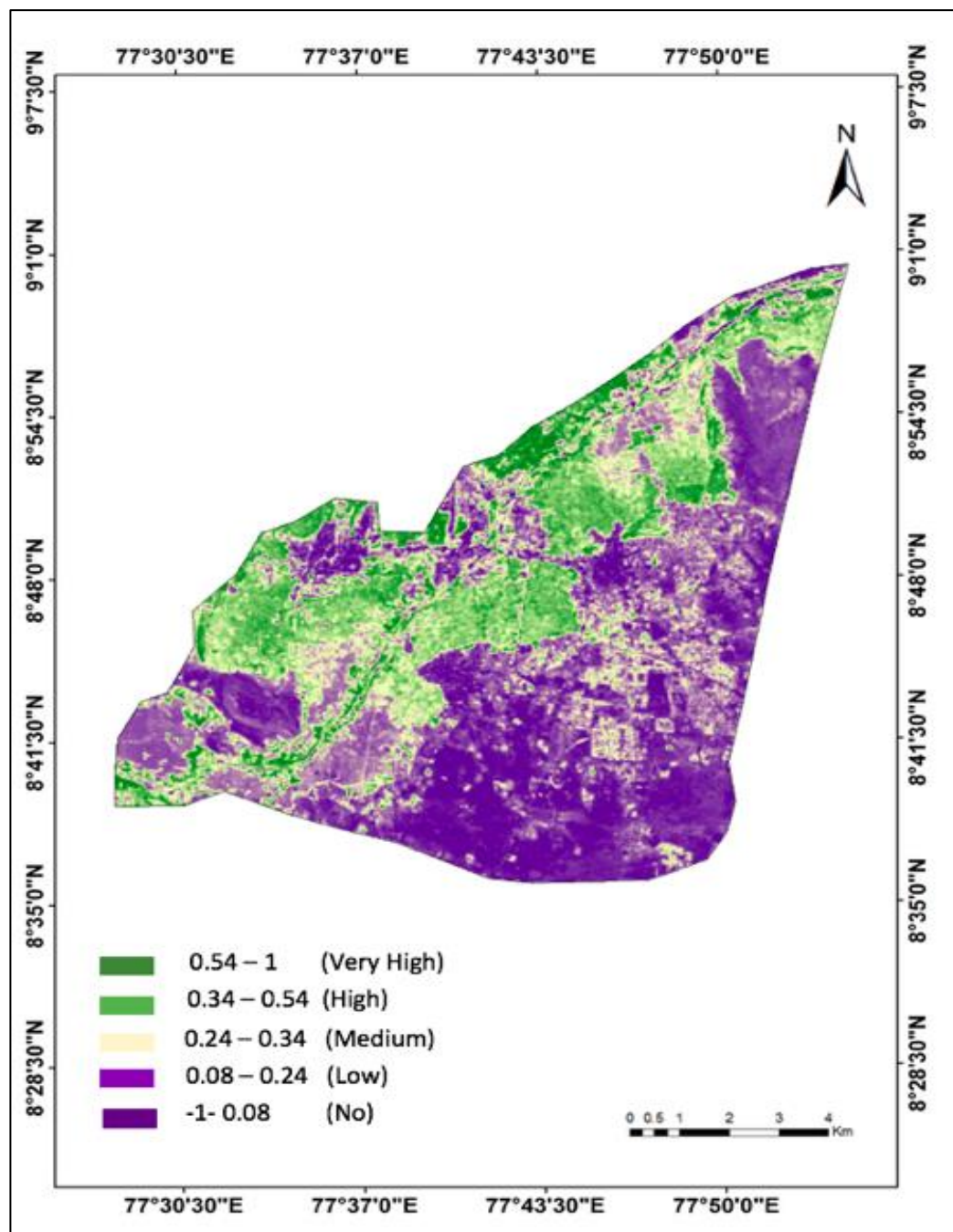
The overall climatic impact of extensive LULC conversion and decrease in surface permeability was evident by an average increase of LST by  $1.3^{\circ}\text{C}$  in Tirunelveli city between 2007 and 2017 (Figure 4.5 and Table 4.6). Particularly, the Western riparian zone, which has undergone the highest conversion of LULC and highest decrease in SAVI, also experienced the highest increase in LST, i.e.  $4^{\circ}\text{C}$  on average from  $28^{\circ}\text{C}$  to  $32^{\circ}\text{C}$ , between 2007 and 2017 (Figure 4.5 and Table 4.6). LST zone  $30\text{--}32^{\circ}\text{C}$  exhibited the highest increase in area coverage (165%) whereas the highest decrease was observed for the coverage of LST zone  $26\text{--}28^{\circ}\text{C}$  (64%) (Table 4.6). Overall, the low temperature zones ( $26\text{--}30^{\circ}\text{C}$ ) showed a decreasing coverage whereas the high temperature zones (more than  $30^{\circ}\text{C}$ ) exhibited an increasing coverage in Tirunelveli between 2007 and 2017 due to extensive LULC conversion and surface permeability deterioration (Table 4.6), which is also in line with [267].

In general, we detected higher LST values for the LULC zones with lower vegetation cover, e.g. barren and fallow land, and urban built-up areas, and with lower surface permeability (lower SAVI), and vice-versa, which is in line with [213] (Table 4.7). The highest areal average LST of above  $34^{\circ}\text{C}$  was observed for the urban built-up areas and barren lands in 2007, which has increased to above  $36^{\circ}\text{C}$  in 2017. In contrast, the lowest areal average LST of below  $27^{\circ}\text{C}$  was observed for croplands, fallow lands, water bodies and wetlands in 2007, which has also

increased to below 28°C in 2017. The highest increase in areal average LST, i.e. 2.4°C, was observed for the urban area and barren lands (Table 4.7). Areal average LSTs of wetland and waterbodies also exhibited an increase of 1°C between 2007 and 2017 (Figure 4.4, 4.5 and Table 4.7). Moreover, the deciduous forest area exhibited a decrease (0.03) and an increase (0.3°C) in the areal average SAVI and LST, respectively, between 2007 and 2017, indicating the adverse impact of overall rapid and extensive urbanization in Tirunelveli (Table 4.5 and 4.7).

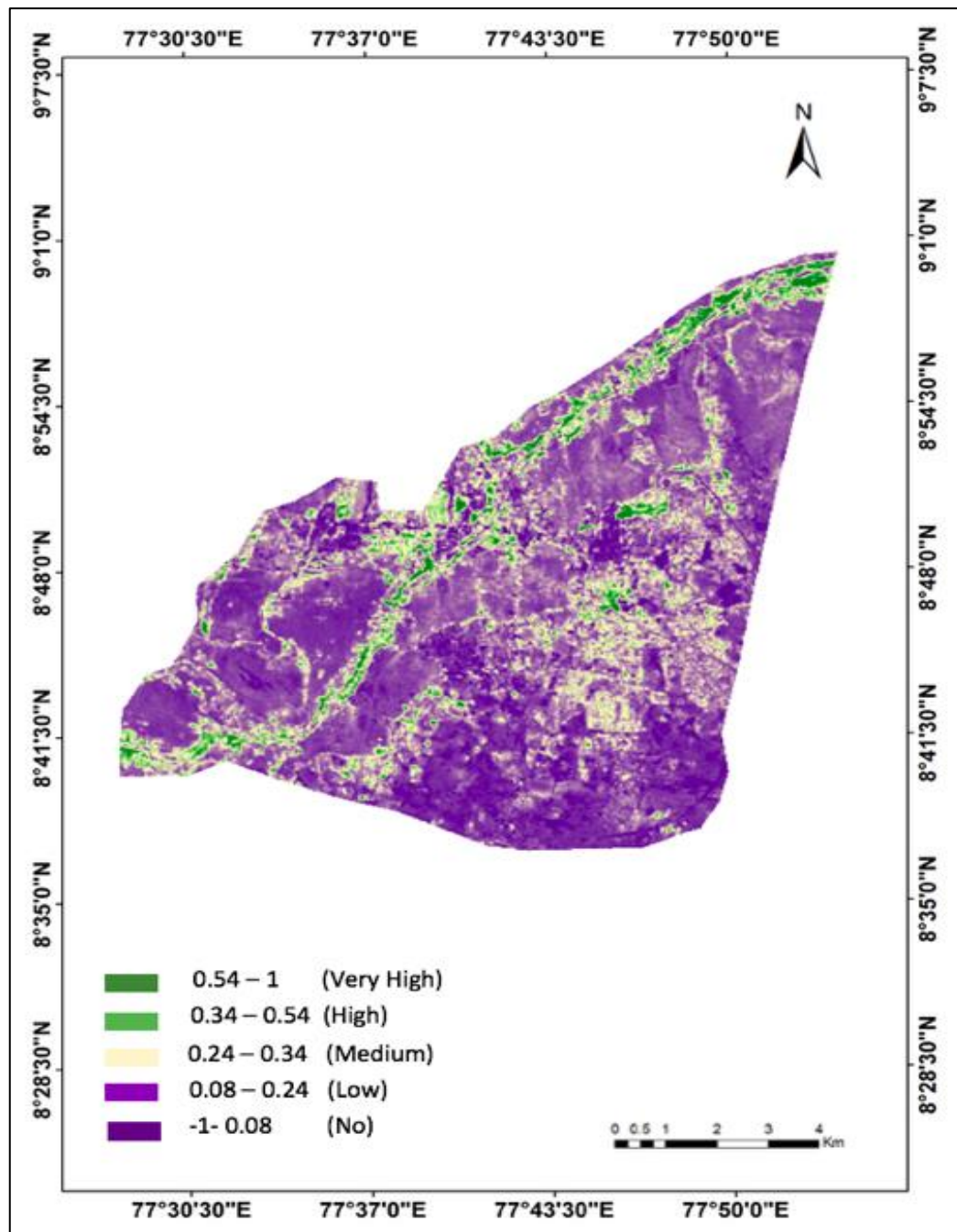
Note that we obtained lower SAVI (lower surface permeability) and higher LST (higher surface temperature) values for the forested area at the North-eastern part of Tirunelveli than other vegetated areas, i.e. cropland pastures and scrubs (Table 4.5 and 4.7). This is because the deciduous forest of Tirunelveli sheds its leaves completely during summer (March - June) [241]. During this season, the surface of the dry forest receives the least precipitation with no other sources of irrigation, and absorbs the highest solar radiation with the highest temperature of the year [269]. Consequently, this dry deciduous forest area exhibits relatively lower surface permeability and higher surface temperature than other vegetated areas during July in our study (Figure 4.4 and 4.5, Table 4.5 and 4.7). Similar climatic responses of deciduous forest were observed in summer by other studies investigating impacts of climatic changes on forests [269]. Nevertheless, this deciduous forest area exhibited a decrease (0.03) and an increase (0.3°C) in the areal average SAVI and LST, respectively, between 2007 and 2017, indicating the adverse impact of overall rapid and extensive urbanization in Tirunelveli (Table 4.5 and 4.7), which is in line with [231].





(a)

**Figure 4.4.** Soil-Adjusted Vegetation Index (SAVI) (surface permeability) maps of the Tirunelveli city in 2007.



(b)

**Figure 4.4.** Soil-Adjusted Vegetation Index (SAVI) (surface permeability) maps of the Tirunelveli city in 2017.

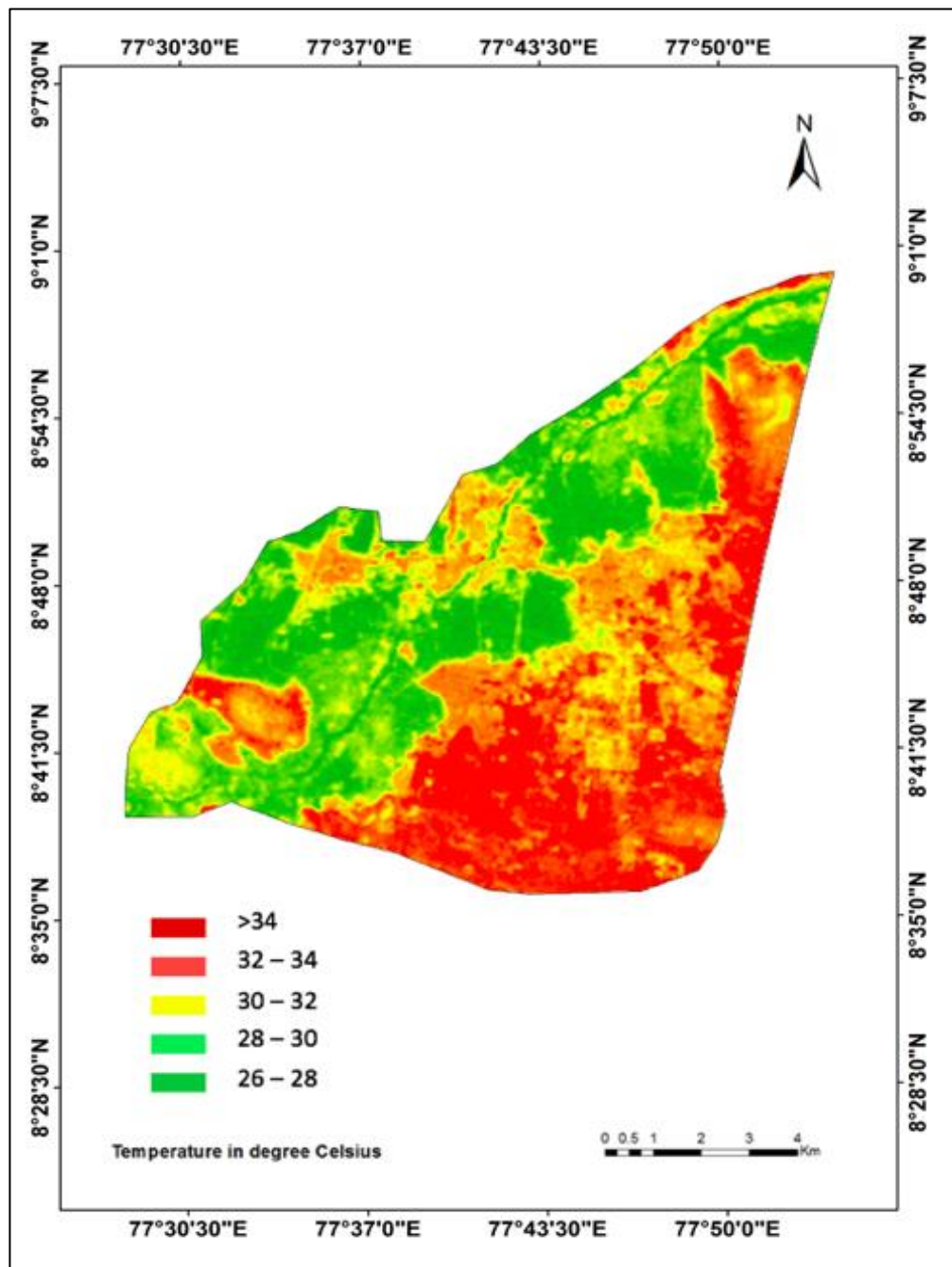


**Table 4.4.** Changes in the coverage of soil permeability (indicated by soil-adjusted vegetation index (SAVI)) classes in Tirunelveli between 2007 and 2017.

SAVI Classes	Surface permeability	Total Area Coverage (Km <sup>2</sup> )		Change in area coverage (%)
		2007	2017	
0.54-1	Very high	12.6	1.64	-86.98
0.34-0.54	High	8.34	0.87	-89.56
0.24-0.34	Medium	5.67	3.13	-44.79
0.08-0.24	Low	11.76	10.54	-10.37
-1-0.08	No	68.15	90.34	32.56

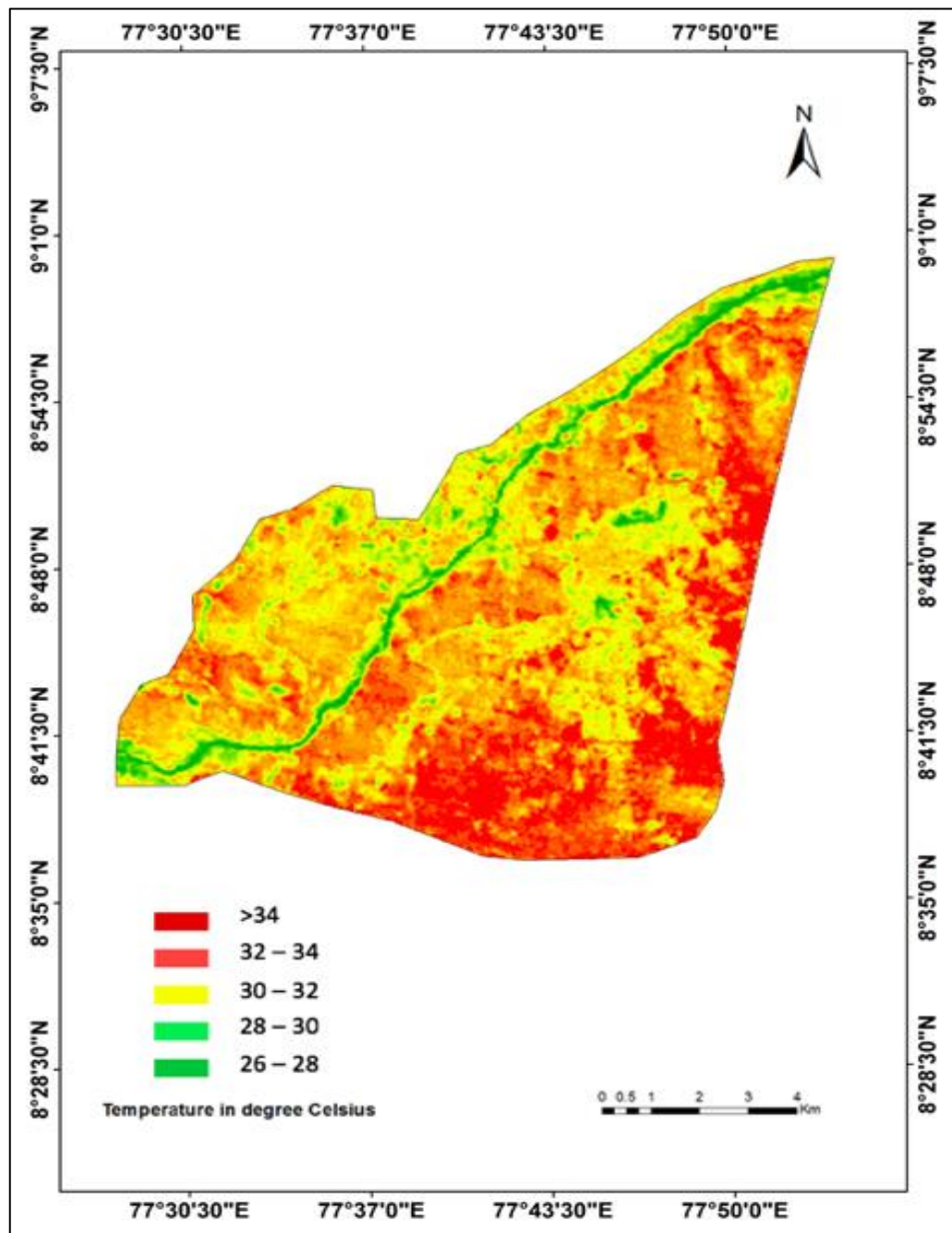
**Table 4.5.** Areal average SAVI values for the LULC zones.

LULC zones	2007	Standard deviation (±)	2017	Standard deviation (±)
Barren land	0.09	0.59	-1	0.70
Cropland pasture	0.42	0.13	0.29	0.08
Fallow land	0.08	0.48	-1	0.61
Forest	0.24	0.03	0.21	0.04
Scrubs	0.54	0.14	0.34	0.12
Urban	0.16	0.10	0.08	0.19
Waterbodies	0.97	0.24	0.54	0.37
Wetland	0.24	0.11	0.34	0.17



(a)

Figure 4.5. Land Surface Temperature (LST) maps of the Tirunelveli city for 2007.



(b)

Figure 4.5. Land Surface Temperature (LST) maps of the Tirunelveli city for 2017.

**Table 4.6.** Statistics of the area between 2007–2017 with corresponding changes in LST.

LST Classes (°C)	Area Coverage (km <sup>2</sup> )		Change in area coverage (%)
	2007	2017	
26 - 28	28.46	10.21	-64.12
28 - 30	19.97	7.21	-63.89
30 - 32	10.43	27.69	165.48
32 - 34	14.77	18.20	23.22
>34	30.57	40.89	33.75

**Table 4.7.** Average land surface temperature (LST) in degrees Celsius by landuse and landcover cover (LULC) zones.

LULC zones	2007	Standard deviation (±)	2017	Standard deviation (±)
Barren land	34.106	5.32	36.604	7.92
Cropland pasture	26.861	5.89	27.112	6.32
Fallow land	34.127	3.21	35.821	6.87
Forest	32.153	3.15	32.462	3.91
Scrubs	26.242	6.13	27.357	7.44
Urban	34.196	1.11	36.620	2.73
Water bodies	26.824	6.98	27.868	8.03
Wetland	26.291	8.44	27.731	9.34

#### 4.4.3 Urban Heat Islands Emergence

We observed a negative correlation between LST and SAVI overall, as well as by the LULC zones (Table 4.8). The overall correlation coefficients obtained for entire Tirunelveli in 2007

and 2017 were -0.24 and -0.72, respectively (both statistically significant at  $p \leq 0.01$ ). Urban built-up areas exhibited the highest correlation coefficients in 2007 and 2017, along with the highest increase in correlation coefficient values (Table 4.8). In general, LULC zones with lower surface permeability exhibited higher correlation coefficient values, and vice-versa. This indicates that a decrease in surface permeability entails an increase in surface temperature [266] and hence, exhibit a high potential for the emergence of UHIs [270].

The emergence potential for UHI was high for the Eastern periphery of Tirunelveli in 2017 with the highest potential for the urban built-up areas at the Southeastern part (Figure 4.6). The Western riparian zone, which has undergone the highest LULC transition from cropland to barren and fallow lands, and urban built-up areas, also exhibited high emergence potential for UHI (Figure 4.6). Consequently, we suggest the Southeastern built-up areas in Tirunelveli as a potential UHI hotspot, while a caution for the Western riparian zone for UHI emergence that requires continuous and detailed monitoring. The waterbodies and wetlands, however, showed the lowest potential for UHI emergence, proving the importance of including waterbodies and greenspaces into urban planning to prevent the emergence of UHI [266].

Note that our analysis is limited to daytime imageries due to the unavailability of nighttime imageries and hence, did not measure nighttime temperature to determine the difference between minimum and maximum surface temperatures. This might affect the accuracy of UHI emergence detection using our SAVI-LST metric. However, since ours is a study on surface temperature and not air temperature, the variation between daytime and nighttime temperatures is marginal due to nighttime surface radiation [267]. Moreover, we used SAVI as an additional surrogate of LST, which provided important proxies for mean, range and variance of surface temperatures [262]. Furthermore, previous studies accurately detected and delineated UHIs based on only daytime imageries [230,239,271]. Hence, we suggest that our SAVI-LST metric is sufficiently robust for detecting UHIs emergence although nighttime imageries should be included when available.

**Table 4.8.** Spearman correlation between soil-adjusted vegetation index (SAVI) and land surface temperature (LST) by landuse and landcover (LULC) zones. All correlation coefficients are statistically significant at  $p \leq 0.01$ .

LULC zones	Correlation coefficients		<i>p</i> -values
	2007	2017	
Barren land	-0.19	-0.25	0.0023
Cropland pasture	-0.11	-0.21	0.0049
Fallow land	-0.17	-0.27	0.0031
Forest	-0.07	-0.13	0.0012
Scrubs	-0.11	-0.13	0.0015
Urban	-0.29	-0.52	0.0062
Water bodies	-0.14	-0.16	0.0017
Wetland	-0.13	-0.25	0.0037

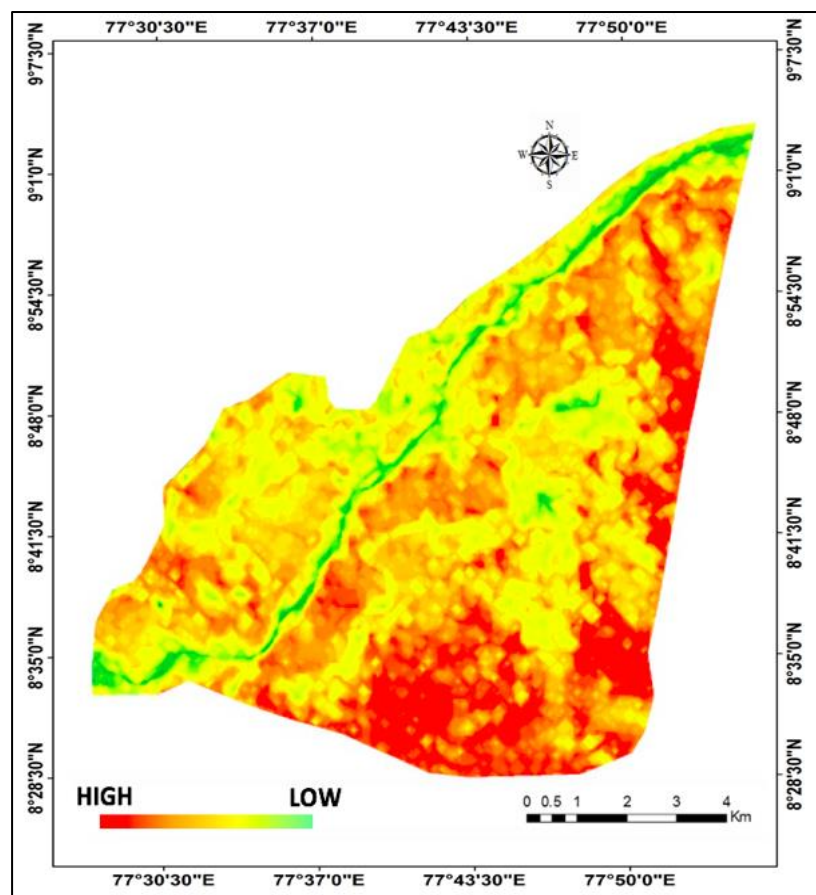


**Figure 4.6.** UHI emergence potential map of Tirunelveli city for 2017.

#### 4.5 Concluding Remarks

We demonstrated the advantage of using fused satellite imageries combining multiple sensors in detecting and monitoring changes in land surface permeability and temperature and emergence of Urban Heat Island (UHI) in fast growing cities like Tirunelveli. Future studies should fuse higher temporal and spectral resolution imageries than the ones used in our study to provide a continuous, seasonal and more detailed assessment of Landuse and Landcover (LULC), Soil-Adjusted Vegetation Index (SAVI) and Land Surface Temperature (LST) changes, and UHI emergence in Tirunelveli [230].

The UHI emergence potential, which was computed by aggregating SAVI and LST provide important metrics for the identification and quantification of UHI zones. These metrics can be integrated in sophisticated UHI detection models for a more accurate and precise identification and quantification of UHI [271].

We suggest that urban landuse measures and zonal planning should be informed by detailed and continuous RS and GIS based assessment of LULC, SAVI and LST [121,265]. Possible measures include the conservation of agriculture and forested lands, and proper management of the reclamations of barren lands to pasture lands to avoid the decrease in surface permeability and ecosystem fragmentation [272]. Urban expansion should include provision of water bodies and afforestation to preserve surface moisture, permeability and radiative capacity, and thus to prevent the increase in surface temperature [25].



## Chapter - 5

What drives a Mangrove degradation?



*"Humanity is cutting down its forests, apparently oblivious to the fact that we may not be able to live without them"*

***Isaac Asimov***

## Chapter 5

### What Drives Mangrove Degradation?

---

#### 5.1 Introduction

The tropical and subtropical climate regions of the world comprise intertidal mangrove swamps forming an unique interface between estuaries, terrestrial and marine ecosystems with enriched biodiversity composed of different species of flora and fauna of which millions people depend upon [273–276]. Mangroves provide unique and valuable provisioning (e.g. aquaculture, fisheries, fuel, medicine, textiles), regulating (e.g. shoreline protection, erosion control, climate regulation), supporting (nutrient cycling, nursery habitat), and cultural (recreation and tourism) ecosystem services [273]. It is estimated that 10 to 15% of coastal sediment retention and carbon storage are due to the global mangrove forest [183]. These values are five times greater than those of tropical forest when including other coastal wetlands [83,277,278]. Mangrove forest acts as an environmental barrier between shore and land from the impact of extreme events, such as hurricanes, storms and tsunamis [279–284].

The mangrove forests are mainly existing in eighteen countries which are Brazil, Mexico, Australia, India, Bangladesh, Indonesia, Nigeria, Malaysia, Papua New Guinea, Colombia, Nigeria, Myanmar, and Cuba, and less importantly in other countries, such as Thailand, Mozambique, Philippines, Guinea-Bissau, and Vietnam. In total, it is estimated that the mangroves forest cover a total area of approximately 150,000km<sup>2</sup> [283,285,286]. Southeast Asia contains about 35% of the mangroves found on earth [283], and has been the site of several mangrove preservation, management, and assessment studies [287]. There are about 50 to 60 known species of mangrove in the world [288], and 35 of these are in the Philippines [273].

The mangrove species in tropical environments are facing major habitat degradation at an alarming rate, possibly even more rapidly than non-coastal tropical forests [74,75]. About 35% of the mangrove forest area has vanished during the past 20 years, and much of the leftovers is in a degraded state [76,77]. This is mainly due to climatic changes and human activities, which cause major alterations over the coastal ecosystem, mostly through deforestation,

agriculture, aquaculture, and urban development [78–83]. Globally, there are many mangrove species identified at risk of extinction, which leads to a tremendous loss of several ecosystem functions, especially in Asia where over-exploitation of mangrove is reported [84,85].

There are several threatened species (*Rhizophora samoensis*, *Conocarpus erectus* and *Avicennia germinans*) found at the Pacific coast and Colombia [289,290]. Another species called *Heritiera fomes*, which protects the coastal land from erosion, salt water intrusion, storms, high tides and floods, is widely available in South Asia and has experienced an extensive decline since the 1990s, which reduces the potential for protection [291]. For instance, Muthurajawela Marsh in Sri Lanka, the water purification processed by this mangrove species were valued in more than 1.8 million (US\$) per year [292]. West Africa and Central Pacific Island are covered by only two species (*Aegicera floridum* and *sonneratia griffithii*), which are globally wide spread species facing regional and local loss [293,294].

Mangrove forest rehabilitation activities have been gradually increasing in different regions especially in Asian countries, such as Indonesia, Bangladesh, Brazil, the East African region and China widely concentrating on mangrove restoration and reforestation, which brings increasing mangrove area and helps to revive fisheries' habitats, ecological restoration, and other forestry purposes [295,296]. But in some cases, it's not viable to restore the mangrove coastal ecosystem [297].

The restoration process of mangroves always needs careful consideration of several factors. One of the main factors which was considered in several studies suggested to identify the distribution of existing and former mangrove forest area [297]. Analyzing the variations to the coastal hydrology which may cause the degradation of mangrove forest and identified the existing watershed can also be considered as the main factor for the restoration process [296]. The study about the temporal changes about the mangrove site is also needed to decide the restoration site selection by considering the several environmental drivers in mangrove forest degradation. Additionally, various parameters have been considered for afforestation site selection including soil characteristics, tidal currents, site stability, depth of the water and fresh water existence [298]. However, efficient policies, an important subject on global drivers, are needed to identify and protect the mangrove forest from further degradation [299].

The monitoring of the distribution and changes in mangrove populations at global and regional scales has been carried out with Remote Sensing (RS) methods [86–90] using different types of data, varying from airborne data (e.g. LiDAR, <sup>42</sup>Radar) to space borne images (e.g. medium and high resolution data) [300], or from <sup>43</sup>hyper-spectral imaging to <sup>44</sup>microwave data [301–304]. These studies enabled the investigation of the human interference on mangroves through the analysis of land use landcover changes (LULCC), at regional and global scales [91]. Additionally, research has been employed to identify several drivers on a regional level, which is geographically limited to small case studies [92–98]. However, such LULCC studies do not allow to detect the drivers of mangrove degradation at the global scale [99]. Thus, identifying the global drivers of mangrove habitat loss is still challenging [100].

In this paper, we review and assess up-to-date information on anthropogenic and environmental drivers of the mangrove degradation, and the causes of disturbance over its ecosystems. First we discussed the global spatial distribution and changes in the mangrove forest. Subsequently we deliberated the identified drivers on mangrove degradation.

## 5.2 Methods

### 5.2.1 Document Search and Categorization

In order to collect different information about mangroves, we followed a detailed search approach related with important functional keywords using two electronic journal sources, <sup>45</sup>Scopus and Web of Science <sup>46</sup>(WOS).

---

<sup>42</sup>**Radar** – Radar is a detection system that uses radio waves to determine the range, angle, or velocity of objects [305].

<sup>43</sup>**Hyperspectral imaging** – Hyperspectral imaging is the spectral imaging process which collects information from across the electromagnetic spectrum. It is used to obtain the spectrum for each pixel in the image of a scene, with the purpose of finding objects, identifying materials, or detecting processes [253].

<sup>44</sup>**Microwaves** – Microwaves are a form of electromagnetic radiation with wavelengths ranging from about one meter to one millimeter; with frequencies between 300 MHz and 300 GHz [306].

We considered all documents published from 1<sup>st</sup> January 1980 to 30<sup>th</sup> December 2018. A total of 231 articles were found using these search terms for the 3 considered categories: status and distribution, drivers, and impacts of degradation (Table 5.1).

**Table 5.1.** List of the combination of mangrove relevant keywords and number of studies considered.

Mangroves	Keywords	Number of studies		Total number of studies
		WOS	Scopus	
<b>Status and Distribution</b>	Global distribution	5	6	11
	Mangrove biomass	6	3	9
	Mangrove species	3	4	7
	Mangrove ecosystem	2	7	9
<b>Drivers</b>	Changes in climate	15	11	26
	Extreme events	20	25	45
	Land changes	19	21	40
	Pollution	12	15	27
	Water flow modification	12	10	22
<b>Impacts of degradation</b>	Ecosystem and Biodiversity changes	3	4	7
	Loss on nutrient cycling and nursery habitat	2	5	7
	Declining raw product	4	3	7
	Loss on natural barriers	1	1	2
	Lost on carbon sequestration	2	4	6
	Influence on culture, tourism and trade	1	5	6
<b>Total number of papers</b>		<b>107</b>	<b>124</b>	<b>231</b>

### 5.2.2 Data Interpretation and Analysis

A database of research studies was built and analyzed to assess the dynamics of research providing an updated overview of the status and distribution, drivers, and impacts of mangrove degradation. Geographical Information System's <sup>47</sup>ArcGIS software [307] was used to map the distribution of the research studies found on mangrove.

## 5.3 Results

### 5.3.1 Global Distribution of Mangrove Forest

The mangrove regions covered in this study as well as the number of studies used are shown in Figure 5.1. A great part of the research papers found were related to Asian countries, which had a high rate of mangrove loss in the last three decades (see Table 5.2) [308,309]. To understand the spatial distribution of global mangrove forest, we assessed a total of 36 studies. Recent studies measured the global total mangrove cover for year 2000 in about 137,760km<sup>2</sup> for 118 countries [310].

However, this estimation differs from the recent valuation by the <sup>48</sup>FAO and other related mangrove cover evaluations (Figure 5.2). An assessment of the rate of mangrove spatial distribution and transformation has differed since the 1980s [310]. This inconsistency may be associated with methodological approaches used in the analyses which depend on the countries covered, degradation level, afforestation activities, and also due to the coarse resolution of satellite imagery [285,310].

Mangroves are mostly situated in equatorial regions, geographically in the tropical and sub-tropical region between 30° N and 30° S [311–313]. Mangroves typically grow in a harsh environment which has high temperatures, extreme tides and high salinity in water. These conditions nourish canopies of mangrove growth up to 30-40m in height [314]. The canopies' height and biomass differences depend on the regional temperature and environmental conditions [75], for instance low temperature conditions decline to nurture canopies of mangrove which drops the growth up to 1-2m in height [314,315].

Mangrove cover mapping can be carried out with the aid of time series of remotely sensed data, such as radar, LIDAR and optical data with a spatial resolution varying from 1m to 30m

[123]. Mangrove cover can also be obtained from the several existing mangrove atlases at regional and global scale [316]. Particularly, these kinds of atlases or FOA and other national examined data provide information about the different kind of species, mangrove covers and situation of mangroves at the local level [317]. Using these datasets, we can attain different mangrove functions, such as carbon stocks, conservation, functionality for biodiversity and changes. However, these kinds of national estimates have a lack of information providing prominent drivers of mangrove degradation at the global scale [186].

---

<sup>45</sup>**Scopus** – Scopus is citation database launched in 2004. Scopus covers nearly 36,377 titles from approximately 11,678 publishers, of which 34,346 are peer-reviewed journals in top-level subject fields [318].

<sup>46</sup>**Web of Science** – Web of Science (previously known as Web of Knowledge) is an online subscription-based scientific citation indexing service [318].

<sup>47</sup>**ArcGIS** – ArcGIS is a geographic information system (GIS) software platform for working with geospatial data, maps and geographic information. It is used for generating and using maps, compiling geographic data, geospatial modelling, analyzing mapped information, sharing and discovering geographic information [307].

<sup>48</sup>**Food and Agriculture Organization (FAO)** – FAO is an agency of the United Nations that centralizes worldwide determinations to defeat hunger [317].

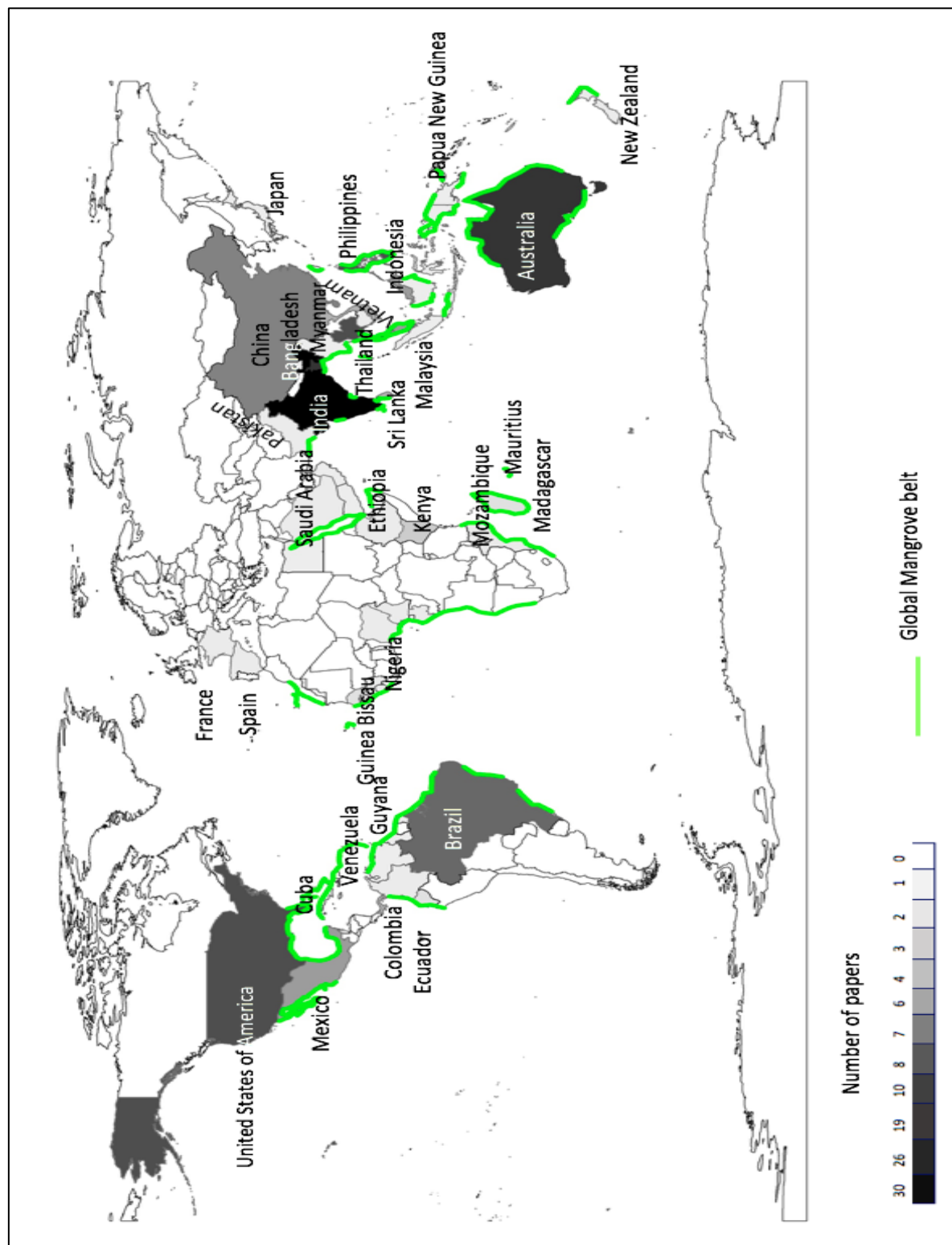
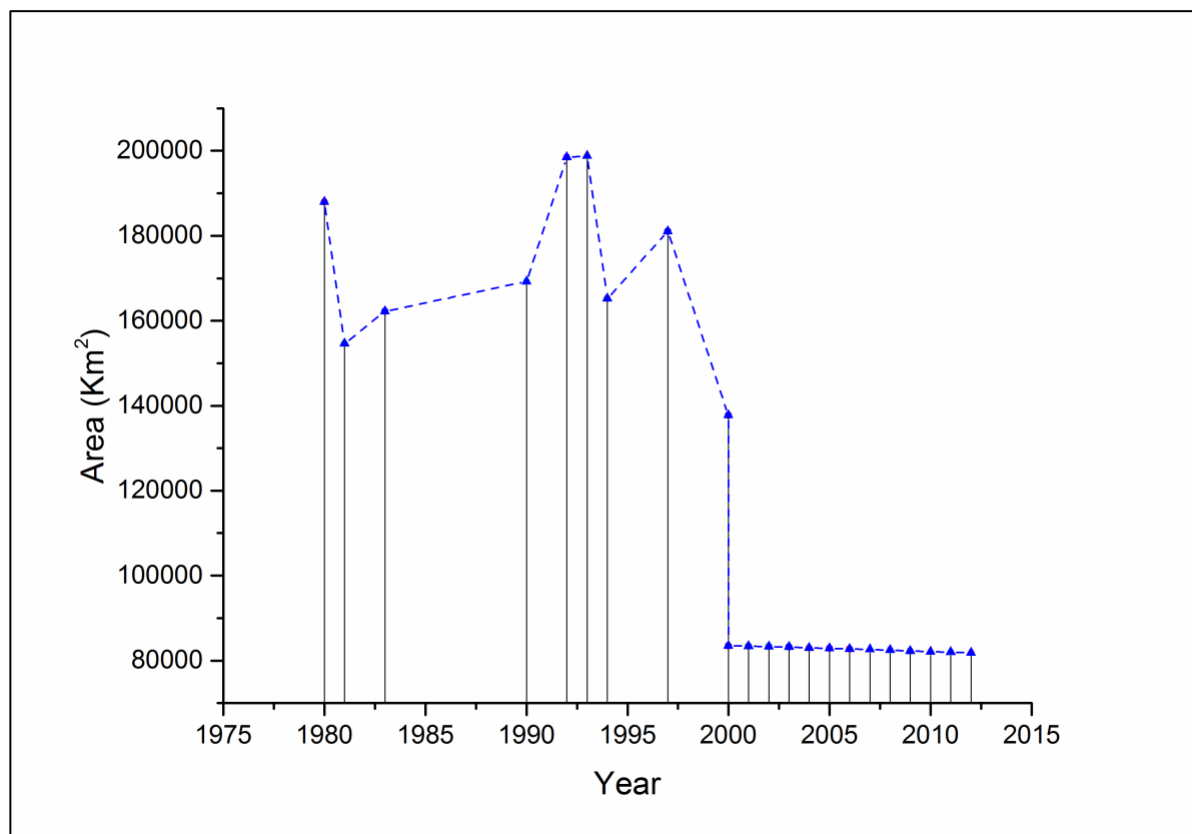


Figure 5.1. Studies covered in this chapter in region wise [260-320].



The major mangrove cover (about 75%) is located in only 15 countries [310]. Asia holds the largest (around 42%) and most diverse mangrove area available in southeast Asia [310]. About 15% of mangrove is situated in Africa. Oceania and South America have 12% and 11% of mangrove forest, respectively. Ramsar wetlands (Sundarbans in Bangladesh and India, Garig Gunak Barlu in Australia, Cayapas-Mataje in Ecuador, Everglades in the United States and Douala Edea in Cameroon) alone held mangrove cover of about 338,482 km<sup>2</sup> in 2012 [106]. Table 5.2 shows the 23 most mangrove-rich countries and their distribution changes between 2000 and 2012 [310].



**Figure 5.2.** Mangroves covers assessment from different sources.

**Table 5.2. 23** Most mangrove-rich countries and their covered area changes from 2000 to 2012. [91,310]

Region	Country	% of global (2000)	Area in km <sup>2</sup> (2000)	% of global (2012)	Area in km <sup>2</sup> (2012)
<b>Asia</b>	Indonesia	28.83	24,073	28.50	23,324
	Malaysia	9.25	4969	5.77	4725
	Myanmar	3.34	2793	3.12	2557
	Bangladesh	2.12	1774	2.17	1772
	India	0.99	825	0.97	797
	Thailand	2.32	1933	2.30	1876
	Philippines	2.50	2091	2.30	1886
<b>Africa</b>	Nigeria	3.18	2657	3.24	2653
	Guinea Bissau	0.89	745	0.91	744
	Mozambique	1.47	1226	1.61	1223
	Madagascar	1.02	852	1.04	849
	Cameroon	1.34	1119	1.36	1112
	Gabon	1.30	1087	1.32	1082
<b>North and central America</b>	Mexico	3.62	3021	3.66	2991
	Cuba	1.99	1660	2.0	1633
	United states	1.93	1612	1.92	1568
<b>South America</b>	Brazil	9.25	7721	9.38	7674
	Venezuela	2.89	2416	2.94	2403
	Colombia	2.01	1674	2.04	1671
	Panama	1.59	1328	1.62	1323
	Ecuador	1.12	938	1.14	935
	Guinea				
<b>Oceania</b>	Australia	3.98	3327	4.05	3316
	Papu New Guinea	5.02	4190	5.10	4172
<b>Total</b>		91.95	74,031	88.46	72,286

### 5.3.2 Drivers in Mangrove Forest Degradation

We found 250 records consisting of 229 studies associated with drivers and 21 on impacts of mangrove degradation. Environmental and anthropogenic pressures are identified as key factors for the continuous mangrove forest degradation [61,319]. In many regions of the world, the decline of mangrove cover rate is increasing rapidly (see table 5.2) [91,310]. However, such changes and causes are not identified globally [320–322].

Worldwide, around 1000km<sup>2</sup> of mangrove cover were converted to other land uses (e.g. agriculture and aquaculture) by implementing the economic policies of the 1970 to the 1980's [323]. Similarly, mangrove forest in Ramsar sites suffered substantial losses between 2000 and 2012 [106] as is listed in Table 5.3.

**Table 5.3.** Ramsar site mangrove loss during 2000 and 2012 [106].

Ramsar site	Area in Km <sup>2</sup> (2000)	Area in Km <sup>2</sup> (2012)	Loss in percentage
Sundarbans, Bangladesh & India	197,994	197,961	0.02
Douala Edea, Cameroon	24,648	24,532	0.47
Garig Gunak Barlu, Australia	11,360	11,296	0.56
Cayapus-Mataje, Ecuador	14,807	14,748	0.40
Everglades, United States	93,090	89,945	3.38

The progressive degradation of the mangrove forest has been associated to pollution, coastal erosion, saline water intrusion, changes in sea resources, flood and deforestation [136]. As a consequence, significant ecosystem services provided by the mangroves have also diminished. These include carbon sequestration, acting as a natural barrier from coastal hazards and biodiversity [324–326]. Table 5.4 shows the number of drivers associated with different regions on mangrove degradation studies covered in this study.

**Table 5.4.** Listed several drivers on mangrove studies covered in this paper. N/A – Not available.

Countries	Climate changes		Anthropogenic activities		
	Temperature, Sea-level rise & Precipitation	Extreme events	Aquaculture, agriculture & plantation	Water and soil Pollutions	Flow modification
Mexico	5	N/A	3	1	N/A
Cuba	N/A	N/A	1	1	N/A
Brazil	3	N/A	3	3	N/A
Guinea Bissau	1	1	N/A	N/A	N/A
Guyana	N/A	N/A	2	1	N/A
Saudi Arabia	1	1	1	N/A	N/A
Ethiopia	2	1	4	N/A	N/A
Mozambique	1	N/A	2	1	N/A
Madagascar	4	2	N/A	N/A	N/A
India	9	4	6	7	4
Bangladesh	6	4	6	2	3
Myanmar	1	2	N/A	N/A	N/A
Malaysia	3	N/A	3	N/A	N/A
Philippines	6	2	6	1	1
Indonesia	7	2	8	1	1
Australia	3	4	1	2	N/A
Papua New Guinea	1	1	1	N/A	N/A
New Zealand	2	2	1	N/A	N/A
Thailand	4	2	6	1	N/A
Colombia	3	2	1	N/A	N/A
Nigeria	2	2	1	N/A	1
Vietnam	1	2	3	N/A	N/A
China	2	N/A	1	2	1
South Africa	1	N/A	N/A	2	1
Ecuador	N/A	N/A	2	1	N/A
Pakistan	1	2	2	1	3
Venezuela	2	N/A	N/A	1	1
United States	2	4	N/A	N/A	N/A
Mauritius	1	1	N/A	2	1

Srilanka	2	2	1	N/A	N/A
Kenya	1	1	N/A	1	N/A
Japan	2	3	N/A	N/A	N/A
Total	79	47	65	31	17

However, the causes of mangrove degradation and its drivers in many parts of the mangrove distributed regions are still poorly comprehended [100]. For effective investigation and policy management it is necessary to analyze global coastal wetland changes and to identify the key answers for mangrove habitat loss. The drivers could be anthropogenic or environmental, or both (Figure 5.3). The environmental drivers comprise of climate, extreme events, and changes in the ecosystem of marine resources [327]. The anthropogenic activities are coastal population, pollution, flow modification and urban development [319].

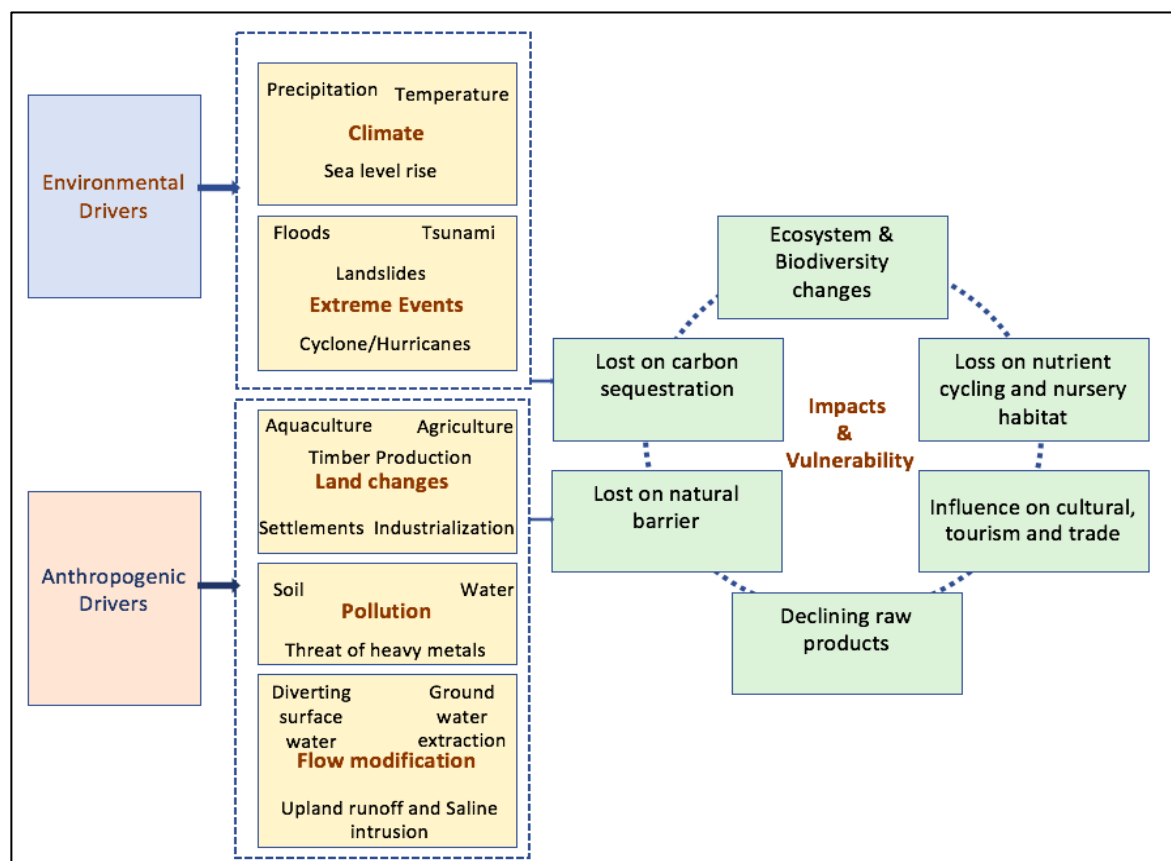


Figure 5.3. Environmental Drivers in mangrove forest and its consequence.

### ***5.3.2.1 Environmental Drivers on Mangrove Degradation and Impacts***

#### ***5.3.2.1.1 Global Sea Level Rise and Extreme High Water Occurrences***

Several types of research have been conducted to identify the cause and impact of sea-level rise [19,328–330]. The main findings is due to global warming related with global and regional sea-level rise is projected to great upsurge between 2090-2099 is 0.18–0.59 m [331]. The recent changes in relative sea-level rise is one of the key drivers of degradation of coastal wetlands including mangroves [19]. Even small increases in the sea level made low-lying coastal land vulnerable, includes Palembang (Indonesia), Sagar Island (India) Sundarbans (Bangladesh) and Shenzhen (China) and small Island states such as Solomon and Nuatambu Island [332–336]. Evidence to that is that mangrove forest in Sagar Island, India is affected by increasing sea level (3.14mm per year) and the rate could upsurge to 3.5 mm per year due to the global warming [337]. Similarly, deltaic subsidence in Bangladesh doubled the rate of sea level rise which threatens the largest tidal halophytic mangroves [338]. Due to the changes in the elevation of the wetland sediment surfaces, there will be differences in the relative measurement of sea-level at tide gauge, and at coastal wetlands [339]. Also, the changes in the coastal wetlands could be caused by the local tectonic progressions, wetland subsidence due to the weight of overlying ice, sedimentation due to erosion, climatological and oceanographic causes [330].

As a consequence of oceanic and temperature factors leading to sea-level changes, the extremely high water events are also likely to increase due to variations in regional climate and ‘El Nino Southern Oscillation <sup>49</sup>(ENSO)’ and ‘Northern Atlantic Oscillation <sup>50</sup>(NAO)’ [340]. An analysis of the records collected from globally distributed stations in the recent years shows every hour sea-level has increased since 1975 [341]. Such increase in the occurrence of severe high water proceedings can drives the condition of the marine ecosystem which poses a great threat to human safety [278] due to increasing water level, coastal sedimentation and sulfide soil toxicity [341].

---

<sup>49</sup>*El Niño–Southern Oscillation (ENSO)* – ENSO is an irregularly periodic variation in winds and sea surface temperatures over the tropical eastern Pacific Ocean, affecting the climate of much of the tropics and subtropics [342].

The sea level changes vary with local to regional dependency on the coastal landscape and situation. With time, change in Eustatic is defined as a variation in sea-level with respect to the earth coordinates system [330]. Eustatic changes are caused by ice melting, increase in the sea water temperature and transfer of Arctic sea ice to water. [328]. Extraction of subsurface ground water has led to coastal subsidence, and variations in thermal expansion across the geography are a few of such factors responsible for the vertical motion of the landform in tectonic movement [170,330,343,344]. These changes cause subsidence along the shoreline and continue with shallow subsidence on mangrove cover area [328]. According to the researchers, the subsidence has been happening since the ice age [19]. There are several delta regions, including Changjiang river delta (China), Chao phraya delta (Thailand) and Mississippi river delta (Gulf of Mexico), that were identified as extremely sensitive to sea level fluctuations, and for which the amount of relative sea level changes is greater than the global average, due to subsidence [345–347]. Coastal erosion and sediment deposition from the banks of large rivers have led to an alarming rate of silt deposition and increased subsidence level [348]. Most of the mangrove area in deltaic plains situated in Brahmaputra, Ganges and Meghna rivers in India (West Bengal) and Bangladesh, and accelerated high water events and sea-level-rise may drive subsidence and erosion due to the monsoons rains which leads to coastal habitat loss of Sundarbans mangroves [338,349–351]. Many studies forecasted the future situation of mangrove inland margin were analyzed based on a) Physio-graphic setting of mangrove forest i.e., information about the neighboring land (slope) and existence of any obstacles, b) a present mangrove boundary delineation, c) forecasting the sea level changes relative to the mangrove swamplands [123,295,352].

#### ***5.3.2.1.2 Extreme Events in a Warming Environment***

As an impact of global climate change, there will be a sharp rise in the tropical cyclone peak wind strengths, with an upsurge in tropical cyclone mean, and highest precipitation intensities in different areas as a result of global climate alteration, which was noted by the Intergovernmental Panel on Climate Change <sup>51</sup>(IPCC) [9,331,353]. If storms become more frequent, storm surge heights are projected to upsurge with strong winds which will affect mangroves and their ecosystems [72], through three different primary means: sediment

deposition, wind damage, and storm flow [354]. The high winds produce sudden and topple stems, defoliate the canopy and cut off the tree branches [355]. A speedy wind flow uproots the taller mangrove trees and knocks them over, but shorter trees may be protected from the hurricanes [356,357]. Evidence to that was the Caribbean hurricane 'Joan' in 1988, which caused extreme damage to the largest mangrove trees and reduced the stability of the stand, loss on several species and forest density [358].

The defoliation and tree mortality to mangroves occurs due to the strong intensity and increased frequency upsurge [359]. This brings high sedimentation rate in wetlands association with changes in soil stability and soil erosion [360]. In addition, it affects the fertility rate of mangroves, variation in seedling season and changes in coastal hydrology causing permanent ecosystem conversion [352]. Sundarbans in Bangladesh and India – the world's largest mangrove forest region - have a high tropical storms frequency and tidal bore since the 60s [361–363]. For instance, Sundarbans in Bangladesh, which is damaged by the cyclone Sidr in 2007, observed 2500 sq.km area of mangroves forest lost due to the cyclone [73]. Similarly, mangrove ecosystems in Orissa and Tamilnadu in India experienced severe damages on mangrove forest due to the super cyclone in 1999 and Vardah cyclone in 2016, Ockhi cyclone in 2017, Gaja cyclone in 2018 respectively [364,365].

Apart from extreme wind induced damages, other natural vulnerabilities such as landslides and Tsunamis can cause severe damages to coastal ecosystems, including mangroves [282]. For instance, the greater Tsunami (2004) occurred in the Indian Ocean after the earthquake hit the epicenter off Sumatra, Indonesia on the Richter magnitude scale of 9.1 – 9.3, which lead to a major loss of human lives and coastal ecosystem in 14 countries [313].

---

<sup>50</sup>**North Atlantic Oscillation (NAO)** – NAO is a weather phenomenon in the North Atlantic Ocean of fluctuations in the difference of atmospheric pressure at sea level (SLP) between the Icelandic Low (semi-permanent centre of low atmospheric pressure found between Iceland and southern Greenland) and the Azores High (High atmospheric pressure typically found south of the Azores) [366].

<sup>51</sup>**Intergovernmental Panel on Climate Change (IPCC)** – IPCC is an international body of the United Nations, committed to delivering the world with an objective, scientific view of climate change and its political and economic impacts [9].



According to FAO studies, these countries have mangrove cover cut-rates from 5,054,900 to 3,660,600 ha [317]. Indonesia has one of the greatest recorded alteration on the mangrove stands, followed by India, Sri Lanka and Thailand [367–369]. Andaman Island, India itself brought 3825–10,200 ha of mangrove forest degradation from 12,750 ha of pre-impact cover, followed by Aceh Province (Sumatra) that lost approximately 750 ha and Andaman cost in Thailand that lost 306 ha [370–372]. As post-tsunami studies clearly disclose, the Tsunami degraded areas in India and Thailand are mostly converted into other land uses [311]. For example, the south and north province in Thailand has significantly mitigated the influence of Tsunami, which is converted into aquaculture and agriculture lands [373]. The Tsunami in Japan in 2011 and Papua New Guinea in 1999 also lead to ecosystem loss [374,375]. Mangrove and other forest were uprooted and broken in tsunami affected places, which brought huge mangrove habitat loss [374].

#### *5.3.2.1.3 Changes in Temperature and Precipitation Patterns*

Anthropogenic greenhouse gas atmospheric concentrations have been linked to the rise in global average surface temperature [376]. Globally, the surface temperature has increased by 0.74 8C between 1906 and 2005 [353] which shows that the linear warming tendency of the past five decades (0.13 8C per decade) is closely twofold that for the last 100 years [353]. Increased surface temperature is expected to affect mangroves by changing the ecosystem and the species [301], mangrove productivity rate [377] and changing phenological patterns [378].

A hard freeze is a natural phenomenon which can deteriorate the growth and expansion of the mangrove forest [88]. The Southwest of Florida is identified as one of the mangrove coasts affected by hard freeze since the 90s, the species death from hoar frost when the temperature reaches -3°C [379]. Therefore, the temperature of the air functions as some physiological barriers, which affects the growth of mangroves into higher altitude [379]. However, the global climate variation and its impact on the growth of the mangrove can slow down the recovery process even after the hard freeze [352]. On the other hand, summer heat waves also produce mangrove habitat loss due to defoliation and intense herbivory, as e.g. Hong Kong experiences strong defoliation in every summer during flowering season that causes low reproductivity and fewer seedlings [380].

Climate change will cause a rise of about 25% in rainfall by 2050 [381]. The regional distribution will be unequal such as boosted precipitation in high-latitudes countries (e.g. New Zealand and South Africa) and reduced precipitation is possible in most subtropical countries [382]. Studies have shown that decline in rainfall and amplified evaporation leads to higher salinity which affects the mangrove productivity, development and sapling and seedling existence, shrinking the diversity of mangrove regions [340]. The degree of changes in rainfall will decline water input to the ground and decreased freshwater supply to mangroves [376], which directly upturns the rate of salinity in coastal wetlands that leads to swelled salt level in mangrove tissues. [343].

Rich biodiversity with the increased productivity in the previously unvegetated areas of the landward fringe within the tidal wetland zone are some of the benefits of increased rainfall [383]. There is a positive correlation between high rainfall and higher mangrove diversity. Productivity has been increased due to a greater source of fluvial sand deposit and nutrients, as well abridged the sulfate level and cut-rate the salinity [378]. However, severe precipitation can produce coastal waterbodies to jump their waterways and introduce fresh channels through the coastal upland, transporting tons of sediment that are accumulated in downstream coastal lands, such as happened in the Choluteca River on the Pacific coast (Honduras) during Hurricane Mitch in 1998 and Tijuana River during the El Niño storm (1993) in southern California, which caused severe damage to the mangrove forest [66,384]. Several ecosystems such as algae, coral reefs and seagrasses also suffered from deteriorated health and changes in cover due to climate changes [385,386]. Mangrove forest is always associated with adjacent coastal ecosystems [333]. Subsequently, effects on the adjacent coastal ecosystems will affect the mangrove health and seedling rate [387]. For example, productive coral reefs supply a proportion of sediment into the low islands of mangroves [377]. This phenomenon will affect the mangroves due to lesser sedimentation rates and boosted regional subsidence if coral reefs and other ecosystem become less productive [330].

### ***5.3.2.2 Anthropogenic Drivers and Impacts***

#### ***5.3.2.2.1 Population Growth and Urbanization***

Human populations occupy an area with-in 60 to 150 kilometers of the coastal land that may contain coastal floodplains, mangroves, tide flats, dunes, and coral reefs [388]. According to the publications from the World Bank group, the human population density in coastal region is around 80 person per square kilometer [339]. Many countries have a higher growth rate in coastal areas than in non-coastal areas [389]. Nearly 50% of population in Africa and Bangladesh lives at the coastline [304]. The high population density poses great demands and exploitation to marine ecosystem [90] and directly motivates fishing, aquaculture, water and soil pollution due to development. Any impact on the coastal areas will directly reflect the economic growth of the country but the growth in the coastal areas comes with a problem in impacting the marine and coastal ecosystem [390,391]. Studies show that 50% of mangroves and 60% of coral reefs are degraded due to anthropogenic activities [99].

The previous studies recorded the rate of mangrove habitat loss in Asia between 2000 and 2012 as an average of 1% per year, which is higher than in other mangrove regions on several continents [100]. Following Asia, the Caribbean mangrove province has the second highest lost over the past three decades due to driving on sewage, oil pollution, solid waste and conversion to landfills and aquaculture [392]. Coastal communities, private industries, and governments in developing countries exploit and transform the resources from mangrove ecosystems for a different purposes. In Asia and Africa, the major drivers that are identified as degradation factors of mangrove forest are agriculture, aquaculture, climate and urbanization [385]. Particularly the Indian coastline, which is acknowledged as one of the richest in biodiversity and includes several countries such as Sri Lanka, Myanmar, Bangladesh, Singapore, Indonesia and Australia, has been losing its mangrove ecosystem in the last three decades due to human interference [385]. Also, in Sub-Saharan countries such as Mauritania, Comoros, Djibouti and Somalia, most of the development progression happens without any strategical plan, which brings mangrove loss [393–397].

Urban development components such as clearing for aquaculture, rice cultivation and timber production have led to the destruction of 25% of global mangroves in past 20 years [71]. This

alarming effect has caused evident modifications in the cover and health of the mangrove forest and its marine environment [398,399]. According to the recent studies, aquaculture is identified as one of the prominent drivers which causes mangroves degradation [400]. Aquaculture destroys the mangroves to create shrimp ponds, which reduces the ground water levels, and causes pollution to the surface water from the pond effluents [401]. However, the governments should invest in infrastructure and development of sewage treatment plants to overcome the loss of coastal habitat [402] because lack of long-term maintenance of natural resources are the greatest shortcoming of shrimp aquaculture [90]. Such developments reduce the environmental contamination to some extent. Researchers have noticed, the world-wide mangroves will vanish in about 50 years if this trend continues [403]. The impacts will be on coastal fisheries, bird life, and other ecosystems which thrive because of mangroves in several parts of the world [285].

#### ***5.3.2.2.2 Aquaculture and Agriculture***

Globally, 38% of mangroves were cleared for shrimp aquaculture and 14% for another fish aquaculture [404]. Thailand and Vietnam are two of the hot spots areas of mangrove degradation which is recorded at a high rate of about 9.535 ha per year [405]. In Thailand alone, records 40% (69,400 ha) of mangrove area were converted into aquaculture [406], 102,000 ha in Vietnam [90], 6500 ha in Bangladesh [304], 21,600 ha in Ecuador, and 11,515 ha in Honduras [153,310,404]. India recorded that about 40% of mangrove habitat on the western coastline has been transformed into urban land and aquaculture [401]. Similarly, Philippines has a high rate of mangrove loss about 50% of the 279,00 ha of mangrove habitat from 1951 to 1988 [407]. About 205,523 ha and 211,000 ha of mangrove marshlands have been transformed into shrimp and other fish farms in the Philippines and Indonesia respectively [81]. An estimation of these ecosystem changes in several Southeast Asian countries (Myanmar, Borneo, Malaysia, and Sumatra) is >10% between 2000 and 2012 [100]. Major decline of mangrove forest in Latin America also due to the wide clearing of mangroves for shrimp farms and agriculture [408].

Agriculture is the dominant influence in all mangrove habitat countries excluding Indonesia, where timber extraction and aquaculture is the major reason [371]. For instance, the

Philippines and Indonesia have most of the deforested mangrove area converted into another ecosystem services such as aquaculture and agriculture, but in West Africa mangrove ecosystems are exploited for wood harvesting and are not transformed [81,97,367]. Likely the conversion of mangrove area into salt pan, river damming and other coastal infrastructure is a major cause of ecosystem degradation recorded in Brazil during 1968 and 1999 but recent research reveals the mangrove biomass of the Pacoti estuary is growing from 0.71 to 1.44 km<sup>2</sup> in the past 10 years, which is formerly occupied with salt marshes [186,409]. Even though the mangrove area in Brazil is affected by human settlements, aquaculture and water pollution, there has been a very low rate of mangrove area loss that has been documented since 1980 [410].

Most of the deforested mangrove areas in the different region was supplanted with agriculture or aquaculture, which is misclassified as mangrove forest in 2012 spatial distribution studies, particularly in Indonesia [367]. But not all mangrove deforested area can be reinstated [404]. For instance, deforestation in Malaysia and Singapore is highly dominant with urban development, which is very improbable to revert back to mangroves [411]. Even some of the agricultural area, previously mangrove forest in Thailand, Burma, Bangladesh, and India, are very hard to afforest or rehabilitate due to the area being spoiled by pesticides and pollution [412]. The mangrove habitat loss rates in Kenya over the 2000-2010 is increasing due to the soil and water pollution [394,395]; Particular studies proved the influence of soil quality for potential agriculture and aquaculture use directly brings on rates of deforestation [413].

The growth of oil palm plantations in Thailand, Malaysia, Sumatra, Colombia and Indonesia is a proximate driver of deforestation [100]. The past transformation of mangrove forest into palm plantations might have been unobserved, because oil palm plantation extension is commonly considered a terrestrial subject, and palm farm that replaces mangrove area may look like those that were replaced in satellite images [411]. The increasing demand for palm oil is expected to bring more production of oil in Indonesia, which is expected to increase by 30% above 2012 levels by 2019, which influences intrusion on mangrove land [100].

### 5.3.2.2.3 Coastal Protection Structures and Flood Control Walls

Coastal erosion structure, seawalls, and other coastal constructions as an effect of rising water level in swamps have affected the mangroves ecosystem [319]. These structures cause surface run-off and flooding of the mangrove immediately during flash flood and increasing down current [414]. Increased rainfall leads to improved construction of storm water drainage, dams and erosion control structures reduce flooding of coastal regions [360]. This diverts the upland water from mangroves and other coastline ecosystems, dropping mangrove productivity [377]. For example, in Asia, the construction of upstream reservoirs and dams is now extremely reducing the supply of sediments to many Delta regions, including Ganges and Cauvery in India and Sundarbans deltas of India and Bangladesh and Indus river delta of Pakistan, which are facing increased wetland erosion with widespread significance [145,246,415,416]. Likewise, China has reduced the annual sediment that is brought to its delta to 0.4 billion metric tons from 1.1 billion metric tons [417]. The costal infrastructure will likely continue to upsurge throughout Asia and globally in coming years [418]. On the other hand, coastal regions with drought or lesser rainfall due to climate change and temperature rise will have higher groundwater extraction [312]. Boosted groundwater withdrawal will increase sea water intrusion to mangrove surfaces and thereby aggregate mangrove marshland vulnerability [304].

In the Mississippi Delta, the wetlands have been reduced drastically because of the building of flood control walls and hydrological disturbance of the deltaic plain [345]. These components led to an isolation of the river from the Delta. Measures have been taken to restore the wetlands by diverting the river water into the wetlands and by creating marshes by pumping the dredged sediments [376]. However, it is important to find a viable and less expensive solution to mitigate the problems since intensive pumping for coastal wetland restoration is expensive and unaffordable in most cases [329].

Industrialization and oil extraction on virgin mangrove forests have increased in the last two decades [419]. But mangrove ecosystems can bioremediate certain industrial and oil pollutants in the limited environment and help in nutrients cycles and sediment

characteristics [335]. It dissolves the metals existent in the deposit by exuding oxygen into the anoxic soil sediment through mangrove aerial roots [420,421]. However, mangroves have adapted to them by acting as biological pollution sinks of low level anthropogenic pollutants [335,412].

Immobilization of metals in mangroves is the major problem due to the chemical contaminant and the organic matter in mangroves [319]. The inundation of the mangrove area leads to depletion of oxygen which reacts with the deposited organic matter [335]. The coastal pollution can be assessed by calculating the presence of heavy and non-toxic metals such as Copper (Cu), Iron (Fe), Magnesium (Mg), Manganese (Mn), and Zinc (Zn) and Mercury (Hg), Lead (Pb), and Tin (Sn) respectively [419]. The presence of heavy metals has led to severe and long-lasting effects in humans and in forest decline due to its environmental direct damages [421,422].

In India, a considerable amount of environmental stress is caused by domestic and industrial waste, heavy metals and other toxic excess from the thermal power stations (Tuticorin), nuclear power plants (Kudankulam & Kalpakkam) and dye factories [146]. In a region like the Arab states in the Persian Gulf, substantial petroleum exploration, oil wells, oil refiners and transportation lead to the oil spill and oil pollution drive on habitat loss on mangroves and other ecosystems [423]. The Gulf of Mexico oil spill in 2010 lead to major threats on costal ecosystems, because oil produces an instant cause with a resident time up to 10 years [424]. Recently, On January, 2017, the tonnes of toxic heavy bunker oil spill in Chennai, Tamilnadu spread some 34 kilometres of Ennore coast and that slick has reached Pichavaram mangrove in south Cuddalore and Pulicat mangroves in northwards, where it brought major ecological damage [425].

Chapter 6

Conclusion



*“The most patriotic thing you can do is to take care of the environment and try to live sustainably”*

***Robert F.Kennedy, Jr***

## Chapter 6

### Major Results and Discussion

---

#### 6.1 Modelling Urban Sprawl using Remotely Sensed Data

In chapter 2, We found fragmented urban growth in the outskirts of Chennai city, with the transformation of vegetation cover and agricultural land into built-up settlements. This alarming extent and level of US will have adverse impacts on the natural resources and land of Chennai. The combined application of geographic information systems, remote sensing, urban change modelling, landscape metrics and entropy measures proved to be a useful and efficient approach for our assessment and modelling US for the Chennai city. Consequently, this study contributes with indicators and metrics to monitor this US in Chennai. It also provides relevant information for sustainable urban growth and efficient urban planning as well as for mitigation of environmental impacts in Chennai. To conclude, our study provides quantitative measures for urban planning and management authorities for mitigating socioecological consequences of US and preventing loss of urban ecosystem services.

#### 6.2 A Remote Sensing Approach to Environmental Monitoring in a Reclaimed Mine Area

In chapter 3, We identified two potential subsidence spots that may be under risk of collapse and overall degradation and damage of vegetation. Thus, our results inform environmental management and mining reclamation experts about land surface and vegetation loss because of subsidence. Environmental management authorities in Kirchheller Heide should prioritize the indicated subsidence areas for further surface and subsurface investigation, as well as for remediation and mitigation. The potential biodiversity and ecosystem impacts of subsidence should also be investigated. In general, our study proves the virtue of RS and GIS for monitoring short-term geological changes and thus for predicting long-term environmental impacts in reclaimed mine areas. Thus, we emphasize the importance of including RS and GIS monitoring in environmental conservation and management projects in addition to field

monitoring [219,426]. Our approach is also useful for identifying ecological stress, and surface erosion and inundation, and thus may provide important metrics for ecological restoration and infrastructure provision [49,53].

### **6.3 Satellite Image Fusion to Detect Changing Surface Permeability and Emerging Urban Heat Islands**

In chapter 4, we demonstrated the advantage of using fused satellite imageries combining multiple sensors in detecting and monitoring changes in land surface permeability and temperature and emergence of Urban Heat Island (UHI) in fast growing cities like Tirunelveli. Future studies should fuse higher temporal and spectral resolution imageries than the ones used in our study to provide a continuous, seasonal and more detailed assessment of Landuse and Landcover (LULC), Soil-Adjusted Vegetation Index (SAVI) and Land Surface Temperature (LST) changes, and UHI emergence in Tirunelveli [230]. We suggest that urban landuse measures and zonal planning should be informed by detailed and continuous RS and GIS based assessment of LULC, SAVI and LST [121,265]. Possible measures include the conservation of agriculture and forested lands, and proper management of the reclamations of barren lands to pasture lands to avoid the decrease in surface permeability and ecosystem fragmentation [272]. Urban expansion should include provision of water bodies and afforestation to preserve surface moisture, permeability and radiative capacity, and thus to prevent the increase in surface temperature [25].

### **6.4 Drives of Mangrove Degradation at Regional to Global Levels**

In chapter 5, we identified several mangrove degradation drivers at regional and global levels resulting from decades of research data of climate variations and human activities. We identified anthropogenic activities, such as encroachment near coastal line, coastal LULC changes, US, exploitation of mangrove forest resources, water withdrawal and pollution in upstreams as the main drivers of mangrove degradation in Asian countries including India, Bangladesh, Thailand and Vietnam. The climatic and associated geological changes, including increased salinity driven by increasing temperatures, are a common reason for mangrove health degradation that was identified in almost all mangrove presence countries. Natural

disasters, e.g. tropical cyclones, entail disruptive damages, whereas climatic changes and anthropogenic activities cause incremental degradation of the global mangrove forest. This information can be useful for future research on mangroves, and to help delineating global planning strategies which consider the correct ecological and economic value of mangroves in order to protect them from further loss.

## 6.5 Contributions

We believe that this dissertation has a comprehensive and rich practical model for quantification of local to global scale socio-ecological impacts of anthropogenic landscape changes by connecting the different aspects, which threaten ecosystem and biodiversity. This research has several contributions in the field of RS and GIS:

First contributes to the field of Urban planning and management. We classified the different land features with the aid of Rotation Forest (ROF) and Random Forest (RF) in the R environment. R facilitates handling large volumes of geospatial data without any technical errors and with high accuracy, when compared to the other existing image processing software and methods. R can easily interface with external databases to handle large amounts of geospatial data [216]. The algorithms for RF and ROF suggested in this dissertation will contribute to classify the LULC area from regional to global extent with low human resource and cost. Thus, the algorithm for LULC introduced in the R environment can effortlessly interface with several geodatabases to classify vast and different kinds of earth landscapes, and contributes to Land monitoring and Landuse department.

We introduced a new approach, Renyi's Entropy method to measure the extent, pattern and level of US of fast-growing cities instead of applying Shannon's entropy in preceding research. Renyi's offers high performance to characterize and identify the degree of spatial dispersion and concentration of urban areas, and can also be computed from remotely sensed images and effectively used to quantify the level of US. We also suggested six landscape metrics to quantify the spatial and physical characteristics of urban features, urban patterns and their forms. This proved practical entropy and metrics method will contribute to city planners and urban developers to provide sustainable urban planning to modern society.

This dissertation moreover contributes a useful metric to identify the mining subsidence spot with the help of freely available spatial data. The presented indices combination of SMA and NDVI that were coded in the R platform will contribute to the field of environmental management and mining reclamation experts to understand the spatio-temporal changes in massive post-mining areas. This research also demonstrated the advantage of fusing imageries from multiple sensors for LULC change assessments as well as for assessing surface permeability and temperature and UHI emergence. Even though the relationship between urbanization and UHI emergence has been well established in previous research. However, there remains a gap at the front of developing early warning signals for the emergence of UHIs using remotely sensed imageries. We overcame this gap and established the advantage of using fused imageries combining multiple sensors in detecting and monitoring UHI in fast growing cities.

This research furthermore contributes to environmental activists and coastal authorities. The broad study on global mangrove forest degradation provides a detailed report on drivers of global mangrove degradation. The identified drivers resulted from decades of published data (from 1981 to present) of climate variations (sea-level rising, storms, precipitation, extremely high-water events and temperature), and human activities (pollution, wood extraction, aquaculture, agriculture and urban expansion). This information can be useful for future research on mangroves, and to help delineating global planning strategies which consider the correct ecological and economic value of mangroves protecting them from further loss.

## 6.6 Outlook and Concluding Remarks

This Ph.D. dissertation investigated the drivers of environmental degradation associated with different landscape changes including urbanization, geological changes, and forest degradation, and thus to contribute to an integrated landscape management. We were interested in the quantification of urban to global scale social-ecological impacts of anthropogenic landscape changes by connecting the different aspects, which threaten the ecosystem and biodiversity. Social-ecological impacts of anthropogenic landscape changes that account for large scale degradation are still constrained by many concerns, which should

be covered by future research. Landscape data scarcity is certainly one of them, not only for resource constraints of developing countries but also globally for many significant variables. For instance, there is no accessibility of the high geometric and thematic accuracy data for specific dates or to cover definite areas. In addition to that, there is the problem of unsuitability of some vegetation and soil indices on the imagery of all sensors.

Remote sensing data for geological changes associated with mining activities have only recently been available for few mining regions and hence, large scale risk assessment related with climate changes and vegetation degradation are lacking. High- and hyperspectral and temporal satellite imageries may deliver mining landscape dynamics with higher accuracy than in our research [62]. For example, a wide-ranging monthly variation analysis may offer detailed information on the emergence and dynamics of subsidence zones when compared to yearly analysis, as subsidence occurs abruptly at the surface level [8]. Moreover, images with higher coverage of bands may classify subsidence spots that are not observed through the growth of waterbodies, e.g., sink holes and landslides [53]. We specifically recommend the usage of high- and hyperspectral and temporal resolution imageries collected in continuous mode for monitoring directly after mining reclamation, when it is most urgent to investigate the surface and subsurface level.

The proposed Renyi's entropy and landscape metrics should be further explored for delineating US extent, level, and patterns in cities of other parts of the world. Though predicted for worldwide applicability, this dissertation could only deliver the test case of one Indian city for US quantification and land change prediction. Associated studies on different cultural landscapes and urban morphologies should be conducted. Even though some landscape metrics examinations have determined the applicability of pattern indices for differentiating landscapes, there is a scarcity of evidence that pattern indices imply ecological progressions. Thus, the advantage of landscape pattern indices for estimating the habitat consequences of unsustainable landscape plans should be handled especially cautiously in creating ecological inferences from landscape pattern index values applied to sustainable landscape plans. Consequently, future studies should develop landscape patterns by considering developments and not merely spatial patterns, associating data of diverse

qualities, generalizing outcomes in space and time, and deliberating culture as a driver of landscape change.

Even though Landsat imagery is worldwide available, the classification of LULC in larger areas is still challenging, as it would need more manpower and a highly efficient geodatabase. As a possible way to overcome this challenge, this dissertation provided the test cases of two Indian cities and one European city for LULC classification from RF and RAF algorithm in the R environment. Though, the proposed classification algorithm should be integrated with external geodatabases and tested to overcome the limitation of LULC classification. However, handling geospatial big data sets outstripping capacity of present computing methods includes R programming [427]. A momentous percentage of big data is actually geospatial data, and the size of such data is rising promptly at least by 20% every year [427]. Besides the drawback in handling geospatial big data, up-to-date data integration, setback in present computer models, incorporation of regional changeability and practise of large scale datasets for analysing landscape dynamics, crowd-sourced geospatial data refers to producing a map using informal social networks have shown substantial to fill geospatial data gaps [428–430].

Though, technologies for efficient use of the spatial data and for interpreting valuable information from the data of RS are still very limited since no single sensor combines the spatial, radiometric, spectral and temporal resolution [35,88,254,431]. To overcome this drawback, we demonstrated the advantage of using fused satellite imageries combining multiple sensors in detecting and monitoring changes in land surface permeability and temperature and emergence of UHI. Nevertheless, future studies should fuse higher temporal and spectral resolution imageries than the ones used in our study to provide a continuous, seasonal and more detailed assessment of LULC, SAVI, and LST changes, and UHI emergence worldwide.

Even though our research identifies several drivers on mangrove degradation, the associations of climatic changes and anthropogenic activities with the incremental degradation of vegetation health in the global mangrove forest have not yet been quantified [145,246,415,416]. Thus, the future project should aim at disentangling and quantifying the relative associations of climatic changes and anthropogenic activities with the vegetation

changes globally and predict the future vegetation health and ecosystem services of mangrove forests. Besides, the data for mangrove degradation drives are only accessible for certain areas and therefore, global drivers related with mangrove health degradation are required for global assessment.





## Reference:

1. Grooten, M.; Almond, R. E. . *Living Planet Report - 2018: Aiming Higher*; Gland, Switzerland, 2018.
2. Watson, R. 75% of Earth's Land Areas Are Degraded  
<https://news.nationalgeographic.com/2018/03/ipbes-land-degradation-environmental-damage-report-spd/>.
3. CMAQ U.S. Environmental Protection Agency. *Www.Cmaq-Model.Org* **2011**, 1–22.
4. O'Neill, R. V.; Riitters, K. H.; Wickham, J. D.; Jones, K. B. Landscape pattern metrics and regional assessment. *Ecosyst. Heal.* **1999**, 5, 225–233.
5. Chapin, F. S.; Zavaleta, E. S.; Eviner, V. T.; Naylor, R. L.; Vitousek, P. M.; Reynolds, H. L.; Hooper, D. U.; Lavorel, S.; Sala, O. E.; Hobbie, S. E.; Mack, M. C.; Díaz, S. Consequences of changing biodiversity. *Nature* 2000, 405, 234–242.
6. Hector, A.; Bagchi, R. Biodiversity and ecosystem multifunctionality. *Nature* **2007**, 448, 188–190.
7. Midgley, G. F. Biodiversity and ecosystem function. *Science* (80-. ). 2012, 335, 174–175.
8. Groombridge, B. Global Biodiversity. *Am. Fish. Soc. Symp.* **1992**, 77, 15–37.
9. IPCC *IPCC Fourth Assessment: Climate Change* 2007; 2008.
10. United Nations Convention on Climate Change *Paris Agreement*; 2015.
11. Pitman, A. J. Greenhouse effect and greenhouse gases. In *Encyclopedia of Earth Sciences Series*; 2005; pp. 391–397.
12. Stern, D. I.; Kaufmann, R. K. Anthropogenic and natural causes of climate change. *Clim. Change* **2014**, 122, 257–269.
13. Gray, R.; Fulton, E.; Little, R.; Scott, R. *Ecosystem model specification with an agent based framework*; 2006.
14. Daily, G. C.; others Introduction: What are ecosystem services? *Nature's Serv. Soc. Depend. Nat. Ecosyst.* **1997**, 1, 3–4.
15. WWF, I. Biodiversity, Ecosystem services, Humanitys Footprint. *Living Planet Rep.* **2008**.
16. Schafer, A.; Victor, D. G. The future mobility of the world population. *Transp. Res. Part A Policy Pract.* **2000**, 34, 171–205.
17. United Nations, D. of E. and S. A. P. D. *World Population Ageing*; 2015; Vol. 5.
18. Reich, D.; Thangaraj, K.; Patterson, N.; Price, A. L.; Singh, L. Reconstructing Indian

population history. *Nature* **2009**.

19. Committee on Sea Level Rise in California Oregon and Washington *Sea-Level Rise for the Coasts of California, Oregon, and Washington: Past, Present, and Future*; 2012.

20. Loveland, T. R.; Reed, B. C.; Brown, J. F.; Ohlen, D. O.; Zhu, Z.; Yang, L.; Merchant, J. W. Development of a global land cover characteristics database and IGBP DISCover from 1 km AVHRR data. *Int. J. Remote Sens.* **2000**, *21*, 1303–1330.

21. Aithal, B. H.; V., R. T. Visualization of Urban Growth Pattern in Chennai Using Geoinformatics and Spatial Metrics. *J. Indian Soc. Remote Sens.* **2016**, *44*, 617–633.

22. Tewolde, M. G.; Cabral, P. Urban sprawl analysis and modeling in Asmara, Eritrea. *Remote Sens.* **2011**, *3*, 2148–2165.

23. Hansen, J.; Ruedy, R.; Sato, M.; Lo, K. Global surface temperature change. *Rev. Geophys.* **2010**, *48*.

24. Boano, C.; Lamarca, M. G.; Hunter, W. The Frontlines of Contested Urbanism: Mega-projects and Mega-resistances in Dharavi. *J. Dev. Soc.* **2011**.

25. Taha, H. Urban climates and heat islands: albedo, evapotranspiration, and anthropogenic heat. *Energy Build.* **1997**, *25*, 99–103.

26. Schneider, A.; Chang, C.; Paulsen, K. The changing spatial form of cities in Western China. *Landsc. Urban Plan.* **2015**, *135*, 40–61.

27. Becerril-Piña, R.; Díaz-Delgado, C.; Mastachi-Loza, C. A.; González-Sosa, E. Integration of remote sensing techniques for monitoring desertification in Mexico. *Hum. Ecol. Risk Assess. An Int. J.* **2016**, *22*, 1–18.

28. Iyer, L.; Macomber, J.; Arora, N. Dhārāvi: Developing Asia ' s Largest Slum. *Harvard Bus. Sch.* **2009**.

29. Schmiedel, U.; Linke, T.; Christiaan, R.; Falk, T.; Grongroft, a; Haarmeyer, D.; Hanke, W.; Henstock, R.; Hoffman, T.; Kunz, N.; Labitzky, T.; Luther-Mosebach, J.; Lutsch, N.; Meyer, S.; Peterson, a; Rower, I.; van der Merwe, H.; van Rooyen, M.; Vollan, B.; Weber, B. Environmental and socio-economic patterns and processes in the Succulent Karoo — frame conditions for the management of this biodiversity hotspot. *Biodivers. South. Africa - Implic. Landuse Manag.* **2010**.

30. Pisharoty, P. R. Introduction to remote sensing. *Proc. Indian Acad. Sci. Sect. C Eng. Sci.* **1983**, *6*, 97–107.

31. Gordon, A.; Simondson, D.; White, M.; Moilanen, A.; Bekessy, S. A. Integrating conservation planning and landuse planning in urban landscapes. *Landsc. Urban Plan.* **2009**, *91*, 183–194.
32. Martin, S. *An introduction to ocean remote sensing*; 2013; Vol. 9781107019.
33. Squires, G. *Urban sprawl causes, consequences and policy responses*; Kathleen corrier, William Gorham, Jack hadley, Adele.V.Harrell, Robert, John, G. and D. S. N., Ed.; The Urban Institute Press: Washington, D.C, 2002.
34. Gao, J. A comparative study on spatial and spectral resolutions of satellite data in mapping mangrove forests. *Int. J. Remote Sens.* **1999**, *20*, 2823–2833.
35. Chander, G.; Markham, B. L.; Helder, D. L. Summary of current radiometric calibration coefficients for Landsat MSS, TM, ETM+, and EO-1 ALI sensors. *Remote Sens. Environ.* **2009**, *113*, 893–903.
36. Sobrino, J. A.; Jiménez-Muñoz, J. C.; Paolini, L. Land surface temperature retrieval from LANDSAT TM 5. *Remote Sens. Environ.* **2004**, *90*, 434–440.
37. Kovacs, J. M.; Vandenberg, C. V.; Wang, J.; Flores-Verdugo, F. The Use of Multipolarized Spaceborne SAR Backscatter for Monitoring the Health of a Degraded Mangrove Forest. *J. Coast. Res.* **2008**.
38. Everitt, J. H.; Escobar, D. E.; Judd, F. W. Evaluation of airborne video imagery for distinguishing black mangrove (*Avicennia crerminans*) on the lower Texas gulf coast. *J Coast. Res* **1991**.
39. Martins, V. N.; Cabral, P.; Silva, D. S. System Sciences Urban modelling for seismic prone areas : the case study of Vila Franca do Campo ( Azores Archipelago , Portugal ). *Nat. Hazards Earth Syst. Sci.* **2012**, *12*, 2731–2741.
40. Gamba, P.; Dell’Acqua, F.; Dasarathy, B. V. Urban remote sensing using multiple data sets: Past, present, and future. *Inf. Fusion* **2005**, *6*, 319–326.
41. McCarthy, M. P.; Best, M. J.; Betts, R. A. Climate change in cities due to global warming and urban effects. *Geophys. Res. Lett.* **2010**, *37*.
42. Dewan, A. M.; Corner, R. J. Spatiotemporal Analysis of Urban Growth, Sprawl and Structure. *Springer Geogr.* **2014**, 99–121.
43. Oke, T. R. The energetic basis of the urban heat island. *Q. J. R. Meteorol. Soc.* **1982**, *108*, 1–24.

44. Brunn, A.; Dittmann, C.; Fischer, C.; Richter, R. Atmospheric correction of 2000 HyMAP data in the framework of the EU-project MINEO. In *Proceedings of SPIE*; 2001; Vol. Volume 454, pp. 382–392.
45. Eikhoff, J. Developments in the German coal mining industry. *Entwicklungen im Dtsch. Steinkohlenbergbau* **2007**, 143, 10–16+4.
46. Brunn, A.; Busch, W.; Dittmann, C.; Fischer, C.; Vosen, P. Monitoring Mining Induced Plant Alteration and Change Detection in a German Coal Mining Area using Airborne Hyperspectral Imagery. ? **2002**, ?, ?
47. Prakash, A.; Gupta, R. P. Land-use mapping and change detection in a coal mining area - a case study in the Jharia coalfield, India. *Int. J. Remote Sens.* **1998**, 19, 391–410.
48. Galvin, J. M. Longwall Mining. In *Ground Engineering - Principles and Practices for Underground Coal Mining*; 2016; pp. 359–420.
49. Song, J.; Han, C.; Li, P.; Zhang, J.; Liu, D.; Jiang, M.; Zheng, L.; Zhang, J.; Song, J. Quantitative prediction of mining subsidence and its impact on the environment. *Int. J. Min. Sci. Technol.* **2012**, 22, 69–73.
50. Morfeld, P.; Ambrosy, J.; Bengtsson, U.; Bicker, H.; Kalkowsky, B.; K??sters, A.; Lenaerts, H.; R??ther, M.; Vautrin, H. J.; Piekarski, C. The risk of developing coal workers' pneumoconiosis in german coal mining under modern mining conditions. *Ann. Occup. Hyg.* **2002**, 46, 251–253.
51. Carnec, C.; Delacourt, C. Three years of mining subsidence monitored by SAR interferometry, near Gardanne, France. In *European Space Agency, (Special Publication) ESA SP*; 2000; pp. 141–149.
52. Allgaier, F. K. Surface Subsidence over Longwall Panels in the Western United States. In *State of the Art of Ground Control in Longwall Mining and Mining Subsidence*; 1982; pp. 199–209.
53. Dittmann, C.; Vosen, P.; Brunn, A. MINEO (Central Europe) environment test site in Germany - Contamination/impact mapping and modelling - Final report; 2002.
54. Scott, M. J.; Statham, I. Development advice maps: mining subsidence. *Geol. Soc. London, Eng. Geol. Spec. Publ.* **1998**, 15, 391–400.
55. Hu, Z.; Hu, F.; Li, J.; Li, H. Impact of coal mining subsidence on farmland in eastern China. *Int. J. Surf. Mining, Reclam. Environ.* **1997**, 11, 91–94.
56. Zuo, C.; Ma, F.; Hou, J. Representatives of mining subsidence analysis visualization of

China. *Liaoning Gongcheng Jishu Daxue Xuebao (Ziran Kexue Ban)/Journal Liaoning Tech. Univ. (Natural Sci. Ed.* **2014**, 33, 788–792.

57. Jat, M. K.; Garg, P. K.; Khare, D. Monitoring and modelling of urban sprawl using remote sensing and GIS techniques. *Int. J. Appl. Earth Obs. Geoinf.* **2008**, 10, 26–43.

58. Rajchandar, P.; Bhowmik, A. K.; Cabral, P.; Zamyatin, A.; Almegdadi, O.; Wang, S. Modelling Urban Sprawl Using Remotely Sensed Data: A Case Study of Chennai City, Tamilnadu. *entropy* **2017**, 19, 163.

59. Deck, O.; Verdel, T.; Salmon, R. Vulnerability assessment of mining subsidence hazards. *Risk Anal.* **2009**, 29, 1381–1394.

60. Venkatesan G; Padmanaban, R. Possibility Studies and Parameter Finding for Interlinking of Thamirabarani and Vaigai Rivers in Tamil Nadu , India. *Int. J. Adv. Earth Sci. Eng.* **2012**, 1, 16–26.

61. Monishiya, B. G.; Padmanaban, R. Mapping and change detection analysis of marine resources in Tuicorin and Vembar group of Islands using remote sensing. *Int. J. Adv. For. Sci. Manag.* **2012**, 1, 1–16.

62. Baek, J.; Kim, S.; Park, H.; Kim, K. Analysis of ground subsidence in coal mining area using SAR interferometry. **2008**, 12, 277–284.

63. Whittaker, B. N.; Reddish, D. J. Mining Subsidence in Longwall Mining with Special Reference to the Prediction of Surface Strains. In *Stability In Underground Mining II*; 1984.

64. Prakash, A.; Gupta, R. P. Land-use mapping and change detection in a coal mining area - a case study in the Jharia coalfield, India. *Int. J. Remote Sens.* **1998**, 19, 391–410.

65. Kairo, J. G.; Kivyatu, B.; Koedam, N. Application of Remote Sensing and Gis in the Management of Mangrove Forests Within and Adjacent To Kiunga Marine Protected Area ., *Environ. Dev. Sustain.* **2002**.

66. Schultz, K. a. El Niño/Southern Oscillation and the Seasonal Predictability of Tropical Cyclones. In *El Nino and the Southern Oscillation*; 2001; Vol. 76, pp. 149–182.

67. Simard, M.; Zhang, K.; Rivera-monroy, V. H.; Ross, M. S.; Ruiz, P. L.; Castañeda-moya, E.; Twilley, R. R.; Rodriguez, E. Mapping Height and Biomass of Mangrove Forests in Everglades National Park with SRTM Elevation Data. **2006**, 72, 299–311.

68. MoEF *Bangladesh Climate Change Strategy and Action Plan*; 2008.

69. Mougin, E.; Proisy, C.; Marty, G.; Fromard, F.; Puig, H.; Betoulle, J. L.; Rudant, J. P.

Multifrequency and multipolarization radar backscattering from mangrove forests. *IEEE Trans. Geosci. Remote Sens.* **1999**.

70. Sirikulchayanon, P.; Sun, W. X.; Oyana, T. J. Assessing the impact of the 2004 tsunami on mangroves using remote sensing and GIS techniques. *Int. J. Remote Sens.* **2008**.

71. Santos, L. C. M.; Matos, H. R.; Schaeffer-Novelli, Y.; Cunha-Lignon, M.; Bitencourt, M. D.; Koedam, N.; Dahdouh-Guebas, F. Anthropogenic activities on mangrove areas (s??o francisco river estuary, brazil northeast): A gis-based analysis of cbers and spot images to aid in local management. *Ocean Coast. Manag.* **2014**.

72. Das, S.; Crépin, A.-S. Mangroves can provide protection against wind damage during storms. *Estuar. Coast. Shelf Sci.* **2013**, *134*, 98–107.

73. Bhowmik, A. K.; Cabral, P. Cyclone Sidr Impacts on the Sundarbans Floristic Diversity. *Earth Sci. Res.* **2013**, *2*, 62–79.

74. Gilman, E. L.; Ellison, J.; Duke, N. C.; Field, C. Threats to mangroves from climate change and adaptation options: A review. *Aquat. Bot.* **2008**.

75. Dahdouh-Guebas, F.; Van Pottelbergh, I.; Kairo, J. G.; Cannicci, S.; Koedam, N. Human-impacted mangroves in Gazi (Kenya): Predicting future vegetation based on retrospective remote sensing, social surveys, and tree distribution. *Mar. Ecol. Prog. Ser.* **2004**, *272*, 77–92.

76. Valiela, I.; Bowen, J.L.; York, J. K. Mangrove forests: One of the world's threatened major tropical environments. *Bioscience* **2001**, *51*, 807–815.

77. Kerr, A. M.; Baird, A. H.; Bhalla, R. S.; Srinivas, V. Reply to “Using remote sensing to assess the protective role of coastal woody vegetation against tsunami waves.” *Int. J. Remote Sens.* **2009**, *30*, 3817–3820.

78. Giridharan, L.; Venugopal, T.; Jayaprakash, M. Evaluation of the seasonal variation on the geochemical parameters and quality assessment of the groundwater in the proximity of River Cooum, Chennai, India. *Environ. Monit. Assess.* **2008**, *143*, 161–178.

79. Blasco, F.; Aizpuru, M.; Gers, C. Depletion of the mangroves of continental Asia. *Wetl. Ecol. Manag.* **2001**, *9*, 245–256.

80. Ellison, A. M.; Farnsworth, E. J. The Global Conservation Status of Mangroves. *Ambio* **1997**.

81. Primavera, J. H. Development and conservation of Philippine mangroves: \rinstitutional issues. *Ecol. Econ.* **2000**.

82. UNEP-WCMC *In the front line : shoreline protection and other ecosystem services from mangroves*



and coral reefs; 2006.

83. Selvam, V.; Ravichandran, K. K.; Gnanappazham, L.; Navamuniyammal, M. Assessment of community-based restoration of Pichavaram mangrove wetland using remote sensing data. *Curr. Sci.* **2003**, *85*, 794–798.
84. Hoppe-Speer, S. C.; Adams, J. B.; Rajkaran, A. Mangrove expansion and population structure at a planted site, East London, South Africa. *South. For. a J. For. Sci.* **2015**, *77*, 131–139.
85. Saenger, P.; Hegerl, E.; Davie, J. Global status of mangrove ecosystems. *Glob. status mangrove ...* **1983**.
86. Jusoff, K. Individual species crown mapping in Taman Rimba Ilmu, University Malaya using airborne hyperspectral imaging. *Am. J. Appl. Sci.* **2010**, *7*, 493–499.
87. Ruiz-Luna, a; Berlanga-Robles, C. a Modifications in Coverage Patterns and Land Use around the Huizache-Caimanero Lagoon System, Sinaloa, Mexico: A Multi-temporal Analysis using LANDSAT Images. *Estuar. Coast. Shelf Sci.* **1999**.
88. Everitt, J.; Judd, F.; Escobar, D.; Davis, M. Integration of Remote Sensing and Spatial Information Technologies for Mapping Black Mangrove on the Texas Gulf Coast. *J. Coast. Res.* **1996**.
89. Mumby, P.J.; Green, E.P.; Edwards, A.J.; Clark, C. D. The cost-effectiveness of remote sensing for tropical coastal resources assessment and management. *J. Environ.* **1999**, *55*, 157–166.
90. Seto, K.C.; Fragkias, M. Mangrove conversion and aquaculture development in Vietnam: A remote sensing-based approach for evaluating the Ramsar Convention on Wetlands. *Glob. Environ. Chang.* **2007**, *17*, 486–500.
91. M, A.; F, A.; F, B. Global assessment of cover change of the mangrove forests using satellite imagery at medium to high resolution. *EEC Res. Proj. no. 15017-1999-05 FIED ISP FR. Jt. Res. Center, Ispra, Italy* **2000**.
92. Green, E.P.; Mumby, P.J.; Edwards, A.J.; Clark, C. D. A review of remote sensing for the assessment and management of tropical coastal resources. *Coast. Manag.* **1996**, *24*, 1–40.
93. Dahdouh-Guebas, F. The use of remote sensing and GIS in the sustainable management of tropical coastal ecosystems. *Environ. Dev. Sustain.* **2002**, *4*, 93–112.
94. Ong, C.C.; Cudahy, T.J.; Caccetta, M.S.; Piggott, M. S. Deriving quantitative dust measurements related to iron ore handling from airborne hyperspectral data. *Min. Technol.*



2003, 112, 158–163.

95. Hirano, A.; Madden, M.; Welch, R. Hyperspectral image data for mapping wetland vegetation. *Wetlands* **2003**, 23, 436–448.

96. Rao, B. R. M.; Dwivedi, R. S.; Kushwaha, S. P. S.; Bhattacharya, S. N.; Anand, J. B.; Dasgupta, S. Monitoring the spatial extent of coastal wetlands using ERS-1 SAR data. *Int. J. Remote Sens.* **1999**, 20, 2509–2517.

97. Simard, M.; Grandi, G. D. E.; Saatchi, S.; Mayaux, P. Mapping tropical coastal vegetation using JERS-1 and ERS-1 radar data with a decision tree classifier. *Int. J. Remote Sens.* **2002**, 23, 1461–1474.

98. Long, B. G.; Skewes, T. D. A Technique for Mapping Mangroves with Landsat TM Satellite Data and Geographic Information System. *Estuar. Coast. Shelf Sci.* **1996**, 43, 373–381.

99. Prasad, P. R. C.; Reddy, C. S.; Rajan, K. S.; Raza, S. H.; Dutt, C. B. S. Assessment of tsunami and anthropogenic impacts on the forest of the North Andaman Islands, India. *Int. J. Remote Sens.* **2009**.

100. Richards, D. R.; Friess, D. A. Rates and drivers of mangrove deforestation in Southeast Asia, 2000–2012. *Proc. Natl. Acad. Sci.* **2016**, 113, 344–349.

101. Megahed, Y.; Cabral, P.; Silva, J.; Caetano, M. Land Cover Mapping Analysis and Urban Growth Modelling Using Remote Sensing Techniques in Greater Cairo Region — Egypt. *ISPRS Int. J. Geo-Information* **2015**, 4, 1750–1769.

102. Sharma, K. P.; Jain, S. C.; Garg, P. K. Monitoring landuse and landcover changes using landsat images. *J. Indian Soc. Photo-Interpretation Remote Sens.* **1984**, 12, 65–70.

103. Drius, M.; Malavasi, M.; Acosta, A. T. R.; Ricotta, C.; Carranza, M. L. Boundary-based analysis for the assessment of coastal dune landscape integrity over time. *Appl. Geogr.* **2013**, 45, 41–48.

104. Tallis, H.; Kareiva, P.; Marvier, M.; Chang, A. Ecosystem Services Special Feature: An ecosystem services framework to support both practical conservation and economic development. *Proc Natl Acad Sci USA* **2008**, 105, 9457–9464.

105. Hara, Y.; Takeuchi, K.; Okubo, S. Urbanization linked with past agricultural landuse patterns in the urban fringe of a deltaic Asian mega-city: A case study in Bangkok. *Landsc. Urban Plan.* **2005**.

106. Hamilton, S. E.; Casey, D. Creation of a high spatio-temporal resolution global database

of continuous mangrove forest cover for the 21st century (CGMFC-21). *Glob. Ecol. Biogeogr.* **2016**, 25, 729–738.

107. Mundia, C. N.; Aniya, M. Dynamics of landuse/cover changes and degradation of Nairobi City, Kenya. *L. Degrad. Dev.* **2006**.

108. Gordon, A.; Simondson, D.; White, M.; Moilanen, A.; Bekessy, S. A. Integrating conservation planning and landuse planning in urban landscapes. *Landsc. Urban Plan.* **2009**.

109. Cabral, P.; Feger, C.; Levrel, H.; Chambolle, M.; Basque, D. Assessing the impact of land-cover changes on ecosystem services: A first step toward integrative planning in Bordeaux, France. *Ecosyst. Serv.* **2015**.

110. Evans, T. P.; Kelley, H. Multi-scale analysis of a household level agent-based model of landcover change. *J. Environ. Manage.* **2004**, 72, 57–72.

111. Sudhira, H. S.; Ramachandra, T. V.; Jagadish, K. S. Urban sprawl pattern recognition and modelling using GIS. *Map India, 2003, New Delhi* **2003**, 1–9.

112. Bhat, P. A.; Shafiq, M. ul; Mir, A. A.; Ahmed, P. Urban sprawl and its impact on landuse/land cover dynamics of Dehradun City, India. *Int. J. Sustain. Built Environ.* **2017**.

113. Cadenasso, M. L.; Pickett, S. T. A.; Schwarz, K. Spatial heterogeneity in urban ecosystems: conceptualizing land cover and a framework for classification. *Front. Ecol. Environ.* **2007**, 5, 80–88.

114. Sabet Sarvestani, M.; Ibrahim, A. L.; Kanaroglou, P. Three decades of urban growth in the city of Shiraz, Iran: A remote sensing and geographic information systems application. *Cities* **2011**, 28, 320–329.

115. Stow, D. A.; Chen, D. M. Sensitivity of multitemporal NOAA AVHRR data of an urbanizing region to land-use/land-cover changes and misregistration. *Remote Sens. Environ.* **2002**, 80, 297–307.

116. Binh, T. N. K. D.; Vromant, N.; Hung, N. T.; Hens, L.; Boon, E. K. Land cover changes between 1968 and 2003 in Cai Nuoc, Ca Mau Peninsula, Vietnam. *Environ. Dev. Sustain.* **2005**.

117. Berlanga-Robles, C. A.; Ruiz-Luna, A.; Berlanga-Robles, C. A.; Ruiz-Luna, A. Land Use Mapping and Change Detection in the Coastal Zone of Northwest Mexico Using Remote Sensing Techniques. *Source J. Coast. Res. J. Coast. Res.* **2002**.

118. Duguma, E. Remote Sensing-Based Urban Land Use/Land Cover Change Detection and Monitoring. *J. Remote Sens. GIS* **2017**, 6.

119. Muttitanon, W.; Tripathi, N. K. Land use/land cover changes in the coastal zone of Ban Don Bay, Thailand using Landsat 5 TM data. *Int. J. Remote Sens.* **2005**.
120. Dhorde, A.; Gadgil, A. Long-term temperature trends at four largest cities of India during the twentieth Century. *J Ind Geophys Union* **2009**, *13*, 85–97.
121. Meza Diaz, B.; Blackburn, G. A. Remote sensing of mangrove biophysical properties : evidence from a laboratory simulation of the possible effects of background variation on spectral vegetation indices. *Int. J. Remote Sens.* **2003**.
122. Wang, C. C.; Lv, Y.; Song, Y. Researches on mining subsidence disaster management GIS's system. In *2012 International Conference on Systems and Informatics, ICSAI 2012*; 2012; pp. 2493–2496.
123. Heumann, B. W. Satellite remote sensing of mangrove forests: Recent advances and future opportunities. *Prog. Phys. Geogr.* **2011**, *35*, 87–108.
124. Kuenzer, C.; Bluemel, A.; Gebhardt, S.; Quoc, T. V.; Dech, S. Remote sensing of mangrove ecosystems: A review. *Remote Sens.* **2011**, *3*, 878–928.
125. Rahman, M. K.; Schmidlin, T. W.; Munro-Stasiuk, M. J.; Curtis, A. Geospatial Analysis of Land Loss, Land Cover Change, and Landuse Patterns of Kutubdia Island, Bangladesh. *Int. J. Appl. Geospatial Res.* **2017**.
126. Lambin, E. F.; Geist, H. *Land-Use and Land-Cover Change: Local Processes and Global Impacts*; 2006.
127. Visalatchi; Padmanaban, R. Land Use and Land Cover Mapping and Shore Line Changes Studies in Tuticorin Coastal Area Using Remote Sensing. *Int. J. Remote Sens.* **2012**, *1*, 1–12.
128. Stow, D. A.; Hope, A.; McGuire, D.; Verbyla, D.; Gamon, J.; Huemmrich, F.; Houston, S.; Racine, C.; Sturm, M.; Tape, K.; Hinzman, L.; Yoshikawa, K.; Tweedie, C.; Noyle, B.; Silapaswan, C.; Douglas, D.; Griffith, B.; Jia, G.; Epstein, H.; Walker, D.; Daeschner, S.; Petersen, A.; Zhou, L.; Myneni, R. Remote sensing of vegetation and land-cover change in Arctic Tundra Ecosystems. *Remote Sens. Environ.* **2004**, *89*, 281–308.
129. Zhang, Q.; Wang, J.; Peng, X.; Gong, P.; Shi, P. Urban built-up land change detection with road density and spectral information from multi-temporal Landsat TM data. *Int. J. Remote Sens.* **2002**, *23*, 3057–3078.
130. Luck, M.; Wu, J. G. A gradient analysis of urban landscape pattern: a case study from the Phoenix metropolitan region, Arizona, USA. *Landsc. Ecol* **2002**, *17*, 327–340.

131. Gowri, V. S.; Ramachandran, S.; Ramesh, R.; Pramiladevi, I. R. R.; Krishnaveni, K. Application of GIS in the study of mass transport of pollutants by Adyar and Cooum Rivers in Chennai, Tamilnadu. *Environ. Monit. Assess.* **2008**, *138*, 41–49.
132. Dewan, A. M.; Yamaguchi, Y. Land use and land cover change in Greater Dhaka , Bangladesh : Using remote sensing to promote sustainable urbanization. *Appl. Geogr.* **2009**, *29*, 390–401.
133. Padmanaban, R. Integrating of Urban Growth Modelling and Utility Management System using Spatio Temporal Data Mining. *Int. J. Adv. Earth Sci. Eng.* **2012**, *1*, 13–15.
134. Padmanaban, R. Modelling the Transformation of Land use and Monitoring and Mapping of Environmental Impact with the help of Remote Sensing and GIS. *Int. J. Adv. Altern. Energy, Environ. Ecol.* **2012**, *1*, 36–38.
135. Herold, M.; Goldstein, N. C.; Clarke, K. C. The spatiotemporal form of urban growth: Measurement, analysis and modeling. *Remote Sens. Environ.* **2003**, *86*, 286–302.
136. De Oliveira Filho, F. J. B.; Metzger, J. P. Thresholds in landscape structure for three common deforestation patterns in the Brazilian Amazon. *Landsc. Ecol.* **2006**, *21*, 1061–1073.
137. Tv, R.; Aithal, B. H.; Sanna, D. D. Insights to urban dynamics through landscape spatial pattern analysis. *Int. J. Appl. Euarth Obs. Geoinf.* **2012**, *18*, 329–343.
138. Byomkesh, T.; Nakagoshi, N.; Dewan, A. M. Urbanization and green space dynamics in Greater Dhaka, Bangladesh. *Landsc. Ecol. Eng.* **2012**, *8*, 45–58.
139. Ferdinent, J.; Padmanaban, R. Development of a Methodology to Estimate Biomass from Tree Height Using Airborne Digital Image. *Int. J. Adv. Remote Sens. GIS* **2013**, *2*, 49–58.
140. Fistola, R. Urban entropy vs sustainability : a new town planning perspective. *WIT Trans. Ecol. Environ.* **2012**, *155*, 195–204.
141. Ji, W.; Ma, J.; Twibell, R. W.; Underhill, K. Characterizing urban sprawl using multi-stage remote sensing images and landscape metrics. *Comput. Environ. Urban Syst.* **2006**, *30*, 861–879.
142. Cabral, P.; Augusto, G.; Tewolde, M.; Araya, Y. Entropy in Urban Systems. *Entropy* **2013**, *15*, 5223–5236.
143. Fan, Y.; Yu, G.; He, Z.; Yu, H.; Bai, R.; Yang, L.; Wu, D. Entropies of the Chinese Land Use / Cover Change from 1990 to 2010 at a County Level. *Entropy* **2010**, *19*, 1–11.
144. Md. Fazlul Haque, M. M. R.; Akhand, D. D. A. Q. Generation of DEM and Ortho-image from High Resolution Stereo Satellite Data for a selected part of Southeast Bangladesh.

*INDIAN J. Appl. Res.* **2014**, 4, 500–502.

145. Dewan, A. M.; Humayun, K.; Nahar, M. K.; Rahman Ziaur Urbanisation and environmental degradation in Dhaka Metropolitan Area of Bangladesh. *Environ. Sustain. Dev.* **2012**, 11, 118–147.

146. Shanmugam, P.; Neelamani, S.; Ahn, Y. H.; Philip, L.; Hong, G. H. Assessment of the levels of coastal marine pollution of Chennai city, Southern India. *Water Resour. Manag.* **2007**, 21, 1187–1206.

147. Raman, N.; Narayanan, D. S. Impact of Solid Waste Effect on Ground Water and Soil Quality Nearer To Pallavaram Solid Waste Landfill Site in Chennai. *Rasayan* **2008**, 1, 828–836.

148. Bl—h, O. Unesco. *Phys. Today* 1949, 2, 3.

149. Arabindoo, P. “City of sand”: Stately Re-Imagination of Marina Beach in Chennai. *Int. J. Urban Reg. Res.* **2011**, 35, 379–401.

150. Rani, C. S. S.; Rema, M.; Deepa, R.; Premalatha, G.; Ravikumar, R.; Mohan, A.; Ramu, M.; Saroja, R.; Kayalvizhi, G.; Mohan, V. the Chennai Urban Population Study ( Cups ) - Methodological Details – ( Cups Paper No . 1 ). **1999**, 19.

151. Jayaprakash, M.; Senthil Kumar, R.; Giridharan, L.; Sujitha, S. B.; Sarkar, S. K.; Jonathan, M. P. Bioaccumulation of metals in fish species from water and sediments in macrotidal Ennore creek, Chennai, SE coast of India: A metropolitan city effect. *Ecotoxicol. Environ. Saf.* **2015**, 120, 243–255.

152. Cabral, P.; Santos, J. A. J. A.; Augusto, G. Monitoring Urban Sprawl and the National Ecological Reserve in Sintra-Cascais, Portugal: Multiple OLS Linear Regression Model Evaluation. *J. Urban Plan. Dev.* **2011**, 137, 346–353.

153. Padmanaban, R.; Sudalaimuthu, K. Marine Fishery Information System and Aquaculture Site Selection Using Remote Sensing and GIS. *Int. J. Adv. Remote Sens. GIS* **2012**, 1, pp 20-33.

154. S, S. L.; Padmanaban, R.; Thomas, V. Inventory of Liquefaction Area and Risk Assessment Region Using Remote Sensing. *Int. J. Adv. Remote Sens. GIS* **2013**, 2, 198–204.

155. Huttner, S.; Bruse, M.; Dostal, P. Using ENVI-met to simulate the impact of global warming on the mi- croclimate in central European cities. *5th Japanese-German Meet. Urban Climatol.* **2008**, 18, 307–312.

156. Khin Mar Yee; Khine Phoo Wai; Bak Jinhyung; Choi Chul Uong Land Use and Land Cover Mapping Based on Band Ratioing with Subpixel Classification by Support Vector

- Machine Techniques (A Case Study on Ngamoeyeik Dam Area, Yangon Region). *J. Geol. Resour. Eng.* **2016**, 4, 127–133.
157. Wilford, J.; Creasey, J.; Exploration, M. Landsat thematic mapper. *Geosci. Aust.* **2002**, 6–12.
158. Vincenzi, S.; Zucchetta, M.; Franzoi, P.; Pellizzato, M.; Pranovi, F.; De Leo, G. A.; Torricelli, P. Application of a Random Forest algorithm to predict spatial distribution of the potential yield of *Ruditapes philippinarum* in the Venice lagoon, Italy. *Ecol. Modell.* **2011**, 222, 1471–1478.
159. Center, U. geological S. E. R. O. and S. USGS.
160. Congalton, R. G. A review of assessing the accuracy of classifications of remotely sensed data. *Remote Sens. Environ.* **1991**, 37, 35–46.
161. Vasconcellos, R. M. De GeoTIFF Uma Abordagem Resumida do Formato. *GeoTIFF Uma Abordagem Resumida do Formato* **2002**.
162. Agency, N. G.; Frame, A.; Trs, A.; Type, G.; Version, D. L.; Epoch, R.; Description, B.; Earth, F.; Pole, I. R.; Conventional, B. I. H.; Pole, T.; Meridian, I. R.; Irm, T.; Meridian, B. I. H. *Z. World Geodetic System 1984*; 2005.
163. Harris Geospatial solutions Environment for Visualizing Image Analysis Software <http://www.harrisgeospatial.com/ProductsandSolutions/GeospatialProducts/ENVI.aspx>.
164. UMass landscape ecology lab FRAGSTATS: Spatial Pattern Analysis Program for Categorical Maps <http://www.umass.edu/landeco/research/fragstats/fragstats.html>.
165. Herold, M.; Scepan, J.; Clarke, K. C. The use of remote sensing and landscape metrics to describe structures and changes in urban land uses. *Environ. Plan. A* **2002**, 34, 1443–1458.
166. Tsallis, C. Possible generalization of Boltzmann-Gibbs statistics. *J. Stat. Phys.* **1988**, 52, 479–487.
167. Lumley, T. *R Fundamentals and Programming Techniques*. *R Man.* **2006**.
168. Maathuis, B. H. P.; Wang, L. Digital Elevation Model Based Hydro Processing. *Geocarto Int.* **2006**, 21, 21–26.
169. Stehman, S. V Estimating the Kappa coefficient and its variance under stratified random sampling. *Photogramm. Eng. Remote Sens.* **1996**, 62, 401–407.
170. USACE *New Jersey Shore Protection Study Manasquan Inlet to Barnegat Inlet - Draft Feasibility Report Integrated Environmental Impact Statement*; 2001; Vol. XXX.



171. ISRO Indian Space Research Organization <https://www.isro.gov.in>.
172. Pontius, R. G. Quantification Error Versus Location Error in Comparison of Categorical Maps. *Photogramm. Eng. Remote Sens.* **2000**, 1610, 1011–1016.
173. Gilmore, R.; Jr, P.; Boersma, W.; Clarke, K.; Nijs, T. De; Dietzel, C.; Duan, Z.; Fotsing, E.; Goldstein, N.; Kok, K.; Koomen, E.; Lippitt, C. D.; Mcconnell, W.; Mohd, A.; Pijanowski, B.; Pithadia, S.; Sweeney, S.; Ngoc, T.; Veldkamp, A. T.; Verburg, P. H. Comparing the input , output , and validation maps for several models of land change. *Springer* **2008**, 11–37.
174. Zyczkowski, K. Renyi Extrapolation of Shannon Entropy. *Cornell Univ. Libr.* **2003**, 1, 297–310.
175. Langley, S. K.; Cheshire, H. M.; Humes, K. S. A comparison of single date and multitemporal satellite image classifications in a semi-arid grassland. *J. Arid Environ.* **2001**, 49, 401–411.
176. Araya, Y. H.; Cabral, P. Analysis and modeling of urban land cover change in Setúbal and Sesimbra, Portugal. *Remote Sens.* **2010**, 2, 1549–1563.
177. Verburg, P. H.; Kok, K.; Pontius Jr., R. G.; Veldkamp, A. Modeling Land-Use and Land-Cover Change. In *Landuse and landcover change Local processes and global impacts Berlin Heidelberg New York Springer S*; 2006.
178. National Remote Sensing Centre Bhuvan.
179. Toz, G. and Erdogan, M. Dem ( Digital Elevation Model ) Production and Accuracy Modeling of Dems From 1 : 35 . 000 Scale Aerial Photographs. *Int. Arch. Photogramm. Remote Sens. Spat. Inf. Sci.* **2008**, 37, 755–780.
180. Flanders, D.; Hall-Beyer, M.; Pereverzoff, J. Preliminary evaluation of eCognition object-based software for cut block delineation and feature extraction. *Can. J. Remote Sens.* **2003**, 29, 441–452.
181. Clarks labs TerrSet Geospatial Monitoring and Modeling Software <https://clarklabs.org/terrset/>.
182. Chaves, A. B.; Lakshumanan, C. Remote Sensing and GIS- Based Integrated Study and Analysis for Mangrove- Wetland Restoration in Ennore Creek , Chennai , South India. In *Proceedings of Taal2007: The 12th World Lake Conference*; 2008; pp. 685–690.
183. Tanaka, N. Vegetation bioshields for tsunami mitigation: Review of effectiveness, limitations, construction, and sustainable management. *Landsc. Ecol. Eng.* **2009**, 5, 71–79.

184. Kim Oanh, N. T.; Upadhyay, N.; Zhuang, Y. H.; Hao, Z. P.; Murthy, D. V. S.; Lestari, P.; Villarin, J. T.; Chengchua, K.; Co, H. X.; Dung, N. T.; Lindgren, E. S. Particulate air pollution in six Asian cities: Spatial and temporal distributions, and associated sources. *Atmos. Environ.* **2006**, *40*, 3367–3380.
185. Chithra, V. S.; Shiva Nagendra, S. M. Indoor air quality investigations in a naturally ventilated school building located close to an urban roadway in Chennai, India. *Build. Environ.* **2012**, *54*, 159–167.
186. Lacerda, L. D. De; Menezes, M. O. T. De; Molisani, M. M. Changes in mangrove extension at the Pacoti River estuary, CE, NE Brazil due to regional environmental changes between 1958 and 2004. *Biota Neotrop.* **2007**, *7*, 67–72.
187. Brunn, A.; Fischer, C.; Dittmann, C.; Richter, R. Quality Assessment , Atmospheric and Geometric Correction of airborne hyperspectral HyMap Data. *Geotech. Eng.* **2003**, 13–16.
188. Kuosmanen, V.; Laitinen, J.; Arkimaa, H. A comparison of hyperspectral airborne HyMap and spaceborne Hyperion data as tools for studying the environmental impact of talc mining in Lahnaslampi, NE. ... *New Qual. Environ.* ... **2005**.
189. Sugimoto, H. *Seimitsu Kogaku Kaishi/Journal of the Japan Society for Precision Engineering*. 2006, pp. 285–288.
190. Ostendorf, A.; Hundertmark, H. Laser. In *Technology Guide: Principles - Applications - Trends*; 2009; pp. 104–109.
191. Pečnik, S.; Mongus, D.; Žalik, B. System for digital elevation model generation from LIDAR data. In *10th International Multidisciplinary Scientific Geoconference and EXPO - Modern Management of Mine Producing, Geology and Environmental Protection, SGEM 2010*; 2010; Vol. 1.
192. Lucas, R.; Ellison, J.; Mitchell, A.; Donnelly, B.; Finlayson, M.; Milne, A. Use of stereo aerial photography for quantifying changes in the extent and height of mangroves in tropical Australia. *Wetl. Ecol. Manag.* **2002**.
193. Ferdinent, J.; Padmanaban, R. Development of a Methodology to Estimate Biomass from Tree Height Using Airborne Digital Image. *Int. J. Adv. Remote Sens. GIS* **2013**, *2*, 49–58.
194. Hinz, C. Wetter dienst [http://www.wetterdienst.de/Deutschlandwetter/Thema\\_des\\_Tages/1653/deutschlandwetter-im-januar-2015](http://www.wetterdienst.de/Deutschlandwetter/Thema_des_Tages/1653/deutschlandwetter-im-januar-2015).
195. Galvin, J. M. Longwall Mining. In *Ground Engineering - Principles and Practices for*



*Underground Coal Mining*; 2016.

196. Svetnik, V.; Liaw, A.; Tong, C.; Christopher Culberson, J.; Sheridan, R. P.; Feuston, B. P. Random Forest: A Classification and Regression Tool for Compound Classification and QSAR Modeling. *J. Chem. Inf. Comput. Sci.* **2003**.
197. Chen, J.; Zhu, X.; Vogelmann, J. .; Gao, F.; Jin, S. A simple and effective method for filling gaps in Landsat ETM+ SLC-off images. *Remote Sens. Environ.* **2011**, 115, 1053–1064.
198. Pebesma, E.; Bivand, R.; Rowlingson, B.; Gomez-Rubio, V. Classes and Methods for Spatial Data. URL <http://CRAN.R-project.org/package=sp>, *R Packag. version* **2013**.
199. Shi, J.; Yuan, X.; Cai, Y.; Wang, G. GPS real-time precise point positioning for aerial triangulation. *GPS Solut.* **2017**, 21, 405–414.
200. Chen, S.-H.; Cioffi-Revilla, C.; Gilbert, N.; Kita, H.; Terano, T.; Yamamoto, R.; Nakamura, M.; Deguchi, H. Agent-Based Simulation Using a Model of Network Formation. *Agent-Based Soc. Syst.* **2011**.
201. Steve Morris; James Tuttle; Jefferson Essic A Partnership Framework for Geospatial Data Preservation in North Carolina. *Libr. Trends* **2009**, 57, 516–540.
202. Gao, J. A hybrid method toward accurate mapping of mangroves in a marginal habitat from SPOT multispectral data. *Int. J. Remote Sens.* **1998**.
203. Hijmans, R. J.; Etten, J. van; Mattiuzzi, M.; Sumner, M.; Greenberg, J. A.; Lamigueiro, O. P.; Bevan, A.; Racine, E. B.; Shortridge, A. Package “raster.” *R* **2014**, 1–27.
204. Breiman, L. Random forests. *Mach. Learn.* **2001**, 45, 5–32.
205. Goslee, S. C. Analyzing Remote Sensing Data in R : The landsat Package. *J. Stat. Softw.* **2011**, 43.
206. Streiner, D. L. An introduction to multivariate statistics. *Can. J. Psychiatry* **1993**, 38, 9–13.
207. Bivand, R. S.; Pebesma, E. J.; Gómez-Rubio, V. *Applied Spatial Data Analysis with R*; 2008; Vol. 65.
208. Hijmans, R. J.; Etten, J. raster: Geographic analysis and modeling with raster data. *R Packag. version 2.0-12*. <http://CRAN.R-project.org/package=raster> **2012**.
209. Assal, T. J.; Anderson, P. J.; Sibold, J. Mapping forest functional type in a forest-shrubland ecotone using SPOT imagery and predictive habitat distribution modelling. *Remote Sens. Lett.* **2015**, 6, 755–764.
210. Walston, L. J.; Cantwell, B. L.; Krummel, J. R. Quantifying spatiotemporal changes in a

- sagebrush ecosystem in relation to energy development. *Ecography (Cop.)*. **2009**, 32, 943–952.
211. Dubovyk, O.; Menz, G.; Conrad, C.; Kan, E.; Machwitz, M.; Khamzina, A. Spatio-temporal analyses of cropland degradation in the irrigated lowlands of Uzbekistan using remote-sensing and logistic regression modeling. *Environ. Monit. Assess.* **2013**, 185, 4775–4790.
212. Assal, T. J.; Anderson, P. J.; Sibold, J. Spatial and temporal trends of drought effects in a heterogeneous semi-arid forest ecosystem. *For. Ecol. Manage.* **2016**, 365, 137–151.
213. Masek, J. G.; Vermote, E. F.; Saleous, N. E.; Wolfe, R.; Hall, F. G.; Huemmrich, K. F.; Gao, F.; Kutler, J.; Lim, T. K. A landsat surface reflectance dataset for North America, 1990-2000. *IEEE Geosci. Remote Sens. Lett.* **2006**, 3, 68–72.
214. Assal, T. J.; Sibold, J.; Reich, R. Modeling a Historical Mountain Pine Beetle Outbreak Using Landsat MSS and Multiple Lines of Evidence. *Remote Sens. Environ.* **2014**, 155, 275–288.
215. Halabisky, M.; Moskal, L. M.; Gillespie, A.; Hannam, M. Reconstructing semi-arid wetland surface water dynamics through spectral mixture analysis of a time series of Landsat satellite images (1984-2011). *Remote Sens. Environ.* **2016**, 177, 171–183.
216. Tippmann, S. Programming tools: Adventures with R. *Nature* 2015.
217. Pebesma, E.; Bivand, R. S. S Classes and Methods for Spatial Data : the sp Package. *Econ. Geogr.* **2005**, 50, 1–21.
218. Clough, B.F.; Ong, J.E.; Gong, W. K. Estimating leaf area index and photosynthetic production in canopies of the mangrove *Rhizophora apiculata*. *Mar. Ecol. Prog. Ser.* **1997**, 159, 285–292.
219. Chevrel, S.; Kopackova, V.; Fischer, C.; Ben Dor, E.; Adar, S.; Shkolnisky, Y.; Misurec, J. Mapping minerals, vegetation health and change detection over the sokolov lignite mine using multirate hyperspectral airborne imagery. In *EAGE/GRSG Remote Sensing Workshop*; 2012.
220. Green, E. P.; Mumby, P. J.; Edwards, A. J.; Clark, C. D.; Ellis, A. C. Estimating leaf area index of mangroves from satellite data. *Aquat. Bot.* **1997**, 58, 11–19.
221. Kovacs, J. M.; Wang, J.; Flores-Verdugo, F. Mapping mangrove leaf area index at the species level using IKONOS and LAI-2000 sensors for the Agua Brava Lagoon, Mexican Pacific. *Estuar. Coast. Shelf Sci.* **2005**, 62, 377–384.
222. Kovacs, J. M.; Flores-Verdugo, F.; Wang, J.; Aspden, L. P. Estimating leaf area index of a degraded mangrove forest using high spatial resolution satellite data. *Aquat. Bot.* **2004**, 80, 13–

22.

223. Kovacs, J. M.; King, J. M. L.; Flores de Santiago, F.; Flores-Verdugo, F. Evaluating the condition of a mangrove forest of the Mexican Pacific based on an estimated leaf area index mapping approach. *Environ. Monit. Assess.* **2009**, *157*, 137–149.

224. Neukermans, G.; Dahdouh-Guebas, F.; Kairo, J. G.; Koedam, N. Mangrove species and stand mapping in Gazi bay (Kenya) using quickbird satellite imagery. *J. Spat. Sci.* **2008**, *53*, 75–86.

225. Giri, C.P.; Kratzschmar, E.; Ofren, R.S.; Pradhan, D.; Shrestha, S. Assessing Land Use/Land Cover Dynamics in Two Identified “Hot Spot” Areas: Oudomxay Province of Lao P.D.R. and Mekong Delta of Vietnam. In *In Proceeding of The 17th Asian Conference on Remote Sensing, Colombo, Sri Lanka*; 1996.

226. Loughner, C. P.; Allen, D. J.; Zhang, D. L.; Pickering, K. E.; Dickerson, R. R.; Landry, L. Roles of urban tree canopy and buildings in urban heat island effects: Parameterization and preliminary results. *J. Appl. Meteorol. Climatol.* **2012**, *51*, 1775–1793.

227. HaiderTaha Characterization of Urban Heat and Exacerbation: Development of a Heat Island Index for California. *Climate* **2017**, *5*, 19–21.

228. Trenberth, K. E.; Shea, D. J. Relationships between precipitation and surface temperature. *Geophys. Res. Lett.* **2005**, *32*, 1–4.

229. W., H. B. The United States Geological Survey. *Nature* 1903, *69*, 115–116.

230. Menberg, K.; Bayer, P.; Zosseder, K.; Rumohr, S.; Blum, P. Subsurface urban heat islands in German cities. *Sci. Total Environ.* **2013**, *442*, 123–133.

231. Narmada, K.; Gobinath, K.; Bhaskaran, G. An Assessment of Resource Potentials for Sustainable Development of Micro-watershed in Tirunelveli District Using Geoinformatics– A Case of Nambiyar Micro-watershed in Tirunelveli District, Tamil Nadu, India. *Aquat. Procedia* **2015**, *4*, 1299–1306.

232. Pande, H.; Tiwari, P. S. High-Resolution and Hyperspectral Data Fusion for Classification. In *New Advances in Image Fusion*; 2013; pp. 57–77.

233. Zhu, L.; Tateishi, R. Fusion of multisensor multitemporal satellite data for land cover mapping. *Int. J. Remote Sens.* **2006**.

234. Kandrika, S.; Ravisankar, T. Multi-temporal satellite imagery and data fusion for improved land cover information extraction. *Int. J. Image Data Fusion* **2011**, *2*, 61–73.

235. Abdikan, S.; Balik Sanli, F.; Sunar, F.; Ehlers, M. A comparative data-fusion analysis of multi-sensor satellite images. *Int. J. Digit. Earth* **2014**, *7*, 671–687.
236. Lillo-Saavedra, M.; Gonzalo, C. Spectral or spatial quality for fused satellite imagery? A trade-off solution using the wavelet à trous algorithm. *Int. J. Remote Sens.* **2006**, *27*, 1453–1464.
237. Per, S. K.; RasmusFensholt; Martin, D. Using Landsat Vegetation Indices to Estimate Impervious Surface Fractions For European Cities. *Remote Sens.* **2015**, *7*, 8224–8249.
238. Zhengming, W. *MODIS Land-Surface Temperature*; China, 1999.
239. Yamamoto, Y. Measures to Mitigate Urban Heat Islands. *Environ. Energy Res. Unit. Quaterly Rev.* **2005**, *18*, 65–83.
240. Gajendran, C.; Jayapriya, S.; Yohannan, D.; Victor, O.; Jacob, C. Assessment of groundwater quality in Tirunelveli District , Tamil Nadu , India. *Int. J. Environ. Sci.* **2013**, *3*, 1874–1880.
241. Ijar, R.; Publications, A. C. E.; Ijar, R. Water Quality Assesement of River Thamirabarani At Tirunelveli District. *Intern. J. Adv. reserch trends Eng. Technol.* **2016**, *3*, 308–313.
242. Tamilnadu Directorate of Census Operations Tamilnadu census <http://www.census2011.co.in>.
243. Alagumuthu, G.; Rajan, M. Chemometric studies of water quality parameters of Sankarankovil block of Tirunelveli, Tamilnadu. *J. Environ. Biol.* **2010**, *31*, 581–586.
244. Kiruba, S.; Jeeva, S.; Kanagappan, M.; Stalin, S. I.; Das, S. S. M. Ethnic storage strategies adopted by farmers of Tirunelveli district of Tamil Nadu , Southern Peninsular India. *J. Agric. Technol.* **2008**, 1–10.
245. Palanisami; Venkatram *NATIONAL AGRICULTURAL DEVELOPMENT PROGRAMME*. 2008, pp. 1–240.
246. Mirza, M. M. Q. VULNERABILITY TO THE GANGES WATER DIVERSION : ADAPTATION AND COPING MECHANISMS. In *The Ganges Water Dispersion: Environmental Effects and Implications*; 2004; pp. 247–285.
247. Lee, T. M.; Yeh, H. C. Applying remote sensing techniques to monitor shifting wetland vegetation: A case study of Danshui River estuary mangrove communities, Taiwan. *Ecol. Eng.* **2009**, *35*, 487–496.
248. Survey, U. S. D. of the I. U. S. G. usgs.
249. Gesch, D. B.; Verdin, K. L.; Greenlee, S. K. New land surface digital elevation model

covers the earth. *Eos (Washington. DC)*. 1999, 80, 69–70.

250. Geymen, A. Digital elevation model (DEM) generation using the SAR interferometry technique. *Arab. J. Geosci.* **2014**, 7, 827–837.

251. Schenk, T. Towards automatic aerial triangulation. *ISPRS J. Photogramm. Remote Sens.* **1997**, 52, 110–121.

252. Daniel, C.; Tennant, Hk. DEM Quality Assessment. In *Digital Elevation Model Technologies and Applications : the DEM Users Manual*; 2001; pp. 395–440.

253. Xu, S.; Ehlers, M. Hyperspectral image sharpening based on Ehlers fusion. In *International Archives of the Photogrammetry, Remote Sensing and Spatial Information Sciences - ISPRS Archives*; 2017; Vol. 42, pp. 941–947.

254. Klonus, S.; Ehlers, M. Image Fusion Using the Ehlers Spectral Characteristics Preservation Algorithm. *GIScience Remote Sens.* **2007**, 44, 93–116.

255. Ling, Y.; Ehlers, M.; Usery, E. L.; Madden, M. FFT-enhanced IHS transform method for fusing high-resolution satellite images. *ISPRS J. Photogramm. Remote Sens.* **2007**, 61, 381–392.

256. Hijmans, R. J.; Etten, J. raster: Geographic analysis and modeling with raster data. *R Packag. version 2.4-20*. <http://CRAN.R-project.org/package=raster> **2012**.

257. Kennedy, M.; Kopp, S. *Understanding map projections*; 2002.

258. Rodríguez, J. J.; Kunchewa, L. I.; Alonso, C. J. Rotation forest: A New classifier ensemble method. *IEEE Trans. Pattern Anal. Mach. Intell.* **2006**, 28, 1619–1630.

259. Ozlem, A. The Rotation Forest algorithm and object-based classification method for land use mapping through UAV images. *Geocarto Int.* **2018**, 33.

260. Franklin, S. E.; Blodgett, C. F. An example of satellite multisensor data fusion. *Comput. Geosci.* **1993**, 19, 577–583.

261. Anderson, J.R., Hardy, E.E., Roach, J.T. et Witmer, R. E. A Land Use And Land Cover Classification System For Use With Remote Sensor Data. *US Gov. Print. Off.* **1976**, 964.

262. Gilabert, M. A.; González-Piqueras, J.; García-Haro, F. J.; Meliá, J. A generalized soil-adjusted vegetation index. *Remote Sens. Environ.* **2002**, 82, 303–310.

263. Qi, J.; Chehbouni, A.; Huete, A. R.; Kerr, Y. H.; Sorooshian, S. A modified soil adjusted vegetation index. *Remote Sens. Environ.* **1994**, 48, 119–126.

264. Huete, A. R. A soil-adjusted vegetation index (SAVI). *Remote Sens. Environ.* **1988**, 25, 295–309.

265. Sun, Y. Retrieval and Application of Land Surface Temperature. *Geo.Utexas.Edu* **2008**, 1, 1–27.
266. Weng, Q.; Lu, D.; Schubring, J. Estimation of land surface temperature-vegetation abundance relationship for urban heat island studies. *Remote Sens. Environ.* **2004**, 89, 467–483.
267. Ulivieri, C.; Cannizzaro, G. Land surface temperature retrievals from satellite measurements. *Acta Astronaut.* **1985**, 12, 977–985.
268. Roth, M. Urban Heat Islands. *Handb. Environ. Fluid Dyn.* **2013**, 2, 143–159.
269. Yingying, X.; Xiaojing, W.; SilanderJohn A, J. . Deciduous forest responses to temperature, precipitation, and drought imply complex climate change impacts. *Proc Natl Acad Sci USA* **2015**, 112, 13585–13590.
270. Gartland, L. *Heat Islands: Understanding and mitigating heat in urban areas*; 2012.
271. Zhao, L.; Lee, X.; Smith, R. B.; Oleson, K. Strong contributions of local background climate to urban heat islands. *Nature* **2014**, 511, 216–219.
272. Ward, K.; Lauf, S.; Kleinschmit, B.; Endlicher, W. Heat waves and urban heat islands in Europe: A review of relevant drivers. *Sci. Total Environ.* **2016**, 569–570, 527–539.
273. Lucas, R.; Rebelo, L. M.; Fatoyinbo, L.; Rosenqvist, A.; Itoh, T.; Shimada, M.; Simard, M.; Souza-Filho, P. W.; Thomas, N.; Trettin, C.; Accad, A.; Carreiras, J.; Hilarides, L. Contribution of L-band SAR to systematic global mangrove monitoring. *Mar. Freshw. Res.* **2014**, 65, 589–603.
274. Vaiphasa, C.; Ongsomwang, S.; Vaiphasa, T.; Skidmore, A. K. Tropical mangrove species discrimination using hyperspectral data: A laboratory study. *Estuar. Coast. Shelf Sci.* **2005**, 65, 371–379.
275. Blasco, F.; Gauquelin, T.; Rasolofoharinoro, M.; Denis, J.; Aizpuru, M.; Caldairou, V. Recent advances in mangrove studies using remote sensing data. *Mar. Freshw. Res.* **1998**, 49, 287.
276. Green, E. P.; Clark, C. D.; Mumby, P. J.; Edwards, a. J.; Ellis, a. C. Remote sensing techniques for mangrove mapping. *Int. J. Remote Sens.* **1998**, 19, 935–956.
277. Fromard, F.; Vega, C.; Proisy, C. Half a century of dynamic coastal change affecting mangrove shorelines of French Guiana. A case study based on remote sensing data analyses and field surveys. *Mar. Geol.* **2004**, 208, 265–280.
278. Blasco, F.; Saenger, P.; Janodet, E. Mangroves as indicator of coastal change. *Catena* **1996**, 27, 167–178.



279. Kathiresan, K.; Rajendran, N. Coastal mangrove forests mitigated tsunami. *Estuar. Coast. Shelf Sci.* **2005**, *65*, 601–606.
280. Danielsen, F.; Sørensen, M. K.; Olwig, M. F.; Selvam, V.; Parish, F.; Burgess, N. D.; Hiraishi, T.; Karunakaran, V. M.; Rasmussen, M. S.; Hansen, L. B.; Quarto, A.; Suryadiputra, N. The Asian tsunami: a protective role for coastal vegetation. *Science (80-. ).* **2005**, *310*, 643.
281. Cochard, R.; Ranamukhaarachchi, S. L.; Shivakoti, G. P.; Shipin, O. V.; Edwards, P. J.; Seeland, K. T. The 2004 tsunami in Aceh and Southern Thailand: A review on coastal ecosystems, wave hazards and vulnerability. *Perspect. Plant Ecol. Evol. Syst.* **2008**, *10*, 3–40.
282. Alongi, D. M. Mangrove forests: Resilience, protection from tsunamis, and responses to global climate change. *Estuar. Coast. Shelf Sci.* **2008**, *76*, 1–13.
283. Giri, C.; Zhu, Z.; Tieszen, L. L.; Singh, A.; Gillette, S.; Kelmelis, J. A. Mangrove forest distributions and dynamics (1975–2005) of the tsunami-affected region of Asia. *J. Biogeogr.* **2008**, *35*, 519–528.
284. Cabral, P.; Augusto, G.; Akande, A.; Costa, A.; Amade, N.; Niquisse, S.; Atumane, A.; Cuna, A.; Kazemi, K.; Mlucasse, R.; Santha, R. Assessing Mozambique's exposure to coastal climate hazards and erosion. *Int. J. Disaster Risk Reduct.* **2017**, *23*, 45–52.
285. Spalding, M. The global distribution and status of mangrove ecosystems. *Int. NewsLett. Coast. Manag.* **1997**, *1*, 20–21.
286. Barbosa, F. M. A.; Cuambe, C. C.; Bandeira, S. O. Status and distribution of mangroves in Mozambique. *South African J. Bot.* **2001**.
287. Walter, V. Object-based classification of remote sensing data for change detection. *ISPRS J. Photogramm. Remote Sens.* **2004**, *58*, 225–238.
288. Hutchison, J.; Manica, A.; Swetnam, R.; Balmford, A.; Spalding, M. Predicting global patterns in mangrove forest biomass. *Conserv. Lett.* **2014**, *7*, 233–240.
289. Jiménez, J. A. 16 - Mangrove Forests of the Pacific Coast of Central America. In *Coastal Plant Communities of Latin America*; 1992; pp. 259–267.
290. Viana, I. G.; Valiela, I.; Martinetto, P.; Monteiro Pierce, R.; Fox, S. E. Isotopic studies in Pacific Panama mangrove estuaries reveal lack of effect of watershed deforestation on food webs. *Mar. Environ. Res.* **2015**, *103*, 95–102.
291. Mazda, Y.; Magi, M.; Kogo, M.; Hong, P. N. Mangroves as coastal protection from waves in the Tong King delta, Vietnam. *Mangroves Salt Marshes* 1997.

292. Ranasinghe, D. M. S. H. K. Agroforestry and community forestry in Sri Lanka. *Sri Lanka For.* **1991**, XX, 45–49.
293. Clough, B. F. Primary productivity and growth of mangrove forests. In *Tropical Mangrove Ecosystems*; 1992; pp. 225–249.
294. Chapman, V. J. *Mangrove vegetation.*; 1976.
295. Alongi, D. M. Present state and future of the world's mangrove forests. *Environ. Conserv.* **2002**, 29, 331–349.
296. Kairo, J. G.; Dahdouh-Guebas, F.; Bosire, J.; Koedam, N. Restoration and management of mangrove systems - a lesson for and from the East African region. *South African J. Bot.* **2001**.
297. Selvam, V.; Ravichandran, K.K.; Gnanappazham, L.; Navamuniyammal, M. Assessment of community-based restoration of Pichavaram mangrove wetland using remote sensing data. *Curr. Sci.* **2003**, 85, 794–798.
298. Field, C. D. Mangrove rehabilitation: Choice and necessity. *Hydrobiologia* **1999**.
299. Lal, P. N. Conservation or Conversion of Mangroves in Fiji- An Ecological Economic Analysis. *Occas. Pap. East-West Environ. Policy Inst.* **1990**, 108.
300. Yang, C.; Everitt, J. H.; Fletcher, R. S.; Jensen, R. R.; Mausel, P. W. Evaluating AISA + Hyperspectral Imagery for Mapping Black Mangrove along the South Texas Gulf Coast. *Photogramm. Eng. Remote Sens.* **2009**, 75, 425–435.
301. Wang, L.; Sousa, W. P. Distinguishing mangrove species with laboratory measurements of hyperspectral leaf reflectance. *Int. J. Remote Sens.* **2009**, 30, 1267–1281.
302. Aschbacher, J.; Ofren, R.; Delsol, J. .; Suselo, T. .; Vibulsresth, S.; Charrupat, T. An integrated comparative approach to mangrove vegetation mapping using advanced remote sensing and GIS technologies: Preliminary results. *Asia-Pacific Symp.* **1995**, 295, 285–295.
303. Everitt, J.H.; Yang, C.; Sriharan, S.; Judd, F. W. Using high resolution satellite imagery to map black mangrove on the Texas Gulf Coast. *J. Coast. Res.* **2008**, 24, 1582–1586.
304. Giri, C.; Pengra, B.; Zhu, Z.; Singh, A.; Tieszen, L. L. Monitoring Mangrove forest dynamics of the Sundarbans in Bangladesh and India using multi-temporal satellite data from 1973 to 2000. *Estuar. Coast. Shelf Sci.* **2007**, 73, 91–100.
305. Hess, L. L.; Melack, J. M.; Simonett, D. S. Radar detection of flooding beneath the forest canopy: a review. *Int. J. Remote Sens.* **1990**, 11, 1313–1325.
306. Oppermann, R. H. Understanding microwaves. *J. Franklin Inst.* **1946**, 242, 430.



307. ESRI ArcGIS 2017.
308. FAO The world's mangroves 1980–2005. *FAO For. Pap. Food Agric. Organ. United Nations*) **2007**, 153.
309. UNEP, F. & Tropical Forest Resources Assessment Project: forest resources of tropical Asia. *FAO, Rome* **1981**.
310. Giri, C.; Ochieng, E.; Tieszen, L. L.; Zhu, Z.; Singh, A.; Loveland, T.; Masek, J.; Duke, N. Status and distribution of mangrove forests of the world using earth observation satellite data. *Glob. Ecol. Biogeogr.* **2011**, 20, 154–159.
311. Giri, Chandra, J. Lomg, S. Abbas, R. Mani Murali, F. M. Q. and D. T. Distribution and dynamics of mangrove forests of South Asia. *J. Environ. Manage.* **2015**, 48, 101–111.
312. Gang, P. O.; Agatsiva, J. L. The current status of mangroves along the Kenyan coast: a case study of Mida Creek mangroves based on remote sensing. *Hydrobiologia* 1992.
313. Giri, C.; Zhu, Z.; Tieszen, L. L.; Singh, A.; Gillette, S.; Kelmelis, J. A. Mangrove forest distributions and dynamics (1975–2005) of the tsunami-affected region of Asia. *J. Biogeogr.* **2008**, 35, 519–528.
314. Simard, M.; Zhang, K.; Rivera-monroy, V. H.; Ross, M. S.; Ruiz, P. L.; Castañeda-moya, E.; Twilley, R. R.; Rodriguez, E. Mapping Height and Biomass of Mangrove Forests in Everglades National Park with SRTM Elevation Data. *Photogramm. Eng. Remote Sens.* **2006**, 72, 299–311.
315. Krauss, K. W.; Lovelock, C. E.; McKee, K. L.; López-Hoffman, L.; Ewe, S. M. L.; Sousa, W. P. Environmental drivers in mangrove establishment and early development: A review. *Aquat. Bot.* 2008.
316. Spalding, M., Blasco, F. & Field, C. World mangrove atlas. *Int. Soc. Mangrove Ecosyst. Okinawa, Japan* **1997**.
317. FAO FAO Fisheries and Aquaculture Department, Mangrove forest management guidelines. *FAO For. Pap. FAO Fish. Aquac. Dep. Rome* **2004**.
318. C, J. Web of Science. *Charlest. Advis.* **2018**, 20, 52–54.
319. Ansari, Z. A.; Matondkar, S. G. P. Anthropogenic activities including pollution and contamination of coastal marine environment. *J. Ecophysiol. Occup. Heal.* **2014**.
320. Liu, K.; Li, X.; Shi, X.; Wang, S.; College, D.; Hampshire, N. Monitoring Mangrove Forest Changes Using Remote Sensing and Gis Data With Decision-Tree Learning. **2005**, 28, 336–346.

321. Thu, P. M.; Populus, J. Status and changes of mangrove forest in Mekong Delta: Case study in Tra Vinh, Vietnam. *Estuar. Coast. Shelf Sci.* **2007**.
322. Kovacs, J. M.; Wang, J.; Blanco-Correa, M. Mapping disturbances in a mangrove forest using multi-date landsat TM imagery. *Environ. Manage.* **2001**, 27, 763–776.
323. Bann, C. The Economic Valuation of Mangroves: A Manual for Researchers. *Econ. Environ. Progr. Southeast Asia* **1998**, 55.
324. Cannicci, S.; Burrows, D.; Fratini, S.; Smith, T. J.; Offenberg, J.; Dahdouh-Guebas, F. Faunal impact on vegetation structure and ecosystem function in mangrove forests: A review. *Aquat. Bot.* **2008**.
325. Vermaat, J. E.; Thampanya, U. Mangroves mitigate tsunami damage: A further response. *Estuar. Coast. Shelf Sci.* **2006**.
326. Wessels, K. J.; De Fries, R. S.; Dempewolf, J.; Anderson, L. O.; Hansen, A. J.; Powell, S. L.; Moran, E. F. Mapping regional land cover with MODIS data for biological conservation: Examples from the Greater Yellowstone Ecosystem, USA and Par?? State, Brazil. *Remote Sens. Environ.* **2004**, 92, 67–83.
327. Barbier, E. B. The protective service of mangrove ecosystems: A review of valuation methods. *Mar. Pollut. Bull.* **2016**, 109, 676–681.
328. Titus, J. G.; Barth, M. C.; Gibbs, M. J.; Hoffman, J. S.; Kenney, M. An overview of the causes and effects of sea level rise. *Greenh. Eff. sea Lev. rise* **1984**.
329. Ar, I.; Federation, I.; Cross, R.; Slr, T.; Coastal, L. E.; Gdp, T.; To, S. L. R. Risk Assessment of Indian Coastal Cities to Sea Level Rise A Development Planning Perspective. *Propos. Risk Assesment Indian Coast. cities to Sea-level Rise* **2009**.
330. Nicholls, R. J. Impacts of and Responses to Sea-Level Rise. In *Understanding Sea-Level Rise and Variability*; 2010.
331. IPCC *Climate change 2007. The physical science basis*; 2007.
332. López, J. M.; Stoner, A. W.; García, J. R.; García-Muñiz, I. Marine food webs associated with Caribbean Islands mangrove wetlands. *Acta Científica* **1988**, 2, 94–123.
333. Manna, S.; Chaudhuri, K.; Bhattacharyya, S.; Bhattacharyya, M. Dynamics of Sundarban estuarine ecosystem: eutrophication induced threat to mangroves. *Saline Systems* **2010**.
334. Seach, J. Vanikoro Island, Solomon Islands.
335. Tam, N. F. Y. Pollution studies on mangroves in Hong Kong and Mainland China. In *The*

*Environment in Asia Pacific Harbours*; 2006.

336. Rahman, M. M. Time-Series Analysis of Coastal Erosion in the Sundarbans Mangrove. *XXII ISPRS Congr. Tech. Comm. VIII* **2012**, XXXIX, 425–429.

337. Mantri, V. A.; Mishra, A. K. On monitoring mangrove vegetation of Sagar Island by remote sensing. *Natl. Acad. Sci. Lett.* **2006**, 29, 45–48.

338. Caesar, J.; Janes, T.; Lindsay, A.; Bhaskaran, B. Temperature and precipitation projections over Bangladesh and the upstream Ganges, Brahmaputra and Meghna systems. *Environ. Sci. Process. Impacts* **2015**, 17, 1047–1056.

339. Neumann, B.; Vafeidis, A. T.; Zimmermann, J.; Nicholls, R. J. Future coastal population growth and exposure to sea-level rise and coastal flooding - A global assessment. *PLoS One* **2015**.

340. Meyers, R. A. *Extreme Environmental Events*; 2011.

341. de Rham, L. P.; Prowse, T. D.; Beltaos, S.; Lacroix, M. P. Assessment of annual high-water events for the Mackenzie River basin, Canada. *Hydrol. Process.* **2008**.

342. Trenberth, K. E. El Niño Southern Oscillation (ENSO). In *Encyclopedia of Ocean Sciences: Second Edition*; 2008; pp. 228–240.

343. Committee, A. T.; Rise, S.; Effects, I. Effects of Sea-Level Rise on Bays and Estuaries. *J. Hydraul. Eng.* **1992**.

344. USACE *Feasibility Report Flood Damage Reduction for Des Moines and Raccoon Rivers Project: Part 1*; 2005; Vol. 1.

345. Day, J. W.; Conner, W. H.; Costanza, R.; Kemp, G. P.; Mendelssohn, I. A. Impacts of sea level rise on coastal systems with special emphasis on the Mississippi River deltaic plain. In *Climate and sea level change: observations, projections and implications*; 1994; pp. 276–296.

346. Umitsu, M. Geo-environment and effect of sea level rise in the Chao Phraya Delta. In *The International Conference on the Chao Phraya Delta: historical development, dynamics and challenges of Thailand's rice bowl*. Kasetsart University, Bangkok; 2002; pp. 1–6.

347. Pinxian, W.; Huanting, S. Changjiang (Yangtze) river delta: a review. In *Coastal Zone: Proceedings of the Symposium on Coastal and Ocean Management*; 1993.

348. Marshall, N. Mangrove conservation in relation to overall environmental considerations. *Hydrobiologia* **1994**.

349. Monirul Qader Mirza, M.; Warrick, R. A.; Ericksen, N. J. The implications of climate

change on floods of the Ganges, Brahmaputra and Meghna rivers in Bangladesh. *Clim. Change* **2003**, 57, 287–318.

350. Ahmad, M. M. Water, water, water everywhere: Experience of Bangladesh in flood disaster management and need for cooperation in the Ganges, Brahmaputra and Meghna Regions. *J. Rural Dev.* **2004**, 23, 279–295.

351. Whitehead, P. G.; Barbour, E.; Futter, M. N.; Sarkar, S.; Rodda, H.; Caesar, J.; Butterfield, D.; Jin, L.; Sinha, R.; Nicholls, R.; Salehin, M. Impacts of climate change and socio-economic scenarios on flow and water quality of the Ganges, Brahmaputra and Meghna (GBM) river systems: low flow and flood statistics. *Environ. Sci. Process. Impacts* **2015**, 17, 1057–1069.

352. Landsea, C. W. Climate Variability of Tropical Cyclones: Past, Present and Future. In *Storms*; 2000.

353. Field, C. D. Impact of expected climate change on mangroves. *Hydrobiologia* **1995**.

354. Grabarek, D. The Sea, the Storm, and the Mangrove Tangle. *Sch. Libr. J.* **2004**, 50, 105.

355. Roth, L. C. Hurricanes and mangrove regeneration: effects of Hurricane Joan, October 1988, on the vegetation of Isla del Venado, Bluefields, Nicaragua. *Biotropica* **1992**, 24, 375–384.

356. Doyle, T. W.; Girod, G. F.; Diaz, H. F.; Pulwarty, R. S. The frequency and intensity of Atlantic hurricanes and their influence on the structure of South Florida mangrove communities. In *Hurricanes*; 1997; p. 109–120 292.

357. Doyle, T. W.; Girod, G. F.; Books, M. A. Chapter 12: modeling mangrove forest migration along the southwest coast of Florida under climate change. *Ning, Z.H., Turner, R.E., Doyle, T.W., Abdollahi, K* **2003**, pp, 211–221.

358. Granzow-de la Cerda, I.; Zamora, N.; Vandermeer, J.; Boucher, D. Tree species diversity in the tropical moist forest (Caribbean of Nicaragua) seven years after Hurricane Joan. *Rev. Biol. Trop.* **1997**, 45, 1409–1419.

359. Das, S. *Can mangroves minimize property loss during big storms?: An analysis of house damages due to the super cyclone in Orissa*; 2009.

360. Granek, E. F.; Ruttenberg, B. I. Protective capacity of mangroves during tropical storms: A case study from “Wilma” and “Gamma” in Belize. *Mar. Ecol. Prog. Ser.* **2007**.

361. Khan, S. R. CYCLONE HAZARD IN BANGLADESH. In *Geomorphic Characterization of cyclone hazards along the coast of Bangladesh*; 1995.

362. Alam, E.; Collins, A. E. Cyclone disaster vulnerability and response experiences in coastal

Bangladesh. *Disasters* **2010**, 34, 931–954.

363. Smith, B. D.; Mansur, E. F. Sundarbans mangrove forest, Bangladesh. In *Climate and Conservation: Landscape and Seascape Science, Planning, and Action*; 2012; pp. 144–154.

364. Panigrahi, N. Disaster management and the need for convergence of services of welfare agencies-A case study of the Super Cyclone of Orissa. *Soc. Change* **2003**, 33, 1–25.

365. Madhu, N. V.; Maheswaran, P. A.; Jyothibabu, R.; Sunil, V.; Revichandran, C.; Balasubramanian, T.; Gopalakrishnan, T. C.; Nair, K. K. C. Enhanced biological production off Chennai triggered by October 1999 super cyclone (Orissa). *Curr. Sci.* **2002**, 82, 1472–1479.

366. Hurrell, J. W.; Kushnir, Y.; Visbeck, M. The North Atlantic oscillation. *Science* (80-. ). 2001, 291, 603–605.

367. Kusmana, C. Distribution and current status of mangrove forests in Indonesia. In *Mangrove Ecosystems of Asia: Status, Challenges and Management Strategies*; 2014; pp. 37–60.

368. Selvam, V. Environmental classification of mangrove wetlands of India. *Curr. Sci.* **2003**, 84, 757–765.

369. Naito, T.; Traesupap, S. The relationship between mangrove deforestation and economic development in Thailand. In *Mangrove Ecosystems of Asia: Status, Challenges and Management Strategies*; 2014; pp. 273–294.

370. KUSMANA, C.; SABIHAM, S.; ABE, K.; WATANABE, H. An Estimation of Above Ground Tree Biomass of a Mangrove Forest in East Sumatra, Indonesia. *Tropics* **1992**, 1, 243–257.

371. Alongi, D. M.; Trott, L. A.; Rachmansyah; Tirendi, F.; McKinnon, A. D.; Undu, M. C. Growth and development of mangrove forests overlying smothered coral reefs, Sulawesi and Sumatra, Indonesia. *Mar. Ecol. Prog. Ser.* **2008**, 370, 97–109.

372. Kanagaratnam, U.; Adhuri, D.; Dey, M. M.; Schwarz, a M. Mangrove Rehabilitation in the West Coast of Aceh ? Issues and Perspectives. *Naga WorldFish Cent. Q.* **2006**, 29, 10–18.

373. Pumijumnong, N. Mangrove forests in Thailand. In *Mangrove Ecosystems of Asia: Status, Challenges and Management Strategies*; 2014; pp. 61–79.

374. Kanaya, G.; Suzuki, T.; Kikuchi, E. Impacts of the 2011 tsunami on sediment characteristics and macrozoobenthic assemblages in a shallow eutrophic lagoon, Sendai Bay, Japan. *PLoS One* **2015**, 10.

375. Williams, N. Tsunami insight to mangrove value. *Curr. Biol.* **2005**, 15, R73.

376. Diop, E. S.; Soumare, A.; Diallo, N.; Guisse, A. Recent changes of the mangroves of the Saloum River estuary, Senegal. *Mangroves Salt Marshes* **1997**.
377. Bouillon, S.; Borges, A. V.; Castañeda-Moya, E.; Diele, K.; Dittmar, T.; Duke, N. C.; Kristensen, E.; Lee, S. Y.; Marchand, C.; Middelburg, J. J.; Rivera-Monroy, V. H.; Smith, T. J.; Twilley, R. R. Mangrove production and carbon sinks: A revision of global budget estimates. *Global Biogeochem. Cycles* **2008**.
378. Kristensen, E.; Bouillon, S.; Dittmar, T.; Marchand, C. Organic carbon dynamics in mangrove ecosystems: A review. *Mangrove Ecol. – Appl. For. Coastal Zo. Manag.* **2008**.
379. Everitt, J.; Judd, F. Using remote sensing techniques to distinguish and monitor black mangrove (*Avicennia germinans*). *J. Coast. Res.* **1989**.
380. Yipp, M. W. *THE DISTRIBUTION OF GROUND DWELLING GASTROPODS IN A SMALL MANGROVE STAND IN HONG-KONG*; 1982.
381. Tebaldi, C.; Lobell, D. B.; Changes, P.; Smith, R. L. Towards probabilistic projections of climate change impacts on global crop yields. *Geophys. Res. Lett.* **2008**.
382. Ruitenbeek, H. J. The rainforest supply price: a tool for evaluating rainforest conservation expenditures. *Ecol. Econ.* **1992**, 6, 57–78.
383. Ramsey, E. W.; Jensen, J. R. Remote Sensing of Mangrove Wetlands: Relating Canopy Spectra to Site-Specific Data. *Photogramm. Eng. Remote Sensing* **1996**.
384. Cahoon, D. R.; Hensel, P.; Rybczyk, J.; McKee, K. L.; Proffitt, C. E.; Perez, B. C. Mass tree mortality leads to mangrove peat collapse at Bay Islands, Honduras after Hurricane Mitch. *J. Ecol.* **2003**, 91, 1093–1105.
385. M. Brander, L.; J. Wagtendonk, A.; S. Hussain, S.; McVittie, A.; Verburg, P. H.; de Groot, R. S.; van der Ploeg, S. Ecosystem service values for mangroves in Southeast Asia: A meta-analysis and value transfer application. *Ecosyst. Serv.* **2012**.
386. Kathiresan, K.; Bingham, B. L. Biology of mangroves and mangrove Ecosystems. *Adv. Mar. Biol.* **2001**, 40, 81–251.
387. Pannier, F. Mangroves impacted by human-induced disturbances: A case study of the Orinoco Delta mangrove ecosystem. *Environ. Manage.* **1979**.
388. Chen, K.; McAneney, J. High-resolution estimates of Australia's coastal population. *Geophys. Res. Lett.* **2006**.
389. Hoque, A. K. F.; Datta, D. K. The mangroves of Bangladesh. *Int. J. Ecol. Environ. Sci.* **2005**.



390. Costanza, R.; Rd' Arge; Groot, R. de; Farber, S. The value of the world's ecosystem services and natural capital. *Ecol. Econ.* **1998**.
391. Manson, F. J.; Loneragan, N. R.; Skilleter, G. a; Phinn, S. R. An evaluation of the evidence for linkages between mangroves and fisheries : A synthesis of the literature and identification of research directions. *Oceanogr. Mar. Biol.* **2005**.
392. Ellison, A.; Farnsworth, E. Anthropogenic distrubance of Caribbean mangrove ecosystems. *Biotropica* 1996, 28, 549–565.
393. Chou, Y.; Jan, J.; Use, L.; Analysis, C. AGRICULTURAL LAND USE CHANGE ANALYSIS : A STUDY OF TAIWAN In the course of the study , we also uses the Python programming language to assist processing and analysis of data , the use of pre-treatment section contains batch download of the data , coordina.
394. Management, M. Mangrove Management and Utilization in Eastern Africa. *Ambio* **1998**, 27, 620–626.
395. Anonymous Annual report of the Kenya Department of Agriculture for 1955. *Kenya* **1956**, I, 70 P.
396. Africa, S. Sub-Saharan Africa. *Popul. English Ed.* **2007**.
397. De Varennes, A.; Qu, G.; Cordovil, C.; Gon??alves, P. Soil quality indicators response to application of hydrophilic polymers to a soil from a sulfide mine. *J. Hazard. Mater.* **2011**, 192, 1836–1841.
398. Al-Hurban, A. E. Effects of recent anthropogenic activities on the surface deposits of Kuwait. *Arab. J. Geosci.* **2014**.
399. Barbier, E. B. Natural barriers to natural disasters: Replanting mangroves after the tsunami. *Front. Ecol. Environ.* **2006**, 4, 124–131.
400. Naylor, R. L.; Goldburg, R. J.; Primavera, J. H.; Kautsky, N.; Beveridge, M. C.; Clay, J.; Folke, C.; Lubchenco, J.; Mooney, H.; Troell, M. Effect of aquaculture on world fish supplies. *Nature* **2000**.
401. Lebel, L.; Tri, N. H.; Saengnoree, A.; Pasong, S.; Buatama, U.; Thoa, L. K. Industrial transformation and shrimp aquaculture in Thailand and Vietnam: pathways to ecological, social, and economic sustainability? *Ambio* **2002**.
402. Das, C. S.; Mandal, R. N. Coastal people and mangroves ecosystem resources vis-??-vis management strategies in Indian Sundarban. *Ocean Coast. Manag.* **2016**.

403. Gilman, E. L.; Ellison, J.; Duke, N. C.; Field, C. Threats to mangroves from climate change and adaptation options. *Aquat. Bot.* 2008.
404. Primavera, J. H. Socio-economic impacts of shrimp culture. *Aquac. Res.* **1997**.
405. Environmental Justice Foundation Thailand's Seafood Slaves.
406. Sathirathai, S.; Barbier, E. B. Valuing Mangrove Conservation in Southern Thailand. *Contemp. Econ. Policy* **2001**.
407. Long, J.; Napton, D.; Giri, C.; Graesser, J. A Mapping and Monitoring Assessment of the Philippines' Mangrove Forests from 1990 to 2010. *J. Coast. Res.* **2014**, 294, 260–271.
408. Lacerda, L. D. Conservation and Sustainable Utilization of Mangrove Forests in Latin America and Africa Regions. *America (NY)*. **1992**, 114190, 44.
409. Silva, E. V.; Farias, J. F.; Barbosa, L. N.; Lima, V. G. F.; Gorayeb, A. Environmental Dynamics of the Estuary of the Pacoti River in Ceará, Brazil: Proposals for Management and Environmental Planning. *J. Coast. Res.* **2016**, 143–147.
410. Fuentes, H. R.; Crisman, T. L.; Bell, S. S.; Koch-Rose, M. S.; Boukerrou, L. Assessment of the Mangrove Ecosystem at São Luis, Maranhão, Brazil. *World Environ. Water Resour. Congr. 2007* **2007**, 1–6.
411. Latiff, A. .; Faridah-Hanum, I. . Mangrove Ecosystem of Malaysia: Status, Challenges and Management Strategies. In *Mangrove Ecosystems of Asia*; 2014; pp. 1–22.
412. IPIECA *Biological impacts of oil pollution: Mangroves*; 2000.
413. Agyen-Sampong, M.; Prakah-Asante, K.; SN, F. Rice improvement in the mangrove swamps of West Africa. In *ILRI Publication*; 1986.
414. Mazda, Y.; Magi, M.; Nanao, H.; Kogo, M.; Miyagi, T.; Kanazawa, N.; Kobashi, D. Coastal erosion due to long-term human impact on mangrove forests. *Wetl. Ecol. Manag.* **2002**.
415. Saito, H.; Bellan, M. F.; Al-Habshi, A.; Aizpuru, M.; Blasco, F. Mangrove research and coastal ecosystem studies with SPOT-4 HRVIR and TERRA ASTER in the Arabian Gulf. *Int. J. Remote Sens.* **2003**, 24, 4073–4092.
416. Rahaman, M. M. Water versus power : Role of dams in geopolitics of Ganges basin. *Water Resour.* **2001**, 1–10.
417. Dong, B. L.; Qin, B. Q.; Gao, G.; Cai, X. L. Submerged macrophyte communities and the controlling factors in large, shallow Lake Taihu (China): Sediment distribution and water depth. *J. Great Lakes Res.* **2014**, 40, 646–655.



418. Paphavasit, N. Wattayakorn, G. Aksornkoae, and B. F. S. C. Mangrove of Thailand: present status of conservation, use and management The Economic and environmental values of mangrove forests and their present state of conservation in the South-east Asia/Pacific region. *Int. Soc. Mangrove Ecosyst. Okinawa Int. Trop. Timber Organ. Yokohama Japan Int. Assoc. Mangroves, Tokyo* **1993**.
419. Padmanaban, R.; Kumar, R. Mapping and Analysis of Marine Pollution in Tuticorin Coastal Area Using Remote Sensing and GIS. *Int. J. Adv. Remote Sens. GIS* **2012**, *1*, 34–48.
420. Ouyang, X.; Guo, F. Paradigms of mangroves in treatment of anthropogenic wastewater pollution. *Sci. Total Environ.* **2016**.
421. Mandura, a S. A mangrove stand under sewage pollution stress: Red Sea. *Mangroves Salt Marshes* **1997**.
422. Lewis, R. R.; Milbrandt, E. C.; Brown, B.; Krauss, K. W.; Rovai, A. S.; Beever, J. W.; Flynn, L. L. Stress in mangrove forests: Early detection and preemptive rehabilitation are essential for future successful worldwide mangrove forest management. *Mar. Pollut. Bull.* **2016**, *109*, 764–771.
423. Goldstein, B. D.; Osofsky, H. J.; Lichtveld, M. Y. The Gulf oil spill. *N. Engl. J. Med.* **2011**, *364*, 1334–1348.
424. Ghasemi, S.; Mola-Hoveizeh, N.; Zakaria, M.; Ismail, A.; Tayefeh, F. H. Relative abundance and diversity of waterbirds in a Persian Gulf mangrove forest, Iran. *Trop. Zool.* **2012**, *25*, 39–53.
425. Hindu, T. *The Hindu*. Chennai 2017, p. 1.
426. Padmanaban, R.; Bhowmik, A.; Cabral, P. A Remote Sensing Approach to Environmental Monitoring in a Reclaimed Mine Area. *ISPRS Int. J. Geo-Information* **2017**, *6*, 401.
427. Lee, J. G.; Kang, M. Geospatial Big Data: Challenges and Opportunities. *Big Data Res.* **2015**, *2*, 74–81.
428. Shan, J.; Qin, K.; Huang, C.; Hu, X.; Yu, Y.; Hu, Q.; Lin, Z.; Chen, J.; Jia, T. Methods of crowd sourcing geographic data processing and analysis. *Wuhan Daxue Xuebao (Xinxi Kexue Ban)/Geomatics Inf. Sci. Wuhan Univ.* **2014**, *39*, 390–396.
429. Jackson, M.; Magro, G. Real-time crowd-sourcing , data and modelling. In *IAIA15 Conference Proceedings*; 2015; pp. 1–6.
430. Hristova, D.; Mashhadi, A.; Quattrone, G.; Capra, L. Mapping Community Engagement

with Urban Crowd-Sourcing. In *In Proceedings of When the City Meets the Citizen Workshop*; 2012.

431. Mitianoudis, N.; Stathaki, T. 12 - Enhancement of multiple sensor images using joint image fusion and blind restoration. In *Image Fusion*; 2008; pp. 299–326.